12-2010

Rare earth element transport in the Yucca Mountain region

Liqiong Zhang
University of Nevada, Las Vegas

RARE EARTH ELEMENT TRANSPORT

IN THE YUCCA MOUNTAIN REGION

by

Liqiong Zhang

Bachelor of Engineering
Science & Technology University of Chengdu, China
1994

Master of Engineering
Hohai University, China
2000

A dissertation submitted in partial fulfillment
of requirements for the

Doctor of Philosophy Degree in Geoscience
Department of Geoscience
College of Sciences

Graduate College
University of Nevada, Las Vegas
December 2010

UNLV
UNIVERSITY OF NEVADA LAS VEGAS

THE GRADUATE COLLEGE

We recommend the dissertation prepared under our supervision by

Liqiong Zhang

entitled

Rare Earth Element Transport in the Yucca Mountain Region

be accepted in partial fulfillment of the requirements for the degree of

Doctor of Philosophy Degree in Geoscience

Zhongbo Yu, Committee Chair

Lambis Papelis, Committee Co-chair

Wanda Taylor, Committee Member

Matthew Lachniet, Committee Member

Zhonghai Ding, Graduate Faculty Representative

Ronald Smith, Ph. D., Vice President for Research and Graduate Studies
and Dean of the Graduate College

December 2010

ABSTRACT

Rare Earth Element Transport in the Yucca Mountain Region

by

Liqiong Zhang

Dr. Zhongbo Yu, Examination Committee Chair
Professor of Hydrology and Hydrogeology
University of Nevada, Las Vegas

Dr. Lambis Papelis, Examination Committee Co-Chair
Associate Professor of Hydrological Science
Desert Research Institute, Las Vegas

In sync with environmental pollution of solutes in nature, from source, process to consequence, geochemical processes (leaching and sorption) and hydraulic transportation of the rare earth elements (REEs) have been investigated at Yucca Mountain (YM), Nevada. This research includes the leaching behavior of trace elements (including REEs) from aquifer rocks, the surface complexation reactions of REEs in synthetic groundwater, and transportation of reactive REEs in the local-scale groundwater system of YM. This dissertation includes three projects. These studies indicate that surface complexation reactions may retard the transportation of REEs along groundwater paths in YM, which suggests a similar behavior of aqueous actinides.

The first project describes the study of leaching characteristics of trace elements (including REEs) from three widely-distributed aquifer host rocks in YM and Nevada Test Site areas. Leachate compositions are significantly impacted by leaching time, pH, grain size, and rock mineralogy. Geochemical modeling was conducted to explore the

redistribution and leaching process of trace elements. Leaching factors of various trace elements were derived to quantify the leached trace elements from each of three aquifer rocks.

The second project describes the adsorption behavior of two REEs, ytterbium (Yb) and europium (Eu), using an integrated approach of laboratory experiments and numerical modeling. Experimental results indicate that Yb and Eu show moderately pH-dependent adsorption behavior, which was simulated by surface complexation models. Due to their advantage of wide relevance to ionic strength, experimentally derived surface complexation models can be used for adsorption reactions in transport modeling.

The third project describes the numerical simulation of REE transport in the mountain-scale groundwater model of YM. A three dimensional reactive groundwater model, PHAST3D, was conceptualized for REE transport modeling by coupling with the experimentally derived surface complexation reactions. Modeling results indicate that sorption reactions may retard transport of REEs and attenuate concentrations of dissolved REEs.

The research demonstrates that surface complexation reactions play an important role in the REE transport in the YM area. As the natural analogue of trivalent-actinides, the simulation results of REEs are expected to help us determine the fate of nuclides stored in the high level nuclear repository in YM.

TABLE OF CONTENTS

LIST OF TABLES

LIST OF FIGURES

ACKNOWLEDGMENTS

Firstly, I would like to thank my examination committee members for their participation and, contributions to my Ph.D. graduate study experience. During the course of my study, they always provide me with instruction, support and patience. Dr. Zhongbo Yu, gives me many valuable advices and guidance. I learn from him about self responsibility, and earnest attitude on research. Dr. Lambis Papelis helps me set up the batch reactor experiments and teaches me a lot of knowledge on Geochemistry. I'm very grateful for Dr. Wanda Taylor for opening a new door in my appreciation for the Tectonics. I would like to thank Dr. Matthew Lachniet for his constant help and cooperation. I also thank Dr. Zhonghai Ding who kindly agreed to be my committee member.

I would like to thank other staff and students from Dr. Papelis's Geochemical Group in the Desert Research Institute for their assistance while doing laboratory work there. I would like to particularly thank Rachael and Tracy for their generous help.

I would also like to thank the University of Nevada and Desert Research Institute for supporting three years of research fellowship.

I thank my family and friends for their encouragement and support, especially, my parents who are always there to support me.

CHAPTER 1

INTRODUCTION

1.1 Background/Problem Statement

Being the proposed future high-level nuclear waste repository, Yucca Mountain (YM) has been a focal point for research since the 1970's. An important question of concern for the public and researchers is whether nuclear waste will access and contaminate the underlying groundwater system by infiltrating across the aquifers or flowing along the fault zones. If contamination happens, the groundwater will become unsafe and unfit for human use. Furthermore, to remove the contaminants from groundwater is more difficult than from surface water. As one of most reliable water resources, groundwater quality is a great concern for people living in this desert area.

Among the major sources of contaminants, radionuclides, especially actinides with high toxicity, cannot be neglected because of various forms of nuclear waste (McPhee and Yeh, 2003). Concerns about groundwater contamination from radionuclides require the understanding of how radionuclides access the groundwater and their behavior in water-rock interaction. Many reactions are usually involved in the interface between rock matrix and groundwater including biodegradation, chemical reactions, precipitation, and dissolution. The focus is what reaction(s) of radionuclides play important roles in and methods to quantify their space-time influence on groundwater quality.

However, it is difficult to investigate directly the complicated geochemical reactions of aqueous radionuclides due to their harmful radioactivity. Previous studies (Johannesson et al., 1997; Dia et al., 2000; Moller et al., 2000) show that REEs have similar charges and sizes as trivalent actinides including neptunium (Np) and plutonium

(Pu). Also, REEs have significant fractionation as a group with small differences in solubility and complex formation, which make them be used as natural analogs of radionuclides. In the past two decades, the studies about REEs have been increased because of their similarities with radionuclides and ability to trace sources.

1.2 Research Objectives

- To characterize the leaching properties of widely distributed aquifer rocks in the YM and adjacent areas. To determine background concentration levels of REEs naturally leached from aquifers.
- To investigate the adsorption behaviors of the selected REEs in batch reactor experiments. The results of these experiments are simulated by using surface complexation models to derive the key adsorption reactions and associated reaction parameters.
- To simulate the selected REEs transport by coupling the experimentally derived surface complexation models. The simulation results are used to evaluate and predict the fate and transport of radionuclides in the YM groundwater system by using REEs as a radionuclide's analogs.

This dissertation is organized in an introduction, and three manuscripts followed by a conclusion. Chapter 1 includes background, objectives, study area, and previous work. Chapter 2 contains the first manuscript describing the study of leaching behavior of trace elements from three main aquifer rocks in southern Nevada region. Chapter 3 is the second manuscript describing the investigation of adsorption behavior of the selected two REEs and the related numerical modeling with surface complexation models. Chapter 4 is the third manuscript presenting the transport modeling of the selected REEs by

coupling the experimentally derived key reactions into a mountain-scale model. Chapter 5 summarizes the conclusions from the study and outlines future work.

1.3 Study Area

Yucca Mountain (YM) is located about 160 kilometers northwest of Las Vegas in southern Nevada (Figure 1.1). On its eastern part is the Nevada Test Site (NTS), on its northwestern part is the Nellis Air Force Range, and on its southwestern part is public lands managed by the Bureau of Land Management (Montazer and Wilson, 1984). The study area belongs to the Basin and Range Province with a desert climate, and is within the Great Basin. In the surrounding area, the lowest altitude is about 80 m below sea level at Badwater in Death Valley and the highest is 3600 m above sea level at Mount Charleston (Scott, 1990). Areas between the basins and mountains generally are above 1500 m. In this area, 25 percent is uplands and 75 percent is intermountain basins filled with alluvium and lower volcanic deposits (D'Agnese et al., 1997). The precipitation distribution differs widely as the mean value in the Spring Mountains is more than 700 mm/yr and 50 mm/yr in Death Valley. Average annual lake-evaporation changes spatially from 1100 mm in the north to 2000 mm in Death Valley (Grasso, 1996).

As a proposed future site for the underground storage of high-level radioactive nuclear wastes, the repository would be located in the tuff of volcanic ash with age of about 11.5 million years, located above the water table (USDOE, 2001). Previous studies showed that the complete set of geologic formations could be divided into approximately ten hydrostratigraphic units (Winograd and Thordarson, 1975). The hydrogeologic properties of these units play an important role in the study area. YM is mainly comprosed of the Quaternary surficial deposits, the Tertiary volcanic aquifer and the

Paleozoic carbonate aquifer in a sequence of three aquifers and three confining units, intersected by variably space-distributed faults that are block bounding, relay structures, strike strip or intrablock as shown in Figure 1.2.

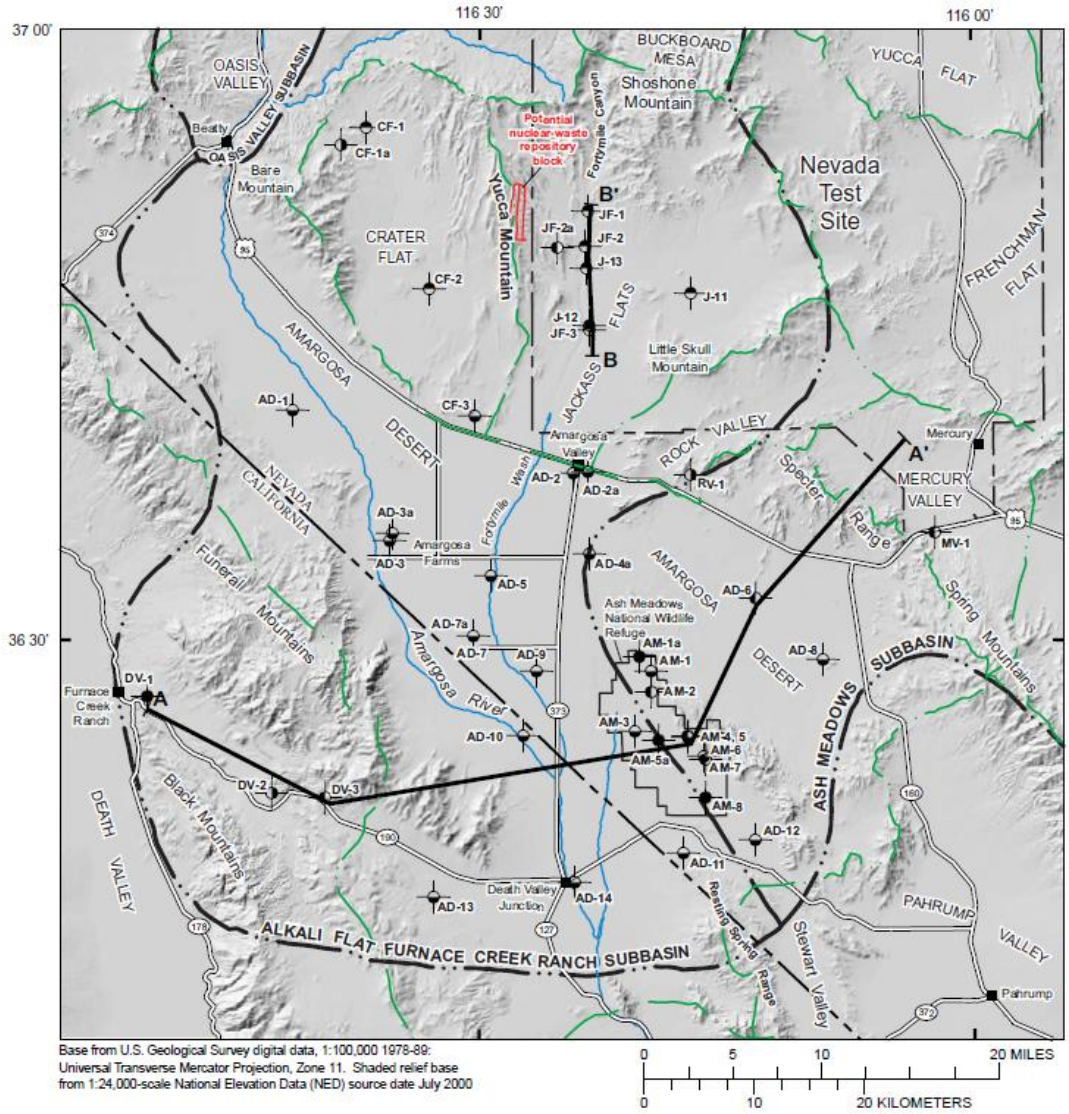

Figure 1.1 Study area and location of primary monitoring wells in the Yucca Mountain. Please note that circle with left half black-Carbonate rock; circle with right half black -Undifferentiated rock; circle with lower half black-Valley fill; circle with upper half black-Volcanic rock; black circle-Combined carbonate rock and valley fill; yellow circle-Miscellaneous monitoring site; black dot dashed line-Ground water subbasin boundary; black dashed line- Nevada Test Site boundary; black solid line-Trace of section; green dot dashed line -hydrographic area boundary (Fenelon and Moreo, 2002).

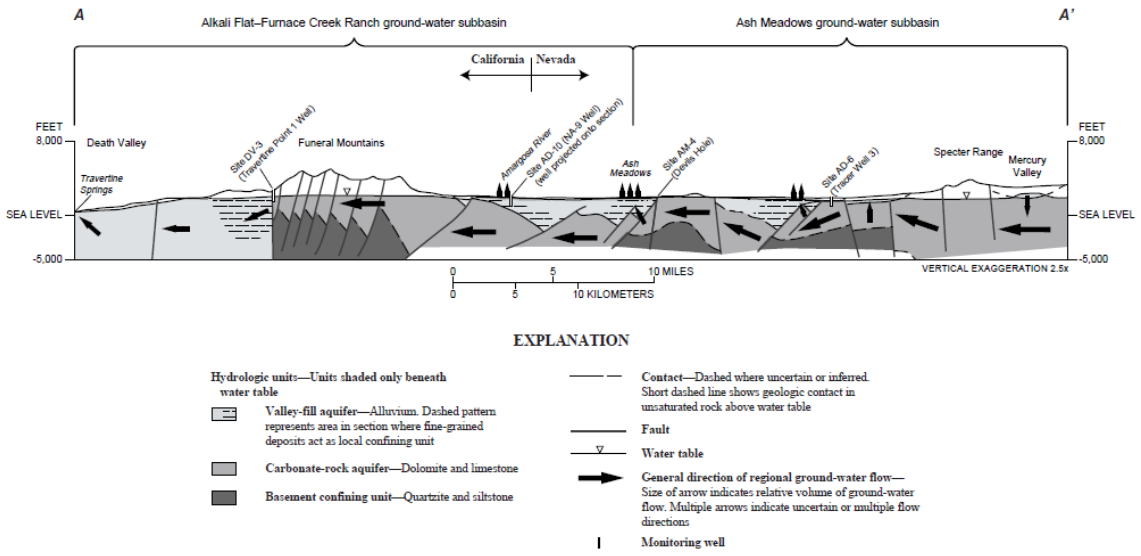

Figure 1.2 Hydrogeologic cross section of A-A' shown in Figure 1.1 (Fenelon and Moreo, 2002)

YM belongs to the Death Valley Regional Flow System (DVRFS), where the primary flow direction of groundwater is from the eastern and northeastern recharge areas to the southwestern discharge area through the carbonate rocks (Patrick, 2003). At YM area, groundwater in north-south direction primarily flows through fractured and faulted volcanic rocks and then into the southern alluvium. Due to a confining unit between the volcanic and carbonate units, they generally are hydraulically separated. Recharge of YM groundwater may be from infiltration of precipitation, infiltration of intermittent streamflow in Fortymile Wash, and underflow from the northern, western, and eastern parts. Groundwater may be discharged as underflow to the south, springs in Death Valley and pumping wells in Jackass Flats and Amargosa Desert (D' Agnese et al., 1997). According to potentiometric surface maps, a large hydraulic-gradient area is located in the north, moderate hydraulic-gradient areas in the west and south, and a small hydraulic-gradient area below Jackass Flats (Daniels et al., 1982).

The groundwater geochemistry in this study area can be described by two dominant types: relatively dilute sodium-bicarbonate water with high silica content mainly due to the influence of volcanic rocks and corresponding sediments, and an elevated calcium-magnesium-bicarbonate water with low silica content mainly due to the influence of carbonate rocks (Luckey et al., 1996). At some locations, groundwater has a combination of characteristics of the above two groundwaters because of mixing along groundwater flow paths. Groundwater under the valley fills may contain significantly concentrated sulfate and chloride ions as a result of extensive evaporation.

1.4 Previous Work

1.4.1 Analogue of Trivalent Radionuclides

The potential migration of radionuclides in groundwater is a key to design and operation of nuclear repositories (Shagalova et al., 2000; Monte, 2002). To simulate the real configuration of radionuclide transport requires adequate understanding of hydrogeologic characteristics of groundwater systems and geochemical behaviors of radionuclides. Understanding of transport and geochemical processes of radionuclides have been challenging due to currently limited knowledge of hydrogeology and geochemistry. Radionuclides' radioactivity prevents people from directly examining and investigating them. Fortunately, previous research studies show that REEs could be used as analogue of trivalent actinides (e.g., plutonium, neptunium) because of similar atom radii and valence (Thompson, 1979; Choppin, 1983; Johannesson et al., 1994, 1995).

Rare earth elements are commonly referred to as the lanthanide series, from La trough Lu, which act as a group and fractionate closely within the group. The reason is that REEs are 4f cations partially filled and shielded from bonding interactions (Thompson,

1979). The dominant mechanism is electrostatic for surface complexation. The REEs are only trivalent except Eu that has another valence of 2+ and Ce with another valence of 4+. With increasing atomic number, the atomic radii decrease results in fractionation of REEs, or lanthanide contraction. Compared with REEs, trivalent actinides are 5f cations showing similar behaviors within the group as well. Despite having fewer redox states than actinides, discussions about lanthanides are mostly applicable to actinides especially in the groundwater in the following studies.

Choppin's study (1983) shows that pronounced chemical similarities exist between actinides and lanthanides. Aqueous complexes of these two series elements can be simulated well with an electrostatic mechanism plus slightly stronger bonding for actinide complexation. In the research of Johannesson et al. (1994), it is shown that all of the REEs (noted as Ln) exist in carbonate complexes and 99% of them are $Ln(CO_3)_2^-$ in alkaline lake waters. Light REEs are prone to form stronger carbonate complexes than relative heavy REEs. Rare earth elements are revealed to act and fractionate as a group, providing very valuable tracer or signature information. A rare earth element, Nd, in groundwater samples from NTS and YM area was investigated by Johannesson et al (1995). Geochemical modeling showed that 92% to >99% of dissolved Nd^{3+} was complexed with carbonate as $NdCO_3^+$ or $(Nd(CO_3)_2^-$, resulting from elevated free CO_3^{2-} in groundwater. Behaviors of aqueous Nd^{3+} indicate that free CO_3^{2-} may increase solubility and decrease retardation of trivalent actinides (Am^{3+}, Cm^{3+}, Cf^{3+}) in groundwater.

Being the analogues of radionuclides, the research of REEs has seen largely increased interest in the last few decades for supporting more insightful information than other

elements or compounds. Dia et al. (2000) identified two different groundwaters by investigating control factors of REEs signature. Their research showed that the two most likely dominant factors are dissolved organic carbon and redox states in groundwater. By studying REE pattern in surface water and groundwater, significant abnormality of Gd was observed in Moeller et al.'s research (2000). Abnormality of the Gd complex finally helped researchers identify the origin and fate of certain waters.

1.4.2 Numerical Transport Modeling

Numerical modeling is one of prevalent techniques which can be applied to various imaginary scenarios for complicated groundwater systems. And multiple time-scale simulations of groundwater systems can be performed with numerical models. Thus, the possibility of radionuclide contamination and the corresponding impact extent can be evaluated (Johnson et al., 2001).

The last several decades have seen a development boom of groundwater transport models. With comparison to the physical mechanisms of groundwater flow, the geochemical characteristics of solutes are more difficult to be determined because of complex and numerous reactions. There are many transport models for the equilibrium/mass transfer in mineral/amorphous phases such as TRANQL (Cederberg et al., 1985), PHREEQC (Parkhurst and Appelo, 1999), HYDROGEOCHEM (Yeh and Tripathi, 1990, 1991) and The Geochemist's Workbench7 (Bethke, 1996). In order to kinetically simulate reactions of solute in the groundwater flow, researchers have been triggered to couple specific reactions into physical-based transport models for their research purposes.

How to simulate the source/sink term in the governing equation of mass transport

directly determines whether the model reflects the important reactions of the solute in the real water-mineral environment and whether the simulated results match well with observed data.

For i^{th} solute species, the one-dimensional governing equation of mass transport can be described as follows:

$$\frac{\partial C_i}{\partial t} = D_{xi} \frac{\partial^2 C_i}{\partial x^2} - v_x \frac{\partial C_i}{\partial x} \pm R \tag{1.1}$$

where C_i is the concentration of i^{th} solute, D_{xi} is the dispersion coefficient, v_x is the flow vector, R is the source/sink term which is determined by the heterogeneous reactions of reactive solute (Domenico and Robbins, 1984; Liu and Narasimhan, 1989; Mangold and Tsang, 1991; Lichtner, 1996; Domenico and Schwartz, 1998).

The chemical behavior of the reactive solute typically includes sorption reactions, redox reactions, and/or radioactive decay, precipitation-dissolution, of the solute along groundwater flow paths.

Specifically, the adsorption reaction can be presented as:

$$R_j^s = \frac{\partial}{\partial t}[\sum_{k=1}^{N_c} V_{kj}^s S_{Xk}] \qquad (\mathrm{k} = 1, \ldots, \mathrm{N_c}) \tag{1.2}$$

where R_{js}, is the sum of the adsorption/desorption process for the j^{th} secondary species, V_{kj} is the stoichiometric coefficient of the adsorbed component k in the adsorbed complex S_{xk}, and N_c is the number of the surface bound complexes of k.

A brief summary of previous work relevant to transport model development follows in this section. Kohler et al. (1996) simulated the retardation of uranium in column experiments by using a transport model with a surface complexation model. Wunderly et al. (1996) developed a versatile model coupled with oxygen diffusion and sulfide-mineral

oxidation to simulate the transport of sulfide mineral oxidation in mine tailing impoundments. Smith and Jaffe (1998) coupled various processes of biodegradation, chemical reactions, precipitation, and dissolution with transport processes of advection, bioturbation, and dispersive mixing to model the trace metals in lake sediments. Zhang and Schwartz (2000) formulated a model to reproduce the coupled process of nonaqueous phase liquid dissolution, chemical reactions and subsequent transport in the chemical oxidation scheme. Zhu (2002) estimated the recharge by using a flow and transport model and the observed radiocarbon ages. Pang and Close (2003) applied the method of temporal moment (MOM) formula to analyze breakthrough data to estimate a first-order degradation rate constant, retardation factor, and sorption distribution coefficient. Comparing to the results of curve fitting, MOM has a better fit with tailing and good application to interpret solute transport with sorption and degradation. Thomasson and Wierenga (2003) conducted a precisely controlled field experiment to study the spatial variability of the retardation coefficient. The study indicated that a range of retardation values may be needed for different depths of soil due to retardation coefficient's wide variability. Kallvenius and Ekberg (2002) designed a transport and chemical kinetics (TACK) program to predict the transport of nuclear waste by coupling a two-dimensional transport model with a geochemical computer program, PHREEQC (Parkhurst and Appelo, 1999). As compared with the software PHAST, TACK showed similar qualitative but different quantitative results. Nelson et al. (2003) used tracers with different diffusivities to investigate the relative contribution of diffusive mass transfer to the solute transport of aquifers in laboratory and field scales. Their research showed that the influence of the diffusive mass transfer to the solute transport could be measured, which

often is accompanied with the diffusion between zones of lower and higher advections in the field scale. Montas (2003) presented an analytical solution for the multidimensional solute transport equation including advection, dispersion and reaction terms. In this study, an advective dispersive-reactive kernel and a coupled advective kernel both with an explicit form are applied and the solution is an exponentially scaled space-time convolution of the two kernels. The results indicated that the solution could accurately predict the mean and range of concentration distribution. Browning et al. (2003) combined the thermodynamic chemistry interpretation of groundwater and formulated a conceptual model to simulate the interactions between mineral/glass, water, and gas of YM area. Their simulated results indicated that chemical compositions of groundwater at YM are influenced more by the percolating waters than by *in situ* chemical reactions. The possible flow paths are influenced mainly by percolation flux and fracture-matrix interactions. A good description of ambient conditions is the key to obtain more reliable results for solute transport.

In order to discern and quantify the major reactions of REEs in the water/mineral medium in the groundwater system, different reactions may be taken into account by employing a closely analogous equation to the above adsorption/desorption treatment in this research. The sum of these reactions can provide a more realistic expression that accounts for the major reactions of the radioactive solutes along the flow paths. Obviously, in the simulation of the equilibrium reactive multicomponent transport, two sets of equations must be solved: hydrodynamic mass transport partial differential equations and equilibrium chemistry nonlinear, algebraic equations. The two sets of equations can be solved independently, and subsequently linked together at each time

step (e.g., Wunderly et al., 1996; Smith and Jaffe, 1998). Yeh and Tripathi (1990) indicated that an iterative coupling of an equilibrium speciation with a kinetic reaction and transport model is computationally most efficient.

1.4.3 Surface Complexation Modeling

Most transport models are not capable of simulating adsorption reactions thermodynamically. Usually, empirical adsorption isotherms are applied to calculate the distribution coefficient, a constant to quantify sorption of solutes. Empirical isotherms are equations developed to quantify the adsorbed adsorbates from solution by curve fitting. It's obvious that the developed isotherm is dependent on adsorbate, adsorbent, and specific conditions. There are three frequently used adsorption isotherms expressed in Equations (1.3)-(1.5).

Linear isotherm:

$$C = K_d C_{aqu} \tag{1.3}$$

where, C is the adsorbed concentration of the adsorbate; K_d is the distribution coefficient; and C_{aqu} is the aqueous concentration of adsorbate at equilibrium.

Freundlich isotherm:

$$C = K_d C_{aqu}^n \tag{1.4}$$

where, *n* is a empirical coefficient, others are defined as above.

Langmuir isotherm:

$$C = \frac{C_{\max} \cdot K_d \cdot C_{aqu}}{1 + K_d \cdot C_{aqu}} \tag{1.5}$$

where, C_{max} is the maximum adsorption capacity of the adsorbate; others are defined as above.

It is obvious that the empirical isotherms can describe an equilibrium system and have application limited within their developed conditions.

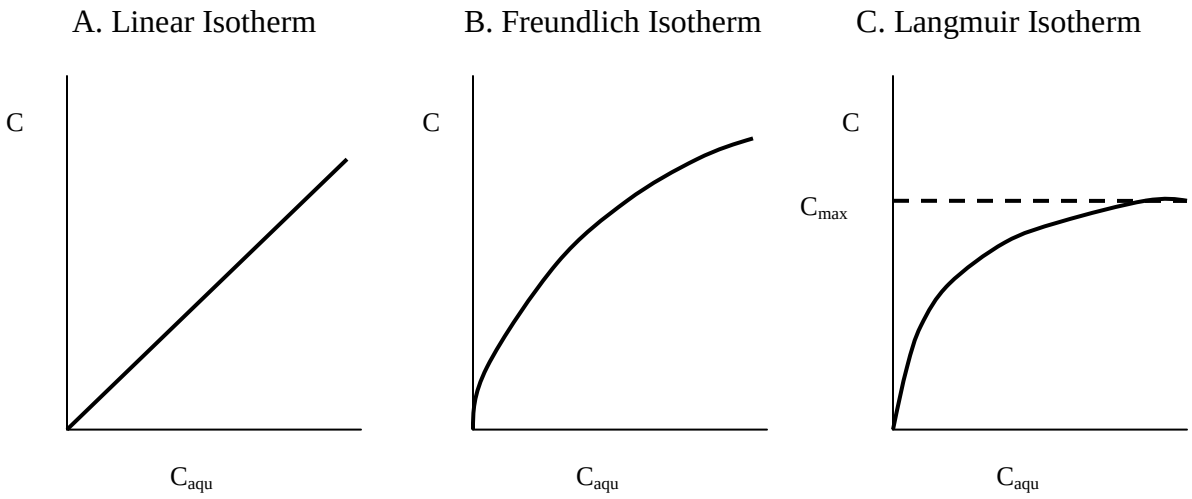

Figure 1.3 Different forms of empirical isotherms: linear isotherm (A), Freundlich isotherm (B), Langmuir isotherm (C), respectively (modified from Goldberg et al., 2007)

Compared with empirical approaches, surface complexation modeling (SCM) approaches directly describes the speciation and distribution of solution and solid surface. Being practiced for 35 years, SCMs have become a prevalent approach of investigating the adsorption process due to its more mechanistic nature. SCMs employ mass action laws analogous to aqueous phase reactions to consider changes in chemical speciation, adsorption, precipitation and other interactions (Davis and Kent, 1990). This makes SCMs more robust than empirical isotherms and applicable to conditions different from the environments in calibration. So far, quite a few transport models are embedded with SCM to account for thermodynamic adsorption. They are CRUNCH (Steefel and Yabusaki, USDOE, 1996), PHREEQC (Parkhurst and Appelo, USGS, 1999), RATEQ

(Curtis, USGS, 2005), UNSATCHEM (Šimůnek et al., USDA, 1996), and UTCHEM (Pope et al., USEPA, 1999).

Generally, there are three basic types of SCMs: constant capacitance model (CCM), diffuse layer model (DLM), and triple layer model (TLM). The schematics of the three models are shown in Figure 1.4A for CCM, Figure 1.4B for DLM, and Figure 1.4C for TLM.

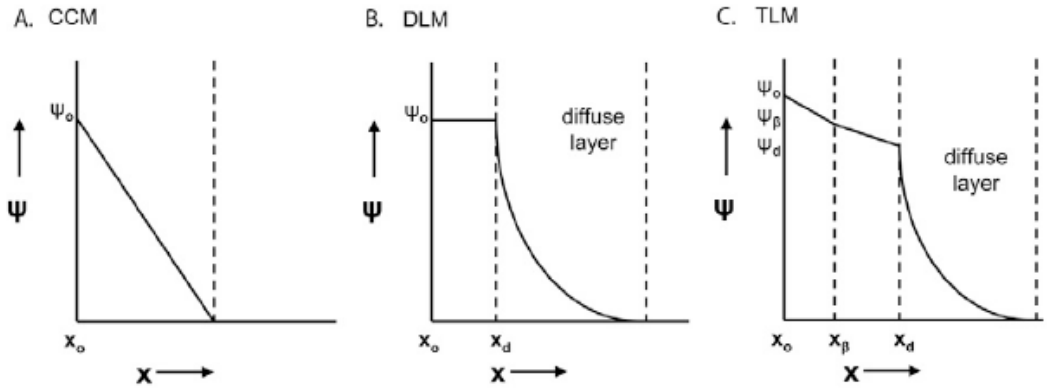

Figure 1.4 Schematics of the interface between solid and solution in A-constant capacitance model (CCM), B-diffuse layer model (DLM), and C-triple layer model (TLM), respectively (from Goldberg et al., 2007). Note that Ψ is the surface potential; x_o is the surface o-plane; x_d is the diffuse layer; x_β is the outer β-plane; *x is* the distance from the surface o-plane.

In the above figure, ψ is the surface potential, x_o denotes the location of the surface o-plane; x_d denotes the location of the diffuse layer; x_β denotes the location of the outer β-plane. It's obvious that TLM can take into account of both strong and weak bonding by inserting a β-plane between the surface plane and the diffuse plane.

The CCM has been used to describe adsorptions of a variety of anions and cations including phosphate, selenite, silicate, lead, arsenate, strontium, cadmium and boron (Goldberg, 1985; Goldberg, 1999; Goldberg at al., 2004; Goldberg at al., 2005). Also

adsorptions of some compounds (e.g., molybdenum) have been studied with CCM (Motta and Miranda, 1989). The investigated adsorbents include natural or synthetic minerals, soils and soil minerals. The CCM is the most limited because the capacity of the surface is simplified as a constant without considering different binding affinity. It is worth mentioning that Lu¨tzenkirchen (1999) first documented estimation and interdependence of surface complexation parameters in CCM. He found that it difficult to obtain a unique and meaningful set of SC parameters by fitting experimental data with CCM.

The DLM has been used to describe adsorptions of a variety of anions and cations including sodium, barium, calcium, cadmium, cobalt, copper, magnate, manganese, nickel, lead, strontium, uranium, and zinc (Zhang et al., 1994; Tonkin et al., 2004; Damaskin et al., 1986; Waite et al., 1994; and Prikryl et al., 2001). The investigated adsorbents include surfaces of Gram negative bacteria, hydrous manganese oxide, ferrihydrite and clays. The DLM has been extensively applied in surface adsorption and produced satisfactory fits of experimental data under some conditions. However, the validation of DLM is still a barrier to robust application because of the imperfect model fundamentals: Derjaguin-Landau-Verwey-Overbeek (DLVO) theory (Murray, 1997).

The TLM has been used to describe adsorptions of a variety of anions and cations including molybdate, sulfate, selenate, zinc, cadmium, baron, lead, europium, sulfate and phosphate (Phan et al., 2004; and Borrok and Fein, 2005; He et al., 1997). The studied adsorbents include hematite, γ-alumina, α-alumina, silica, river sediments, and soils among others (Hwang and Lenhart, 2008; Kosmulski, 1996; Wu et al., 2001). Generally, the TLM can provide more flexibility in simulating adsorption reactions than CCM and DLM at the expense of simplicity. Consequently, more model parameters are involved

and need to be calibrated and verified. Compared with CCM and DLM, TLM has the same reactions for inner-sphere surface complexation, plus reactions for outer-sphere surface complexation. TLM is capable of describing surface competition between inner- and outer-sphere complexes.

It is important to mention that obtained model parameters are applicable only to the same or similar sets of specific adsorbate-adsorbent pair. Furthermore, parameters in CCM, DLM, and TLM are not comparable and convertible due to different assumptions made respectively in their own conceptualization. Theoretically, it is not clear which of the above three SCMs is best in describing adsorption behavior in natural environments (Westall, 1987). Generally, to select an appropriate SCM is highly dependent on the specific adsorbates and adsorbents of interest. Generally, the method of trial and error is employed and testified through the simulation comparison among different SCMs.

Specification of surface complexes and associated equilibrium constants are crucial to SCM modeling. There are usually two techniques applied to investigate adsorption behaviors including macroscopies and spectroscopy. Macroscopic technique mainly includes batch reactor experiment and column experiment providing experimental adsorption isotherms or edges and breakthrough curves. Based on macroscopic investigation, specifying surface complexation reactions and associated equilibrium constants can be experimental derived by using curve fitting. No single technique can fully investigate adsorption mechanisms because surface complexes are complicated and affected by multiple factors in nature. Sometimes, molecular level information is necessary to constrain surface complexation reactions in the SCM modeling. Spectroscopic techniques help us identify the interactions between ions and surface, types

of adsorbed species, structures of surface complexes. An integrated method of the two techniques is always preferred given the incomplete understanding of adsorption.

1.4.4 Groundwater Modeling of YM and NTS areas

In the 1970's, numerous computer codes were available for modeling groundwater and solute transport owing to the magnificent development of computer techniques. It is worth to mention that J.R. Harrill is the person who firstly simulated the groundwater flow in the basin fill of Las Vegas Valley, Southern Nevada (Prudic, 2003). Presently groundwater models have been a prevalent tool capable of simulating complex underground environments. The NTS and YM, low-level nuclear test site and high-level radionuclide repositories respectively, are the most intensely studied sites in Southern Nevada. The potential contamination of groundwater by nuclear waste is a great concern which triggered thorough investigations of YM and NTS. Groundwater models of YM and NTS can be divided into two types including regional and local according to spatial scales. The two kinds of models are different in purposes of study and usages in practice. Usually, a regional model is used to evaluate global response to groundwater withdrawal, estimate rough travel time of solutes, and provide boundaries for local groundwater models. A local model is used to study specific area and detailed information of interest. In southern Nevada, most local models are related to radionuclide transport in the YM and NTS areas.

1.4.4.1 Regional-scale models

In 1982, a 2-D steady inverse model was developed to simulate the flow beneath the NTS and vicinity (Waddell, 1982, USGS). The typical aquifer assemblage consisting of carbonate rocks, volcanic rocks and alluvium was implemented into the groundwater

model besides some large ranges and faults in this area. Impacts of model parameters including recharge, discharge, and transmissivity to hydraulic heads and fluxes were analyzed, providing the support of field study and estimation of prediction uncertainty.

A regional model was developed to simulate groundwater flow and tritium transport in NTS area by considering detailed geologic stratigraphy (USDOE, 1997). This is a steady-state finite difference model, covering 26,200 square miles of area, and consisting of 76 rows, 68 columns and 20 vertical layers. In the simulation of solute transport, a particle tracking technique was used to simulate 1-D tritium transport in a 200-year time frame. The study provided some valuable information for the regional groundwater modeling. They are as follows: the regional geology controls the locations of flow paths; matrix diffusion dominates the migration of tritium; the uncertainty of the source term impacts decreases with increasing distances from the waste repository; and recharge coefficients are as important as matrix diffusion (USDOE, 1997).

The USGS (Belcher, editor, 2004) developed a 3-D transient model for the groundwater simulation in YM and NTS areas on the basis of a 3-D steady-state model through carbonate rocks (Prudic et al., 1995). Twenty seven hydrogeologic units are included in a 3-D digital hydrogeologic framework model besides faults and fractures. The regional model-Death Valley region flow system (DVRFS) is composed of 16 layers, finite-difference mesh including 194 uniform rows and 160 uniform columns spacing 1,500 m (Prudic et al., 2003). By incorporating many valuable miscellaneous research results, the model helps us appropriately estimate pumping effects, recharge, and discharge and flow patterns of the groundwater system.

1.4.4.2 Site-scale models

According to locations, there are two groups of site-scale model, local model of NTS and local model of YM. Pohlmann et al. (1999) developed a groundwater and transport model-FAULTLESS at Central Nevada Test Area (CNTA) in order to evaluate underground nuclear tests. The model covers about 20 square miles of area made up of 130×160×27 cubic cells of 50 m length. Using the fracture flow/matrix diffusion approach, the model simulates the transport of radionuclides firstly from cavity to control cross section through the particle tracking approach. Also the sensitivity analysis of some parameters was conducted to assess their impacts on the most reducing travel time of nuclides.

Pawloski et al. (2001) conducted a series of unclassified simulations of radionuclide release and transport underground at the CHESHIRE test at Pahute Mesa of NTS. Focusing on impacts of the CHESHIRE test, a flow and transport model was developed to predict radionuclide migration in the sub-region of Pahute Mesa Corrective Action Unit (CAU). These unclassified simulations were developed for defining hydrologic source term boundary conditions in the CAU model. This research is of significance in interpreting sources term behavior which may be applied to other areas.

Wolfsberg et al. (2002) employed an integrated approach to simulate the groundwater flow and radionuclides transport beneath the BENHAM and TYBO underground nuclide tests at Pahute Mesa of NTS. Main components of the model include source-term model considering radionuclide release following complex processes, and site-scale transport models considering solutes transport in volcanic rocks with fractures. These components produced results that match well with laboratory and field data after coupling together.

Sensitivity analysis was performed to assess possible ranges of model parameters.

The last three decades have seen extensive studies of YM to characterize the heterogeneous hydrogeologic system and complex transport processes under this proposed geologic waste repository. Results of these fundamental studies enhance the conceptualization and development of groundwater models for this site. It is worth mentioning that two significant groundwater models frequently were applied at the study area of YM, FEHM by Los Alamos National Laboratory (Birdsell et al., 1995) and TOUGH2 by Lawrence Berkeley Laboratory (Pruess, 1991). The FEHM is a finite-element heat and mass- transfer computer code which can simulate the groundwater flow and solute transport in unsaturated and saturated zones (Zyvoloski and Robinson, 1999). In the FEHM, there are three main modules including fluid flow and transport, reactive solute transport and particle tracking, and configuration control and verification. The air-water transport is assumed isothermal and gas is considered as noncondensible in the FEHM. The component of dual-porosity and double-porosity/double permeability was designed for simulating fracture flow; and reactive-transport and particle tracking components were designed for simulating multiple solute transports (Zyvoloski et al., 1997).

TOUGH2 is a numerical simulation program for non-isothermal multiphase, multicomponent flow in porous and fractured media (Pruess, 1991). It has been successfully used for simulations of the unsaturated zone at YM. It is a family code including MULKOM module, which is the core part of TOUGH for modeling the water-air two phase flow and transport and was updated as TOUGH2 in 1999 (Pruess, 1991). Module T2VOC (Falta et al., 1995) was designed to simulate a volatile organic

compound (VOC) in a 3-phase flow of water, air and non-aqueous phase liquids (NAPLs). As the extension of T2VOC, module TMVOC (Pruess and Battistelli, 2002) was designed to simulate three-phase non-isothermal flow of water, soil gas, and a multicomponent mixture of VOCs in heterogeneous saturated and unsaturated zones. This module is usually used in problems of hydrocarbon fuel spill, organic solvents spills, and stream-assisted source remediation (Pruess and Battistelli, 2002). Module TOUGHREACT was designed for introducing reactive geochemical reactions into the multiphase flow in porous and fractural media (Xu and Pruess, 2001). These reactions include equilibrium and kinetic reactions, precipitation and dissolution, chemically active gas phase, and interactions between mineral assemblages and fluids. iTOUGH 2 is a numerical inverse model providing parameter calibration and uncertainty analysis for TOUGH2 (Finsterle, 1999). By applying a minimization procedure, the estimated parameters can yield minimum error residuals as compared with observed data, which is a key to the model calibration and prediction uncertainty.

The two local-scale models, FEHM and TOUGH2, are both 3-D groundwater flow and reactive multi-component transport models for saturated and unsaturated zones. They are widely used in complex groundwater simulation underneath the YM after years of calibration and verification. Their flexible unstructured grids both can conform to the geologically complex aquifer systems. It is worth to mention that FHEM is an isotherm model and TOUGH2 a non-isotherm model, enabling the latter to consider heat-related phenomena. That they most interest us is how the two important models simulate adsorption effects (or retardation) in the groundwater system. There are four equilibrium adsorption isotherms embedded in the FEHM to quantify the adsorbed contaminants,

including linear, Freundlich, Modified Freundlich, and Langmuir isotherms (Zyvoloski et al., 1997). In TOUGH2, the distribution coefficients for each rock type are used for adsorption effects. As discussed above, using a lumped single parameter, the distribution coefficient, to count for complex adsorption may considerably increase the prediction uncertainty. Thus, the uncertainty analysis, e.g., Monte Carlo simulation, is an absolute necessity for simulated results with TOUGH2.

1.4.5 Summary

The HST3D model (Kipp, 1997) and the PHREEQC model (Parkhurst and Appelo, 1999) with the newly developed surface complexation model will be assembled with some necessary and effective improvements specifically for the YM groundwater system. In the developed numerical system, the most efficient solution will be employed for the equilibrium speciation with the kinetic reaction and transport. Due to the flexible function of PHREEQC, the system can simulate different reaction processes such as adsorption/desorption, ion exchange and precipitation/dissolution. So the transport of radioactive solutes will be modeled and compared closely to the groundwater environment with a full use of the above experimental results and the numerical system.

From previous studies, it is obvious that more complicated models have been conceptualized and developed with the enhanced understanding of geochemical behaviors of REEs and other trace elements in the groundwater flow. More models can take all accounts of heat, solute, and flow transport by coupling three sets of partial differential equations of groundwater flow, heat transport, and solute transport. Dimension levels of numerical models are increased from one- or two-dimensions to three-dimensions for the requirement of complex geometric study domains. The crucial

problem is how to describe reaction terms in the solute transport equation, a key to simulation capacities of models. Chemical behavior of a reactive solute is involved with adsorption/desorption reaction, redox reaction and/or radioactive decay along groundwater flow paths. However, only the adsorption/desorption reaction is generally taken into account as the source/sink term by using a constant distribution coefficient. Meanwhile, the other reactions are simply neglected which might play important roles in the transport process.

This dissertation is composed of an introduction, three manuscripts including leaching of tracer elements, adsorption of rare earth elements, solute transport of groundwater system in YM area, followed by a general conclusion section.

1.5 References

Belcher, W.R., (editor) 2004. Death Valley regional ground-water flow system, Nevada and California -- hydrogeologic framework and transient ground-water flow model, WRI 2004-5205. U. S. Geological Survey, Denver, Colorado, 408 pp.

Birdsell, K., Soil, W., Rosenberg, N., and Robinson, B., 1995. Numerical modeling of unsaturated groundwater flow and radionuclide transport at MDAG. LA-UR-95-2735, Los Alamos National Laboratory, NM

Borrok, M.D., and Fein, B.J., 2005. The impact of ionic strength on the adsorption of protons, Pb, Cd, and Sr onto the surfaces of Gram negative bacteria: testing non-electrostatic, diffuse, and triple-layer models. Journal of Colloid and Interface Science. 286, p. 110–126.

Browning, L., Murphy, M.W., Manepally, C., and Fedors, R., 2003, Reactive transport model for the ambient unsaturated hydrogeochemical system at Yucca Mountain,

Nevada. Computer & Geosciences. 29, p. 247-263.

Cederberg, G.A., Street, R.L., and Leckie, J.O., 1985, A groundwater mass transport and equilibrium chemistry model for multicomponent systems. Water Resources Research 21, p. 1095-1104.

Choppin, G.R., 1983. Comparison of the solution chemistry of the actinides and lanthanides. Journal of the Less-Common Metals. 93, p. 323-330.

Curtis, P.G., 2005. Documentation and applications of the reactive geochemical transport model RATEQ. NUREG/CR-6871, U. S. Geological Survey, Menlo Park, California, 111 pp.

Damaskin, B.B., Perchenko, O.A., and Karpov, S.I., 1986. Description of ionic adsorption in terms of the model of two parallel capacitors with common diffuse layer and underlying virial adsorption isotherm. Soviet Electrochemistry (English Translation of Elektro-Khimiia). 22, p. 405-409.

D' Agnese, Faunt, C.C, Turner, A.K., and Hill, M.C., 1997. Hydrogeologic evaluation and numerical simulation of the Death Valley regional ground-water flow system, Nevada and California. Water-Resources Investigations - U. S. Geological Survey, Report: WRI 96-4300, p. 72-77.

Daniels, W.R., Wolfsberg, K., Rundberg, R.S., Ogard, A.E., Kerrisk, J.F., Duffy, C.J., and Newton, T., 1982. Summary report on the geochemistry of Yucca Mountain and environs. Los Alamos, N.M.: Los Alamos National Laboratory.

Dia, A., Grua, G., Olivie-Lauquet, G., Riou, C., Molenat, J., and Curmi, P., 2000. The distribution of rare earth elements in groundwaters: Assessing the role of source-rock composition, redox changes, and colloidal particles. Geochimica et

Cosmochimica Acta, 64, p. 4131-4152.

Domenico, P.A., and Robbins, G.A., 1984. A dispersion scale effect in model calibrations and field tracer experiments. Journal of Hydrology, 70, p. 123-132.

Domenico, P.A., and Schwartz, F.W., 1998. Physical and chemical hydrogeology. 2nd edition, John Wiley and Sons (New York), p. 506.

Falta, R.W., Pruess, K., Finsterle, S., and Battistelli, A., 1995. T2VOC User's Guide. Report LBL-36400, Lawrence Berkeley Laboratory, Berkeley, California, pp. 158.

Fenelon, M.J., and Moreo, T.M., 2002. Trend analysis of ground-water levels and spring discharge in the Yucca Mountain region, Nevada and California, 1960–2000. WRIR- 02-4178, U.S. Geological survey, Denver, Colorado, p. 5-7.

Finsterle, S., 1999. iTOUGH2 User's Guide. Report LBNL-40040, Lawrence Berkeley National Laboratory, Berkeley, California, 137 pp.

Goldberg, S., Criscenti, J.L., Turner, R.D., Davis, A.J., and Cantrell, J.K., 2007. Adsorption –desorption processes in subsurface reactive transport modeling. Vadose Zone Journal, 6, p. 407–435.

Goldberg, S., 1985. Chemical modeling of anion competition on goethite using the constant capacitance model. Soil Science Society of America Journal. 49, p 851-856.

Goldberg, S., 1999. Reanalysis of boron adsorption on soils and soil minerals using the constant capacitance model. Soil Science Society of America Journal, 63, p 823-829.

Goldberg, S., Suarez, L.D., Basta, T.N., and Lesch, M.S., 2004. Predicting boron adsorption isotherms by midwestern soils using the constant capacitance model. Soil Science Society of America Journal, 68, p. 795–801.

Goldberg, S., Lesch, M.S., Suarez, L.D., and Basta, T.N., 2005. Predicting arsenate adsorption by soils using soil chemical parameters in the constant capacitance model. Soil Science Society of America Journal, 69, p. 1389–1398.

Grasso, D.N., 1996. Hydrology of modern and late Holocene lakes, Death Valley, California. Water-Resources Investigations Report 95-4237, U.S. Geological Survey, Denver, Colorado.

He, M.L., Zelazny, L.W., Baligar, V.C., Ritchey, K.D., and Martens, D.C., 1997. Ionic strength effects on sulfate and phosphate adsorption on γ-alumina and kaolinite: triple-layer model. Soil Science Society of America Journal, 61, p. 784-793.

Hwang, S.Y., and Lenhart, J.J., 2008. The dependence of hematite site-occupancy standard state triple-layer model parameters on inner-layer capacitance. Journal of Colloid and Interface Science, 319, p. 206–213.

Johannesson, H.K., Lyons, W.B., and Bird, A.D., 1994. Rare erath element concentrations and speciation in alkine lakes from the western U.S.A. Geophysical Research Letters, 21, p. 773-776.

Johannesson, H.K., Stetzenbach, J.K., and Hodge, F.H., 1995. Speciation of the rare earth element neodymium in groundwaters of the Nevada Test Site and Yucca Mountain and implications for actinide solubility. Applied Geochemistr, 10, p. 565-572.

Johannesson, H.K., Stetzenbach, J.K., Hodge, F.H., Kreamer, K.D., and Zhou, X., 1997. Delieaton of groundwater flow systems in the southern Great Basin using aqueous

rare earth element distribution. Ground Water, 35, p. 807-819.

Johnson, M.S., Copplestone, D., Fox, W.M., and Jones, S.R., 2001. Annual cycle of radionuclide contamination on tide-washed pasture in the Mersey Estuary, NW England. Estuaries, 24, p. 198-203.

Kallvenius, G., and Ekberg, C., 2002, TACK-a program coupling chemical kinetics with a two-dimensional transport model in geochemical systems. Computers & Geosciences. 29, p. 511-521.

Kipp, L.K., 1997. Guide to the Revised Heat and Solute Transport Simulator: HST3D -- Version 2. Water-Resources Investigations Report 97-4157, U.S. Geological Survey, Denver, Colorado, 149 pp.

Kohler, M., Curtis, G.P., Kent, D.B., and Davis, J.A., 1996. Experimental investigation and modeling of uranium (VI) transport under variable chemical conditions. Water Resources Research, 32, p. 3539-3551.

Kosmulski, M., 1996. Adsorption of cadmium on alumina and silica: analysis of the values of stability constants of surface complexes calculated for different parameters of triple layer model. Colloids and Surfaces: SURFACES. 117, p. 201-214.

Lichtner, P.C., 1996, Continuum formulation of multicomponent-multiphase reactive transport. in: P. C. Lichtner, C. I. Steefel, and E. H. Oellkers (eds.) Reactive transport in porous media. 34. Mineralological Society American, Washington, DC, p. 1-81.

Liu, C.W., and Narasimhan, T.N., 1989. Redox-controlled multiple-species reactive transport, 1. Model development. Water Resources Research, 25, p. 883-910.

Luckey, R.R., Tucci, P., Faunt, C.C., Ervin, E.M., Steinkampf, W.C., Dognese, F.A., and

Patterson, G.L., 1996. Status of Understanding of the Saturated-Zone Ground-Water Flow System at Yucca Mountain, Nevada, as of 1995. Water-Resources Investigations Report 96-4077, Denver, Colorado: U.S. Geological Survey. ACC: MOL.19970513.0209.

Lu¨tzenkirchen, J., 1999. Parameter estimation for the constant capacitance surface complexation model: analysis of parameter interdependencies. Journal of Colloid and Interface Science, 210, p 384–390.

Mangold, D.C., and Tsang, C.F., 1991. A summary of subsurface hydrological and hydrochemical models. Reviews of Geophysics, 29, p. 51-79.

McPhee, J, and Yeh, W.G., 2003. Groundwater quality modeling and management under uncertainty; proceedings. Symposium on Groundwater quality modeling and management under uncertainty, Philadelphia, PA, United States.

Moller, P., Dulski, P., Bau, M., Knappe, A., Pkedeger, A., and Sommer-von Jarmersted, C., 2000. Anthropogenic gadolinium as a conservative tracers in hydrology. Journal of Geochemical Exploration, 69-70, p. 409-414.

Montas, J.H., 2003. An analytical solution of the three-component transport equation with application to third-order transport. Water Resources Research, 39, p. 1036.

Montazer, P., and Wilson, W.E., 1984. Conceptual hydrologic model of flow in the unsaturated zone, Yucca Mountain, Nevada, Water Resources Investigations Report 84-4355, USGS, Denver, Colorado.

Monte, L., 2002. A general methodology for structuring models to predict the long-term migration of radionuclides from catchments. Journal of Environmental Radioactivity, 59, p. 153-168.

Motta, M.M., and Miranda, C.F., 1989. Molybdate adsorption on kaolinite, montmorillonite, and illite: Constant capacitance modeling. Soil Science Society of America Journal, 53, p. 380-385.

Nelson, N.T., Hu, Q., and Brusseau, M.L., 2003, Characterizing the contribution of diffusive mass transfer to solute transport in sedimentary aquifer systems at laboratory and filed scales. Journal of Hydrology, 276, p. 275-286.

Pang, L., and Close, M., 2003. A field study of nonequilibrium and facilitated transport of Cd in an alluvial gravel aquifer. Ground Water, 37, p. 785-792.

Parkhurst, D.L., and Appelo, C.A.J., 1999. Users guide to PHREEQC: A computer model for speciation, reaction path, advective transport, and inverse geochemical calculations. WRIR/99-4259, U. S. Geologic Survey, Denver, Colorado, 326 pp.

Patrick, T., 2003, Saturated-zone hydrology at Yucca Mountain. Geological Society of America Abstracts with Programs. 35, p. 435.

Pawloski, G.A., Tompson, A.F.B., Carle, S.F., Bourcier, W.L., Bruton, C.J., Daniels, J.I., Maxwell, R.M., Shumaker, D.E., Smith, D.K., and Zavarin, M., 2001. Evaluation of the hydrologic source term from underground nuclear tests on pahute mesa at the nevada test site: the CHESHIRE Test. W-7405-ENG-48, US Department of Energy.

Phan, T.N.T., Louvard, N., Bachiri, A.S., Persello, J., and Foissy, A., 2004. Modeling Competitive Adsorption of Molybdate, Sulfate, Adsorption of zinc on colloidal silica, triple layer modelization and aggregation data. Colloids and Surfaces A: Physicochemical and Engineering Aspects, 244, p. 131–140.

Pohlmann, K., Chapman, J., Hassan, A., and Papelis, L., 1999. Evaluation of Groundwater

Flow and Transport at the Faultless Underground Nuclear Test Area. DRI Publication 45165, DRI, Las Vegas, Nevada, 245 pp.

Pope, A.G., Sepehrnoori, K., Sharma, M.M., McKinney, C.D., Speitel, E.G., and Jackson, E.R., 1999. Three-dimensional napl fate and transport model. EPA/600/R-99/011, Center for Petroleum and Geosystems Engineering, The University of Texas at Austin, Austin, Texas, 361 pp.

Prikryl, D.J., Jain, A., Turner, R.D., and Pabalan, T.R., 2001. UraniumVI sorption behavior on silicate mineral mixtures. Journal of Contaminant Hydrology, 47, p. 241–253.

Prudic, E.D., Harrill, J.R., and Burbey, T.J., 1995. Conceptual evaluation of regional ground-water flow in the carbonate-rock province of the Great Basin, Nevada, Utah, and adjacent states. Professional Paper 1409–D, U.S. Geological Survey, Denver, Colorado, 102 pp.

Prudic, E.D., 2003. Development of numerical models to assess ground-water flow patterns in the great basin of Southern Nevada. Geological Society of America Abstracts with Programs, 35, p. 616

Pruess, K., 1991. TOUGH2: A general numerical simulator for multiphase fluid and heat flow. LBL-29400, Lawrence Berkeley Laboratory, Berkeley, California, 210 pp.

Pruess, K., and Battistelli, A., 2002. TMVOC, A numerical simulator for three-phase non-isothermal flows of multicomponent hydrocarbon mixtures in saturated-unsaturated heterogeneous media. LBNL-49375, Lawrence Berkeley National Laboratory, Berkeley, California, and Aquater S.p.A., San Lorenzo in Campo (PU), Italy, 204 pp.

Scott, B.R., 1990. Structural geology of Yucca Mountain. Proceedings of the topical meeting on Nuclear waste isolation in the unsaturated zone, Focus '89. American Nuclear Society, La Grange Park, IL, United States .

Shagalova, E., Zhukova, O., Germenchuk, M., Matveenko, I., and Bakarikova, Z., 2000. Dynamics of radiation situation on the territory of Belarus and migration of radionuclides in different types of soils after Chernobyl catastrophe. Journal of Radioanalytical and Nuclear Chemistry, 246. p. 521-525

Šimůnek, J., Suarez, L.D., and Šejna, M., 1996. The UNSATCHEM software package for simulating one-dimensional variably saturated water flow, heat transport, carbon dioxide production and transport, and multicomponent solute transport with major ion equilibrium and kinetic chemistry (Version 2.0). Research Report No. 141, U.S. Salinity Laboratory, USDA, Riverside, California, 186 p.

Smith, S.L., and Jaffe, P.R., 1998, Modeling the transport and reaction of trace metals in water-saturated soils and sediments. Water Resources Research, 34, p. 3135-3147.

Steefel, C.I., and Yabusaki, S.B., 1996. OS3D/GIMRT, Software for multicomponent-multidimensional reactive transport: User's Manual and Programmer's Guide. PNL-11166, Pacific Northwest National Laboratory, Richland, Washington, 63 p.

Thomasson, J.M., and Wierenga, J.P., 2003. Spatial variability of the effective retardation factor in an unsaturated field soil. Journal of Hydrology, 272, p. 213–225.

Thompson, L.C., 1979. Complexes. In handbook on the physics and chemistry of rare earths, editor Gschneider, K.A., and Eyring, L., Elsevire, pp. 209-295.

Tonkin, W.J., Balistrieri, S.L., Murray, W.J., 2004. Modeling sorption of divalent metal cations on hydrous manganese oxide using the diffuse double layer model. Applied Geochemistry. 19, p. 29–53.

USDOE, 1997. Regional groundwater flow and tritium transport modeling and risk assessment of the Underground Test Area, Nevada Test Site, Nevada. Report DOE/NV–477, U.S. Department of Energy, DOE Nevada Operations Office Las Vegas, Nevada, 396 pp.

USDOE, 2001. Yucca Mountain Science and Engineering Report: Technical Information Supporting Site Recommendation Consideration. DOE/RW-0539, U.S. DOE Office of Civilian Radioactive Waste Management, 46 pp.

Waddell, R.W., 1982. Two-dimensional, steady-state model of ground-water flow, Nevada Test Site and vicinity, Nevada-California. USGS-WRI-82-4085, U.S. Geological Survey, Denver, Colorado, 77 pp.

Waite, D.T., Davis, A.J., Payne, E.T., Waychunas, G.A., and Xu, N., 1994. Uranium(VI) adsorption to ferrihydrite: Application of a surface complexation model. Geochimica et Cosmochimica Acta., 58, p. 5465-5478

Westall, J., 1987. Adsorption mechanisms in aquatic chemistry. Aquatic Surface Chemistry, editor Stumm, W., John Wile & Sons, New York, p. 3-32.

Winograd, T.J., and Thordarson, W., 1975. Hydrogeologic and hydrochemical framework, south central Great Basin, Nevada-California, with special reference to the Nevada Test Site: U. S. Geological Survey, Professional Paper 712-C, p. 126.

Wolfsberg, A., Glascoe, L., Lu, G., Olson, A., Lichtner, P., McGraw, M., Cherry, T., and Roemer, G., 2002. Tybo / Benham: Model analysis of groundwater flow and

radionuclide migration from underground nuclear tests in southwestern Pahute Mesa, Nevada. LA-13977, Los Alamos National Laboratory, NM, 490 pp.

Wu, C.H., Lo, S.L., Lin, C.F., and Kuoy, C.Y., 2001. Modeling Competitive Adsorption of Molybdate, Sulfate, and Selenate on γ-Al_2O_3 by the Triple-Layer Model. Journal of Colloid and Interface Science, 233, p. 259–264.

Wunderly, M.D., Blowes, D.W., Frind, E.O., and Ptacek, C.J., 1996. Sulfide mineral oxidation and subsequent reactive transport of oxidation products in mine tailings impoundments: A numerical model. Water Resources Research, 32, p. 3173-3187.

Xu, T., and Pruess, K., 2001. Modeling multiphase non-isothermal fluid flow and reactive geochemical transport in variably saturated fractured rocks: 1. Methodology. American Journal of Science, 301, p. 16-33.

Yeh, G.T., and Tripathi, V.S., 1990. A critical evaluation of recent developments in hydrochemical transport models of reactive multichemical components. Water Resources Research, 32, p. 3173-3187.

Yeh, G.T., and Tripathi, V.S., 1991. HYDROGEOCHEM: A coupled model of hydrological and geochemical equilibrium of multicomponent systems. Oak Ridge National Lab., Rep. ORNL-5522, Oak Ridge, TN, p. 312.

Zhang, H., and Schwartz, F.W., 2000. Simulating the in situ oxidative treatment pf chlorinated ethylenes by potassium permanganate. Water Resources Research, 36, p. 3031-3042.

Zhang, Z.Z., Sparks, L.D., and Scrivner, C.N., 1994. Characterization and modeling of the Al-Oxide/Aqueous solution interface. Journal of Colloid and Interface Science, 162, p. 244-251.

Zhu, C., 2002. Estimate of recharge from radiocarbon dating of groundwater and numerical flow and transport modeling. Water Resources Research, 36, p. 2607-2620.

Zyvoloski, A.G., Robinson, A.B., Dash, V.Z., Trease, L.L., 1997. User's Manual for the FEHM Application-A Finite-Element Heat- and Mass-Transfer Code. OSTI ID 14902, Los Alamos National Laboratory, Los Alamos, NM, 155 pp.

CHAPTER 2

WATER-ROCK INTERACTIONS OF TRACE ELEMENTS IN THREE DIFFERENT AQUIFERS: LABORATORY LEACHING EXPERIMENTS AND NUMERICAL MODELING

Measurements of trace elements leached from host rocks can indicate the source of flowing groundwater and provide the host rock's fingerprint, information which may be useful in the transport modeling and remediation of groundwater systems. In this study, the leaching characteristics of three widely-distributed aquifer host rocks in southern Nevada were investigated through leaching experiments of thirteen trace elements under different experimental conditions (leaching time, pH, grain size, and rock mineralogy). Experimental analysis indicated that leaching time, pH, and grain size all have significant impacts on the leaching of trace elements. The effect of host rock mineralogy on leachate composition also provides useful clues about groundwater sources. Solute speciation and saturation indices were simulated using geochemical modeling to further explore the redistribution and leaching process of trace elements. Based on experimentally derived leaching fractions, a simple conceptual model was developed to consider the leaching of trace elements from host rocks into the groundwater. As a practical application, the conceptual leaching model was linked with a transport model of uranium (U) along the groundwater flow path from the Spring Mountains (recharge zone) to Amargosa Desert (discharge zone) in southern Nevada. In this way, additional U from rainfall-induced direct recharge from the Spring Mountains could be considered in the transport modeling. The significance of this research lies in the quantification of the fraction of leached trace elements from different aquifer host rocks and the provision of fundamental datasets for

transport modeling in this region.

2.1 Introduction

Low precipitation, extensive evaporation, and sparse population make arid Southern Nevada a favored site for the storage of nuclear waste. Consequently, Yucca Mountain (YM) has been selected as the first future high-level nuclear waste repository. In addition, hundreds of nuclear tests have been conducted underground at the nearby Nevada Test Site (NTS), the largest outdoor national experimental laboratory since 1961. The NTS and YM have been of great concern to hydrogeologists and geochemists in water-limited Nevada, where the contamination of groundwater is inevitably a crucial environmental issue. The key to the protection of groundwater in this region is to detect contaminant movement and change in groundwater flow (CRTD, 2002). However, the heterogeneity of arid soils and the complexity of geochemical interaction between water and rock limit our understanding of the actual processes of groundwater movement and contaminant transport (Yu and Hu, 2003).

Trace elements are regarded as informative fingerprints of groundwater and host rocks. Studies on trace elements at the aquifer rock/water interface can provide very valuable information on the source and evolution process of groundwater. Previous studies on the leaching of trace elements under different conditions have been conducted in many different study areas (Wagner and Hlatshwayo, 2005; Sohlenius and O¨ born, 2004; Al-Masri et al., 2004; Gaskova et al., 2003; and Quejido et al., 2005). Contamination by arsenic (As) and uranium (U) is a hot issue prompting many studies, while various kinds of slags, tails, and coals are the most commonly studied host materials. Gaskova et al. (2003) conducted laboratory-based experiments to study the

leaching of As-containing tailings with different solutions and water/rock ratios, and over different leaching times. The results showed that, in alkaline environments, As is more easily leached from the particle surfaces than other trace elements (Co, Ni, Fe). Host rock is an important factor in that it provides the source and habitation for the leaching of trace elements. Wagner and Hlatshwayo (2005) determined the concentrations of fourteen trace elements in the Highveld coals by digestion and compared them with those of the reference material. The measured concentrations were generally lower than the global level for coals, except in the enriched siderophile elements. In order to obtain more systematic and general information about leaching, researchers have expanded studies to include additional trace elements, resulting in a wider spectrum of those that are studied. Al-Masri et al. (2004) calculated the leaching factors, which quantify the fraction leached from host rocks, for trace elements in Syrian phosphogypsum. Their results suggest that trace elements can either be adsorbed on the surface of gypsum, occur inside the gypsum lattice, associate with organic materials or dissolve in acids.

It is worth mentioning that further investigations of the mineralogical properties of host rocks have better explained the leaching mechanism of trace elements. Microscopic and spectroscopic techniques are now frequently used in the study of water and rock particle interactions. Scanning electron microscopy (SEM), X-ray diffraction (XRD) and X-ray fluorescence spectroscopy (XRF) are commonly used. Sohlenius and O¨ born (2004) studied the leaching and partitioning behaviors of some trace elements in oxidized and non-oxidized sulphidic sediments using XRF. Quejido et al. (2005) used sequential leaching methods to investigate the mineralogical distribution of some trace elements, including U, Ce, and La-Nd. In their research, XRF and scanning electron (SE) images

were applied to the Fe (III)-U (VI) fracture filling materials from the "Mina Fe" U deposit to explore the mechanisms of leaching. While microscopic and spectroscopic analytical techniques allow for the discovery of leaching phenomena beyond certain detection thresholds, geochemical modeling based on the principles of geochemistry are used to interpret the experimental results. Geochemical modeling may include solute speciation, saturation calculation, and surface complexation. Parsons et al. (2000) investigated the mineralogy of base-metal slags with the aid of backscattered scanning electron (BSE) and secondary electron images. Geochemical simulation results with the EQ 6 model showed that the equilibrium solubilities of secondary minerals control the aqueous concentrations of Al, Ba, Cu, Fe, Si, and SO_4. Piatak et al. (2004) studied the mineralogy of three slags at different sample sites through the analysis of BSE images and calculation of speciation and saturation. Silicates, sulfide, and secondary minerals were shown to influence the leaching process of slags. Lee et al. (2005) studied the leaching behavior of As and other trace elements from waste rock and contaminated soil. Integrating X-ray analyses, speciation, and saturation calculations, they found that Fe-hydroxides, Fe (Mn)-hydroxides and Fe-sulfates, appearing as secondary minerals, adsorbed the dissolved metals.

Meanwhile, other researchers have investigated trace elements in groundwater to trace back its possible sources or evolution processes. Edet et al. (2003) collected and analyzed 43 groundwater samples from 33 aquifer monitoring wells. With factor analysis and statistical methods, four types of groundwater and two groups of trace elements were found in the samples. Their research suggested that the trace elements arise from a process that is geogenic rather than anthropogenic (e.g., tidal flushing). Farnham et al.

(2003) used principal component analysis (PCA), Q-mode factor analysis, and correspondence analysis to study the trace elements in groundwater samples collected from YM. These statistical studies showed enhanced levels of trace elements in groundwater flowing through different aquifer rock types (volcanic or carbonate) and in groundwater at different oxidizing/reducing stages.

Most of these previous studies, however, were focused on the assessment of specific contaminated sites for remediation rather than the simulation of contaminant transport in the regional groundwater. Published studies on the leaching of trace elements from natural regional aquifer assemblages, instead of from synthetic host material are scarce. Such studies would enhance our understanding of the source, movement, and transport of regional groundwater.

The objectives of this study were: (1) to characterize trace elements in leachates from different aquifer host rocks in southern Nevada through leaching experiments; (2) to document and assess the influences of grain size, pH, and leaching time, in addition to rock mineralogy on leachate composition; (3) to explore water/rock interaction in the leaching process with geochemical modeling; and (4) to provide preliminary datasets for quantifying the fraction of trace elements leached from aquifer host rocks; (5) to test advantages of using the experimentally derived fraction in the transport modeling.

In this study, the bulk concentrations of trace elements in host rocks were measured and leaching fractions were calculated. Experimental analysis was used to distinguish the effects of the host rock, grain size, pH value, and leaching time. An interactive geochemical model, PHREEQC 2.8 (Parkhurst, 1995), was used to calculate the speciation states and saturation indices to further explore the interaction between host

rocks and leachates. PHREEQC 2.8 was also used to simulate one-dimensional solute transport in the application case study.

2.2 Materials and Methods

2.2.1 Study Area

Southern Nevada with a desert climate is part of the central Basin and Range Province (Figure 2.1). Regional elevation varies from about 80 m below sea level in Badwater, in California, to 3,600 m above sea level at the top of Peak Charleston. The mountain ranges separating the basins are generally above 1,500 m (Scott, 1990). Twenty five percent of the area is uplands and 75 percent is intermountain basin filled with alluvium and lower volcanic deposits (Grasso, 1996). The precipitation distribution varies widely dominated by altitude, with the mean value ranging from more than 700 mm/yr in The Spring Mountains to only 50 mm/yr in Death Valley. Average annual lake-evaporation varies spatially from 1,100 mm in the north to 2,000 mm in Death Valley (D' Agnese et al., 1997).

Many previous studies have indicated that hydrostratigraphic units usually have geohydrologic impacts on the groundwater movement and geochemistry. Although there is a wide spatial variation of hydrostatigraphic units within or close to the NTS, aquifer rocks in the vertical direction primarily consist of Quaternary surficial deposits, Tertiary felsic volcanic aquifer, and Paleozoic limestone or dolomite (Winograd and Thordarson, 1975). Paleozoic limestone and dolomite are transmissive because they can dissolve in groundwater. However, the hydrogeologic characteristics of the Tertiary volcanic rocks are unpredictable due to the complex effects of volcanic eruption, cooling, and secondary alteration (Laczniak et al., 1996). These three kinds of aquifer rocks were collected from

exposures in southern Nevada and used for leaching experiments in this study.

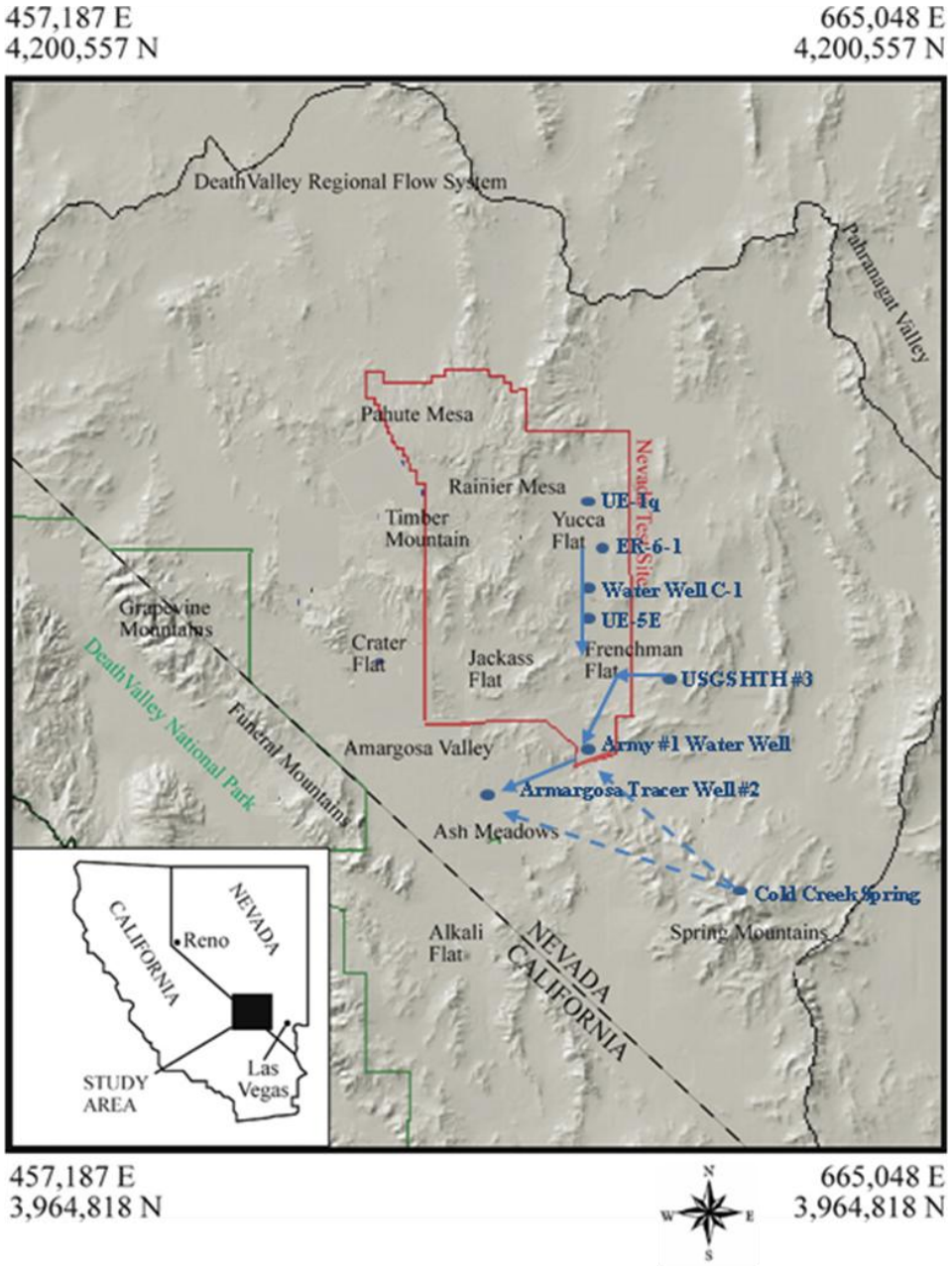

Figure 2.1 Study area showing locations of wells used in flow path analysis and the possible recharge flow paths from the eastern area and from the Spring Mountains (from Koonce et al., 2006 and Hershey and Acheampong, 1997). Please note blue ellipse representing monitoring well; blue solid line representing flow path; and blue dashed line representing possible flow path.

2.2.2 Sample Collection and Rock Sample Analysis

The Cambrian Bonanza King Formation (dolomite) and the Permian Toroweap Formation (limestone) samples were collected at Frenchman Mountain and the Tertiary Surprise Formation (volcanic rocks) samples were collected at the NTS. These sample sites are stratigraphically and lithologically related to the aquifer rocks in the vicinity of NTS and YM (Zhou, 2004). Selecting representative hydrostratigraphic units of aquifer rocks allowed us to evaluate the leaching process in the natural environment of Southern Nevada. Raw rock samples were selected in the field to ensure absence of weathering rinds, calcite veins, or obvious signs of possible alteration.

Samples were rinsed with distilled water and dried in air to measure accurate weights. After being crushed into powder, 0.25 g of each rock sample was placed into clean Teflon digestion bombs. Five mL of ultrapure HF (Seastar, double sub-boiling, distilled in Teflon®) and 5 mL of ultrapure HNO_3 (Seastar, double sub-boiling, distilled in quartz) were then added. After being sealed and placed in a microwave oven (CEM Corporation MDS-2100), the digestion bombs were heated to 189 °C and pressurized to 8.62×10^5 Pa (8.5 atm) for 25 minutes. The closed Teflon bombs were cooled naturally, after which 30 mL of a saturated boric acid solution were added into each bomb. Each sample was subsequently heated again in the microwave at 100 °C and 6.9×10^4 Pa to 1.38×10^5 Pa (0.68 to 1.36 atm) for 5 minutes. Finally, the dissolved rock samples were decanted into clean polyethylene bottles and diluted by a factor of 180 for the analysis with an inductively-coupled plasma mass spectrometer (ICP-MS, Perkin Elmer Elan 5000) (Zhou, 2004).

2.2.3 Leaching Experiments

Laboratory batch tests were conducted to study the leaching behavior and concentration of trace elements in low-temperature aqueous solutions. In the leaching experiments, the rock samples were crushed and fractioned into three groups whose grain sizes fell into either the #10 to #20 (841 μm to 2.0 mm), #20 to #45 (354 to 841 μm), or <#45 (<354 μm) U.S. standard sieve sizes. After adding 60 g of distilled water into each test tube to achieve a rock-water mass ratio of 1:3, the test tubes were placed on a rotator for three periods of 7, 30 and 90 days respectively. Sodium bicarbonate ($NaHCO_3$) and nitric acid (HNO_3) were used to adjust each solution's pH so that it fell into one of three designated ranges (acidic 3-4, neutral 7-8 and alkali 10-11). At the end of the test periods, the rock samples and leaching solutions were separated with a centrifuge and filtered with 0.45 μm Nuclepore® filters (Johannesson and Zhou, 1999). The concentrations of trace elements in leached solutions were obtained with ICP-MS (Perkin Elmer Elan 5000), based on subtracted concentrations in method blanks. An atomic absorption flame spectrometer (AA) was used for the analysis of the major cations, and an ion chromatograph (IC) for major anions (Zhou, 2004).

In sum, 81 experimental sets were obtained, indicating the effects of wide parameter variation, which included three pH ranges (acidic, neutral, and alkaline), three leaching times, three host rocks, and three particle sizes.

2.2.4 Mineralogy of Host Rocks

Based on preliminary examination, the Lower Cambrian Bonanza King Formation rocks are non-fossiliferous and light or dark gray dolomites. Approximately 80-90% of the unit is dolomite, 4-6% is chert, and the remaining few percent is other minerals. The

Permian Toroweap Formation is slightly fossiliferous, containing approximately 70% limestone, 20% dolomite, and small amounts of sandstone and mudstone. The Tertiary Surprise Formation is composed of rhyolitic volcanic rocks that consist of 60-70% of quartz and 20-30% of chert, limestone, and mudstone.

In order to quantify the fraction of trace elements leached from different rock types, the following equation was used:

$$x = \frac{\text{concentration of trace element leached into distilled water}}{\text{rock solid total surface} \times \text{mass ratio of water to rock solid}} \quad (2.1)$$

where the concentration of trace element leached into distilled water and mass ratio of water to rock solid are known parameters in the leaching experiments. Because the specific surface area of the individual size fractions was not measured, the surface area of each sample was estimated based on particle size, using the geometric mean of the corresponding size fraction cutoff. Thus, the leaching fraction (ppb/cm^2), x, can be calculated to reflect the amount of trace metal leached from the host rocks. The leaching fraction is influenced by pH, leaching time, grain size, and the nature of host rocks (including mineralogy and chemical composition).

2.3 Results and Discussion

2.3.1 Aquifer Rock Analysis

Each of three aquifer rocks showed a different bulk concentration of trace elements, as determined by ICP-MS rock analysis. Mn was the most abundant element in both the Bonanza King and Surprise formations, while Cr was the most abundant in the Toroweap Formation. For all the three rocks, Ti bulk concentration was the lowest. In order to evaluate the enrichment of trace elements in the aquifer host rocks, the measured bulk concentrations were normalized by concentrations in continental crust (Newsom, 1995).

The calculated crust-normalization distributions, shown in Figure 2.2, make it apparent that the enrichment of Toroweap Formation is between that of the other two formations. Bonanza King Formation is depleted in Mn, Cs, and Ti, relative to Surprise Formation. The different distributions of trace elements may reflect the different origins, crystallization process and metamorphic histories of the host rocks.

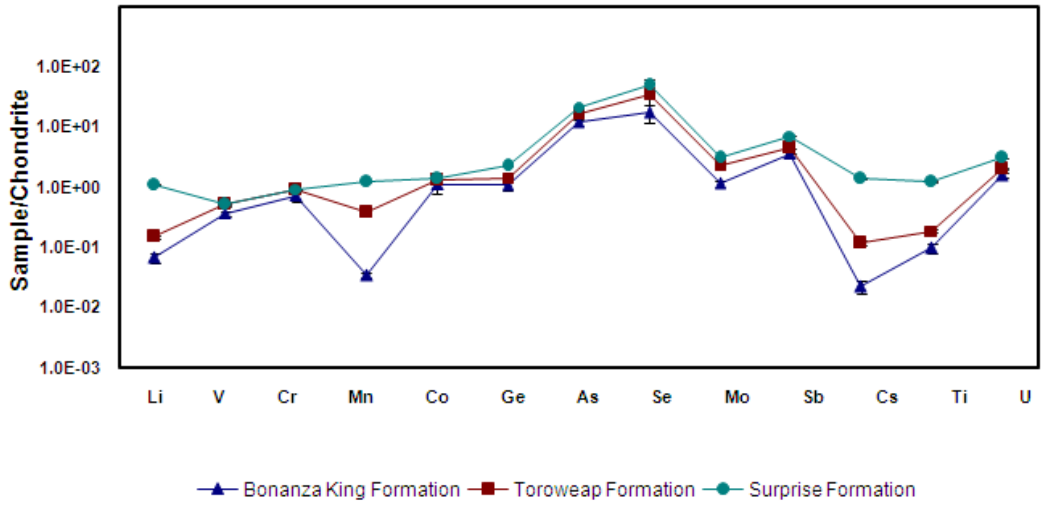

Figure 2.2 Crust-normalized trace element distributions for three host rock samples. The data shows the enrichments of the three host rocks are different for each trace element.

2.3.2 Leaching Results

The results of 81 experimental sets showed that a big difference exists in the leaching fraction of different elements. Mn, the most abundant element in the three rocks, had the largest calculated fractions at least over one order of magnitude than other trace elements. For the Bonanza King Formation, Toroweap Formation, and Surprise Formation, the second largest leaching fractions, respectively, are about 4.32×10^{-7}, 1.81×10^{-5}, and 5.73×10^{-4} ppb/cm^2 for Cr, and the minimums, respectively, are about 9.36×10^{-12},

9.76×10^{-9}, and 9.91×10^{-9} ppb/cm^2 for Cs. The reason that Mn is easily leached may be its high abundance in host rocks. Cu, Mn, and Fe are often found in secondary minerals due to antagonistic reactions, so secondary minerals in fractures might contribute too. The low leaching fraction of Cs results from its low abundance in the host rocks, relative to other elements. The leaching fraction of each trace element from the Bonanza King Formation was less than those from the other two rocks. For example, the measured Mn concentration was the largest in the Bonanza King rock too, but its calculated leaching fraction was significantly less by 2 or 3 orders of magnitude of that in the other two rocks.

Leaching fraction plots were used to analyze the effects of individual parameters (e.g., pH) on the leaching of trace elements, thus eliminating interfering effects of the other parameters (e.g., grain size and leaching time). Each plot represented the experimental sets dealing with each combination of a single parameter and rock type (Figures 2.3-2.5). Different rocks showed different trends in the variation of their leaching characteristics. Increased amounts of trace elements were released into aqueous solution from Bonanza King Formation and Toroweap Formation rocks with enhanced pH values; while Surprise Formation rocks were the opposite. As expected, fine grains tended to leach out more trace elements than coarse grains shown as Figure 2.6. Spikes in the leaching fraction trend, which were more significant in the Bonanza King Formation than in the Surprise Formation results, demonstrated the existence of selective leaching. This may have to do with variation in chemical composition, mineralogy, and content of trace elements in the different rock formations.

2.3.2.1 Leaching Time

Generally, the concentrations of leached trace elements increased continuously before a dynamic equilibrium between the leached solution and host rock was achieved. Figure 2.3 shows the pattern and range of variation in leaching fractions of trace elements from 354 -841 μm rock samples at pH 7-8 solution. The Surprise Formation and Toroweap Formation had the similar variation ranges. In general, the leaching fractions of trace elements at 7 days are lower than those at 90 days from same experimental conditions. According to the difference between leaching fractions at 7 and 90 days, some trace elements seemed to reach equilibrium sooner than others. The experimental results may indicate that leaching process reached equilibrium close after leaching for 90 days. The rates of leaching of most trace elements decreased as leaching time increased. However, due to the reversible dissolution/adsorption and unknown controls on the leaching, not all sample sets followed this pattern, as shown in Figure 2.3, especially except for Mo. Due to the limited experimental time, it was assumed that trace elements reached pseudo equilibrium after 90 days. Figure 2.4 shows that changing leaching times produced less than one order of magnitude variation in leaching fractions, with the exception of large variation of Mn released from the Toroweap Formation, respectively, after 7 days and 90 days.

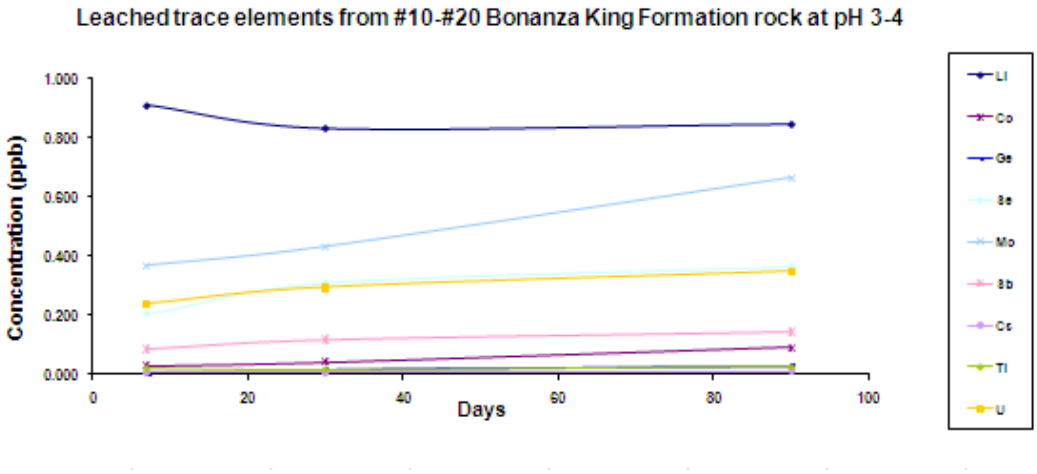

Figure 2.3 Concentration of each leached trace elements is a function of leaching time at 7 days, 30 days and 90 days, respectively. The concentrations of most leached trace elements obtain equilibrium with increasing time except Molybdenum (Mo).

2.3.2.2 pH Values

Figure 2.5 shows trace elements leached from the three different rock samples, with same grain size and leaching times but with the different pH ranges. The Toroweap Formation and the Bonanza King Formation showed similar decreased concentrations with increasing pH, whose decreased solubilities caused lower leaching fractions of most trace elements. The Surprise Formation instead showed increased concentrations with increasing pH because its solubility is negative proportional to pH values. In the alkaline condition, more trace elements dissolved into solution from Surprise Formation rocks.

(A)

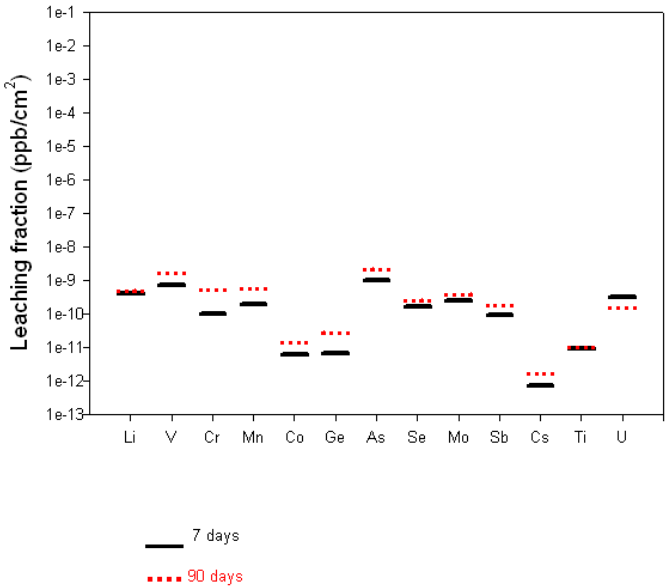

(B)

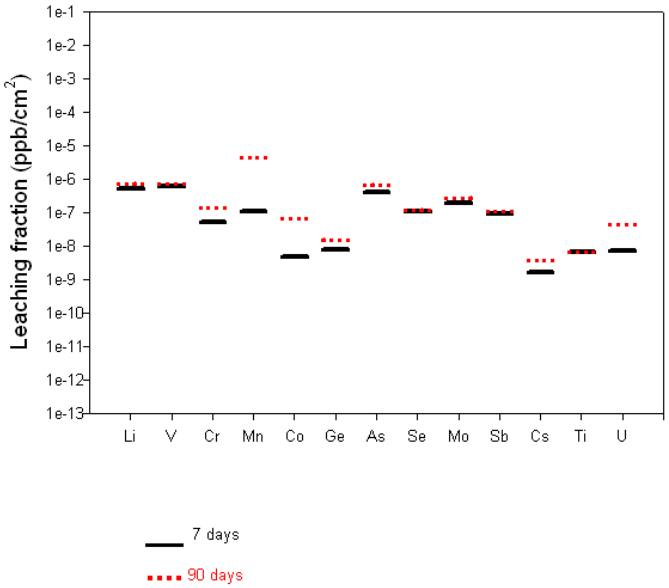

(C)

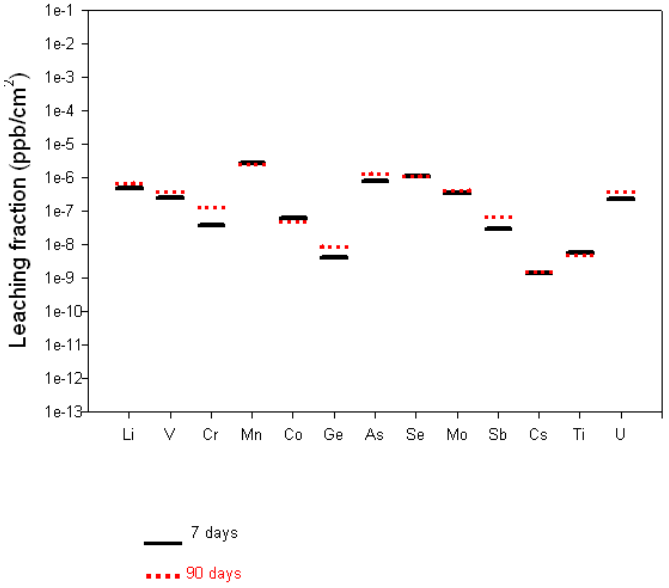

Figure 2.4 (A) Leaching fractions of trace elements from dolomite rock with gain size from 841 μm to 2.0 mm and at pH 7-8 by accumulating leaching time from 7 to 90 days. (B) Leaching fractions of trace elements from limestone rock with gain size from 841 μm to 2.0 mm and at pH 7-8 by accumulating leaching time from 7 to 90 days. (C) Leaching fractions of trace elements from volcanic rock with gain size from 841 μm to 2.0 mm and at pH 7-8 by accumulating leaching time from 7 to 90 days.

In general, the variation in leaching fractions of trace elements did not exceed one order of magnitude for Bonanza King Formation rocks. However, the other two formation rocks had a wider variation of leaching fractions from pH 3 to 4 to pH 10 to11. The special variation patterns provide some valuable information about the host rock sources of leachates. In Figure 2.5, different trace elements were influenced by pH change to different extents for all three types of rock samples. The most affected elements by pH were V, Cr, As and U in Toroweap Formation; and Li, Mn, Ge and U in the Surprise Formation. Bonanza King Formation had undergone less influence by pH possibly due to its less solubility and vulnerability to leaching. The alkalinity of the solution decreased the solubility of mineral phases contained in the dolomitic rocks. It can also be explained by that a different insoluble solute speciation was produced in a high pH solution. Based on the experimental results, a smaller amount of Ti and more of V dissolved, respectively, from the Toroweap Formation and from the Surprise Formation in acidic solution than in an alkaline solution. They both are exceptional cases which cannot be explained by change in mineral solubility with increasing pH. The reason is unknown, and measurement errors could play a role.

(A)

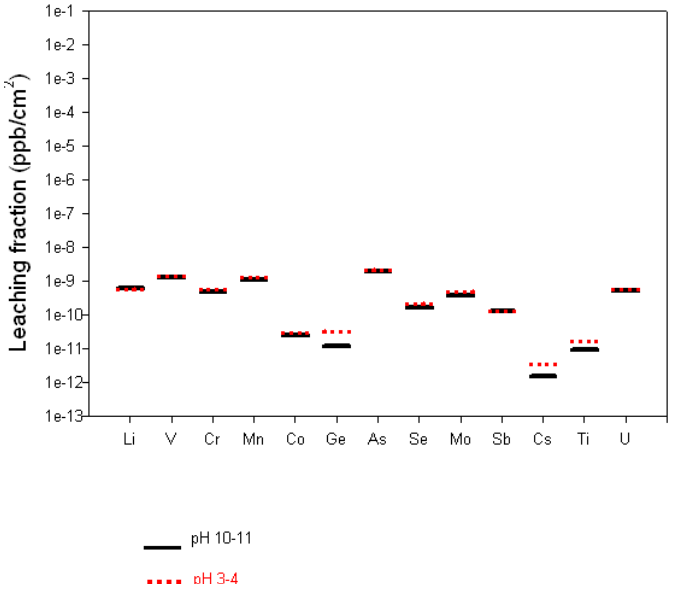

(B)

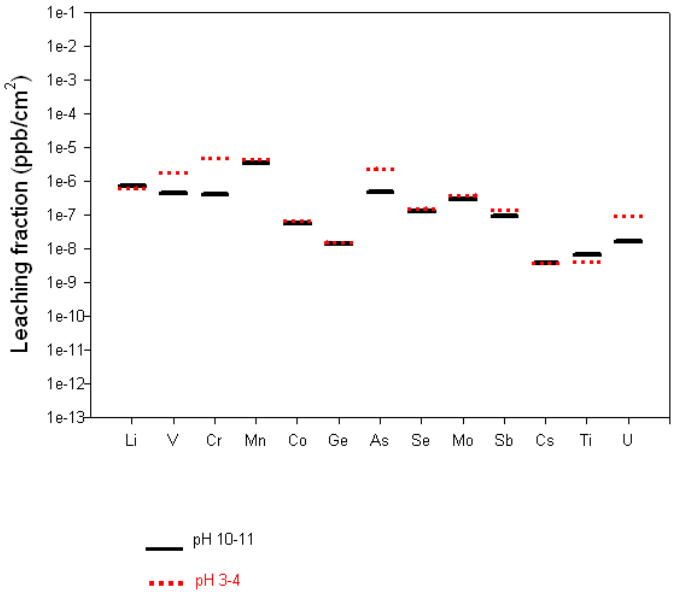

(C)

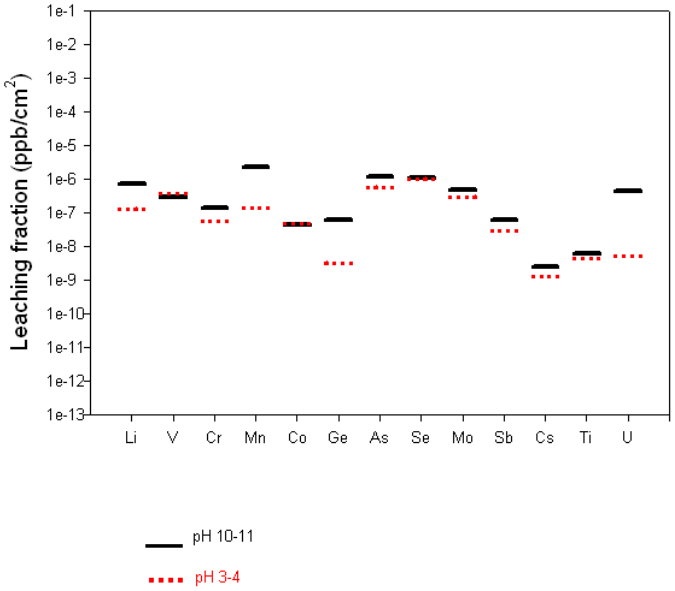

Figure 2.5 (A) Leaching fractions of trace elements from dolomite rock after 90 days of leaching under pH varying between 3-4, and 10-11 with gain size from 841 μm to 2.0 mm. (B) Leaching fractions of trace elements from limestone rock after 90 days of leaching under pH varying between 3-4, and 10-11 with gain size from 841 μm to 2.0 mm. (C) Leaching fractions of trace elements from volcanic rock after 90 days of leaching under pH varying between 3-4, and 10-11 with gain size from 841 μm to 2.0 mm.

2.3.2.3 Grain Size

Under the same experimental conditions, more absolute amounts of trace elements were released from fine grains than from coarse grains shown in Figure 2.6. This is reasonable, and may be explained by the increased particle surface area and interaction with the solution.

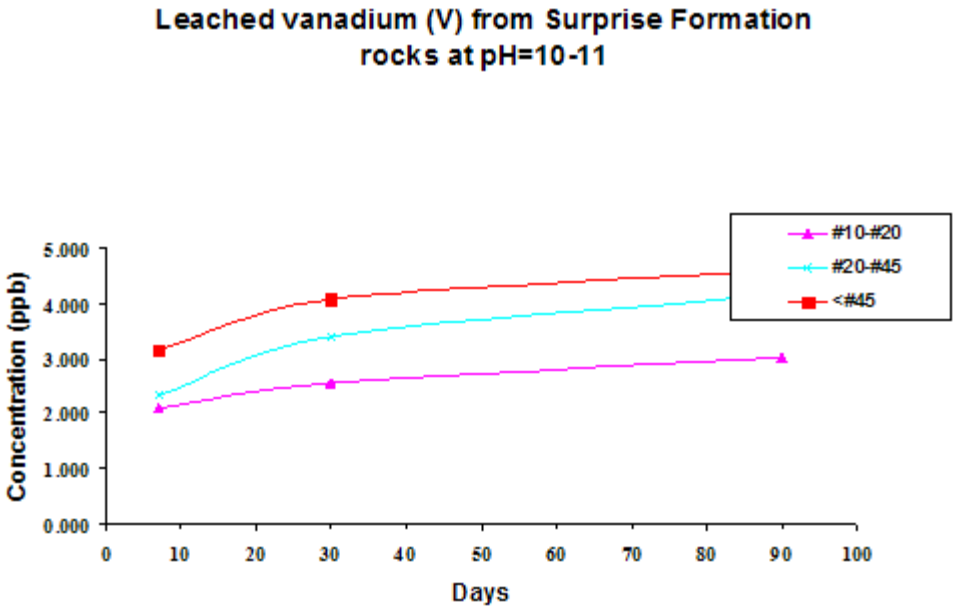

Figure 2.6 Leaching process of vanadium from volcanic rocks with different grain sizes including #10 to #20, #20 to #45, and less than #45 under pH 10-11 and 90 days of leaching showing the trend of progressively leached vanadium as grain size decreases

Figure 2.6 shows trace elements released from 1 g of different grain-sized rock samples at pH 10-11 and 90 days after leaching. Because the leaching fraction calculated in this study has already taken grain size into account by normalizing by the surface area of the particles, the leached trace elements (ppb/g) were supposed to be same in different grain-size samples with unit weight. This is true for the 13 investigated elements leached

from the two carbonate rocks (1 gram) except Mn and Cr. Relatively, volcanic rocks kept quite constant leaching behavior for 1g of different grain-sized samples. In other words, the constancy suggested that the influence of grain size on most trace elements is similar for all the three rock types, indicating that the most leached trace elements from fine grains are higher than those from coarse grains. This may be due to the fact that the fine-sized grains are allowed more continuous interaction with water, which results in more rapid attainment of equilibrium than coarse-sized grains. Judging from the scale of leaching fractions, it indicated that fewer quantities of trace elements were leached from the Bonanza King than from the other two rock formations.

The influences of pH value, grain size, and leaching time on the leaching of trace elements in real environments are complicated and overlapping. Different rock types showed different variations under the impacts of grain size, leaching time, and especially pH. The patterns and scales of variation in different rocks in response to changes in pH, grain size, and leaching time can provide some insights about their sources. These factors were considered to cause the leaching fractions to vary from 10^{-11} to 10^{-4} ppb/cm^2 for Toroweap Formation and Surprise Formation, but from 10^{-12} to 10^{-6} ppb/cm^2 for Bonanza King Formation (Figures 2.4, 2.5, and 2.7). Thus, it is apparent that different rock types show different leaching behavior, and the effect of rock type requires further study.

(A)

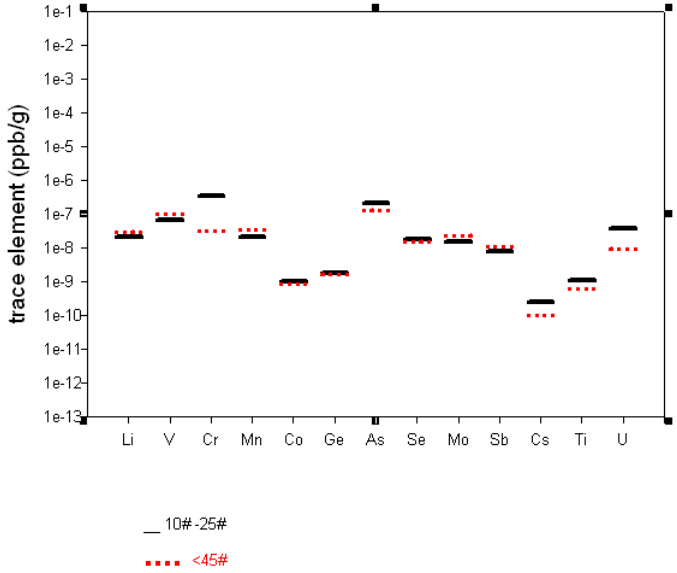

(B)

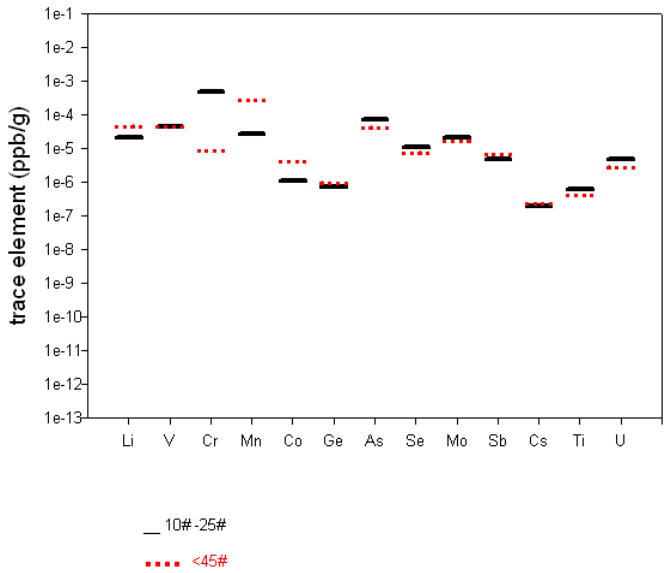

(C)

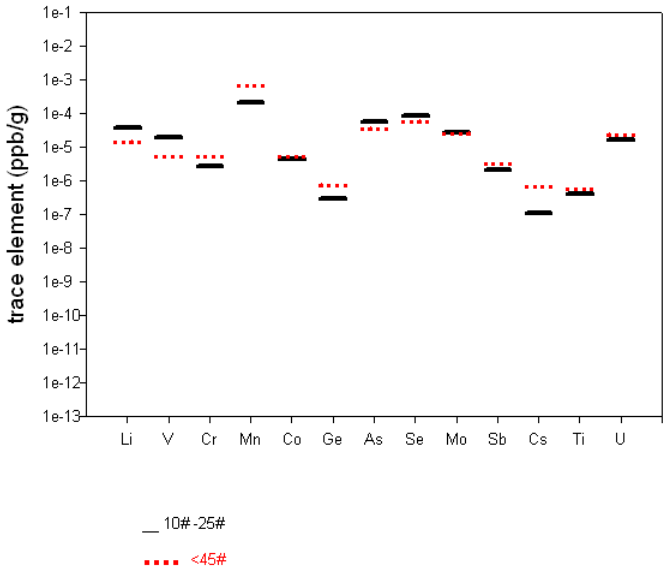

Figure 2.7 (A) Leached trace elements from dolimte rock with two gain sizes from 841 μm to 2.0 mm, and less than 354 μm under pH 7-8 and 90 days of leaching. (B) Leached trace elements from limestone rock with two gain sizes from 841 μm to 2.0 mm, and less than 354 μm under pH 7-8 and 90 days of leaching. (C) Leached trace elements from volcanic rock with two gain sizes from 841 μm to 2.0 mm, and less than 354 μm under pH 7-8 and 90 days of leaching.

2.3.2.4 Rock Type

According to the analysis by Mariner et al. (1983), the Bonanza King Formation is composed primarily of dolomite and trace amounts of quartz and aragonite. The major constituents of the Toroweap Formation are limestone, quartz and trace amounts of feldspar. The purities of both dolomite and limestone in the study area are quite high. The high bulk concentrations of Mn and Cr in all the three rock types resulted in their high concentrations in leached solutions. Surprise Formation released the highest concentrations of Cs in all experimental sample sets. This coincides with Farnham et al. (2003) observation that groundwater flowing through volcanic rocks might contain elevated concentration of Cs. In the case of this study, this was probably caused by the very high Cs concentration in the Surprise Formation bulk rock as compared to the other two rock formations.

The lower leaching fractions of trace elements leached from the Bonanza King Formation were generally less than those of the other two types of rock. It can be concluded that the rock of the Bonanza King Formation is less vulnerable than the other rocks, and less easily affected by pH, grain size, and leaching time.

2.3.3 Speciation and Solubility of Leachates

Geochemical modeling (e.g., solute speciation and solubility indices) can help us analyze the experiment results and fully explain the leaching process. The concentrations of major and minor cations and anions in leachates were measured for this purpose. In all of the leachates, dominant cations were Ca^{2+} and Mg^{2+}. The highest concentrations of

Ca^{2+} and Mg^{2+} were 237.2 mg/L in <345 um volcanic rocks and 43.44 mg/L in <345 um limestone rocks, respectively, while the lowest concentrations were 12.4 mg/L in 841 μm -2.0 mm limestone rocks and 1.18 mg/L in 841 μm -2.0 mm dolomite rocks. The prevalence of Na^+ and K^+ were similar in the leachates of all samples sets. Generally, the major cation concentrations increased with increasing leaching time and decreasing grain size, except for some anomalies possibly resulting from incongruent dissolution. In leachates, the dominant anion was SO_4^{2-}, with the highest concentration being 278.7 mg/L from <345 um volcanic rocks and the lowest 14.3 mg/L from 841 μm -2.0 mm limestone rocks. Obviously, the leaching of Ca^{2+}, Mg^{2+}, and SO_4^{2-} was controlled by the chemical composition and mineralogy of the bulk samples. Farnham et al.'s research (2003) on the groundwater in the YM area found a correlation coefficient among Ca^{2+}, Mg^{2+} and SO_4^{2-} of 0.93. The similarity of aquifer rocks of YM to the rock formations included in this study support the dominance of Ca^{2+}, Mg^{2+}, and SO_4^{2-} in our results.

Potential geochemical controls on leached trace elements were numerically simulated with model fitting, using PHREEQC Interactive 2.8, a geochemical model, along with its database phreeqc.dat. In PHREEQC, if the saturation index of the solution to a specific mineral phase is positive (or negative), the solution is over-saturated (or under-saturated). A zero saturation index (SI) value means the solution is at equilibrium.

Speciation calculations indicate that free ions Li^+, and their corresponding SO_4^{2-} complexes are the dominant species of these elements at low pH solutions. Li^+, free ions and their corresponding F^- and Cl^- complexes comprise major fractions of the dissolved

elements in the solution leached from the host rocks. For Mn^{2+}, free ions were the first dominant species and Mn^{2+} hydrolysis products were elevated, while Mn^{2+} and SO_4^{2-} complexes were attenuated with increasing pH. The second dominant species of Mn^{2+} in alkaline conditions was Mn^{2+} hydrolysis products, and in acidic conditions, Mn^{2+} and SO_4^{2-}. This means that some part of Mn exists in the high pH value as insoluble Mn^{2+} hydroxides and in the low pH value as soluble Mn^{2+} sulfates. This may be why Mn is one of the elements most influenced by pH in all three rock formations.

Results of saturation modeling showed that some mineral phases have more constant saturation indices with respect to changing grain sizes, pH values, and rock types. These minerals were anhydrite, celestite, fluorite, and gypsum, and all their saturation indices (SIs) were under-saturated, ranging from -2.32 to -1.03, -3.46 to -1.04, -3.38 to -1.41, and -2.97 to -0.81, respectively. Other kinds of mineral phases such as manganite and pyrolusite showed strong pH dependences. The calculated SIs of all leachates with respect to these minerals were under-saturated when pH values were less than 7.5 and saturated when pH values were equal or larger than 7.5. SIs of all samples ranged from -6.41 to 8.09 for manganite and -15.24 to 11.02 for pyrolusite. The change of SIs was less significant for samples with different grain size, but from the same rock formation and with the same pH value. There were no consistently positive or negative variation trends between fine and coarse particles, based on the saturation calculations. This lack also indicates that the impact of grain size on the leaching of trace elements may be limited to 1 order of SI. The positive SIs (partial precipitations) of mineral phase might be caused

by the abundance of corresponding metals in bulk samples. Other geologically reasonable mineral phases were obviously under-saturated.

2.4 Application in Transport Modeling

The leaching fractions derived from the leaching experiments of trace elements were used in the simple conceptual model to consider the fraction of trace elements released from host aquifer rocks into groundwater transport. An application case study, the transport modeling of major cations, major anions, and U from Yucca Flat to the Amargosa Desert, was conducted to take advantage of these preliminary datasets. The fraction conceptual model was used to describe the addition of U infiltrating to the groundwater system from rainfall on Spring Mountain. The mixing of groundwater from different aquifer rocks and recharge sources was also considered. The fitness of the measured and simulated concentrations in the groundwater of monitoring wells supported the possibility of the groundwater system being partially recharged by the precipitation on Spring Mountain. Observed geochemical data were taken from eight wells, shown in Figure 2.1. The chemical equilibrium speciation and saturation states of important minerals in groundwater from these wells were calculated with PHREEQC INTERACTIVE 2.8. All of them were saturated with respect to magnesite, quartz and talc. Furthermore, groundwater from Army #1 Water Well, UE 1-q well, and ER 6-1 well was saturated with aragonite, calcite, dolomite, iolite, and K-mica, providing control information on the mineral phases used in inverse modeling.

2.4.1 Inverse Modeling

Five possible scenarios of currently unknown flow paths (listed in Table 2.1) were evaluated through inverse modeling. All inverse modeling scenarios were constrained by the measured isotopes $\delta^{18}O$, δD and $\delta^{13}C$ (from Hershey and Acheampong, 1997), and were required to balance the measured Ca^{2+}, Mg^{2+}, SO_4^{2-} and alkalinity as HCO_3^-. Further constraints were added by allowing magnesite and quartz to precipitate while allowing dolomite and gypsum to dissolve according to the calculated saturation indices of groundwater in the different wells. The UE –5e PW-3 well was not used in examining the possible recharge from USGS HTH #3 well, due to its location in the mixing zone of Frenchman Flat, which implies that the groundwater in this well may be a mixture of lower carbonate and upper volcanic groundwater (Laczniak et al., 1996). If geochemical models can be found to reproduce the geochemical evolutions through inverse modeling, under the strict controls mentioned above, flow paths may be delineated. In Table 2.1, two valid models were fund through inverse modeling, which are capable to explain the difference in composition between the groundwater mixture of Cold Creek Spring and Water Well C-1 and the groundwater of Army #1well due to reactions. Similarly, another two valid models were found to explain the difference in composition between the groundwater mixture of Cold Creek Spring and Army #1 Water Well and the groundwater of Amargosa Tracer Well #2. It can be concluded either that groundwater recharge in the eastern part of the study area may be impossible or that USGS HTH #3 well is not a good representative of groundwater in the eastern part, which coincides with Hershey and Acheampong's (1997)

work. As for whether the groundwater is recharged from The Spring Mountains (represented by Cold Creek Spring), the inverse modeling verified two potential flow paths: one from Cold Creek Spring and Water Well C-1 to Army #1 Water Well to Amargosa Tracer Well #2, and another from Cold Creek Spring and Army #1 Water Well to Amargosa Tracer Well #2. Both scenarios produced models that were capable of determining the transfers of phases explaining the possible agrochemical groundwater evolution along the two assumed flow paths. The groundwater from The Spring Mountains may flow medially, providing recharge either to the south, to the north, or to both the south and the north of Army #1. Based on Koonce et al.'s (2006) study using principal component analysis (PCA) of 118 groundwater samples, the conclusion was drawn that groundwater may also flow from the Spring Mountains to Ash Meadow and to the adjacent area.

Table 2.1 Numbers of models and valid models for different flow paths

Groundwater inverse model scenario	No. of models	No. of valid models
From USGS HTH #3 and Water Well C-1 to Army #1	4	0
From USGS HTH #3 and Water Well C-1 to Amargosa Tracer Well #2	4	0
From USGS HTH #3 to Amargosa Tracer Well #2	3	0
From Cold Creek Spring and Water Well C-1 to Army #1	18	2
From Cold Creek Spring and Army #1 Water Well to Amargosa Tracer Well #2	18	2

2.4.2 Transport Modeling

Inverse modeling suggested that the Spring Mountains might be a source of recharge to the groundwater system from Yucca Flat to Amargosa Desert. Thus, one-dimensional advective and diffusive transport modeling was conducted, using PHREEQC, along this groundwater flow path (from Cold Creek Spring and Army #1 Water Well to Amargosa Tracer Well #2). Because of uranium's stable behavior (Hodge et al., 1996), which may provide more valuable hints as to the source tracking and evolution process of groundwater, its transport was simulated. The effects of mineral phase, mixing and kinetic sorption were also considered in the simulations. Based on Hughes's research (1966), precipitation on the Spring Mountains can recharge the underlying groundwater directly by infiltrating into a Carbonate Karst system. In the fraction conceptual model, the rainfall-induced U was assumed to be released from the carbonate aquifer, which consisted of the upper/middle Toroweap Formation and lower Bonanza King Formation. The rock solid surface areas were estimated based on the bulk density and average porosity of the carbonate rocks in Southern Nevada aquifers (Berger, 1992) and of the volcanic rocks in YM (Flint, 1997). The derived leaching fractions of U from the three grain sizes, in a pH 7-8 solution, were averaged to estimate the amount of U leached from aquifer rocks during precipitation infiltration, which would probably not vary widely in a natural formation, composed of many different grain sizes. Complex mechanisms that are often used to consider the difference between laboratory and natural conditions were not included in this study, the reason being that there is not yet a representative and good way to account for the

upscale transformation in the leaching process. The calculated fraction of leached U can be used as a conservative estimation of contamination due to leaching. The mean concentrations of major cations and anions in the precipitation (snow) in the Spring Mountains were referenced from Gűler and Thyne (2004). It was suggested that the rate of the infiltrated rainfall discharged to the Spring Mountains through the karst system was over 400 m^3/mon (Hughes, 1966). The U contained in rainfall was also neglected, because of the minute amount and absence of data. The arithmetic mean of the U leaching fraction of three grain sizes in Bonanza King Formation and of Toroweap Formation was used to quantify the extra U leached from Karst. Then, the U carried by infiltrated precipitation was added into the groundwater and allowed to migrate along the flow paths. The calculated results match well with the measured values, except for those of chloride and sodium, as shown in Figures 2.8 and 2.9, and Table 2.2. Along the modeled flow path, the concentration of calcium decreased, as a result of the precipitation of calcium minerals, while the concentration of sodium increased due to the intensive evaporation and the influence of the mineral phase. The calculated sodium concentration is lower than the measured concentrations. One of possible reasons is that the recharge from Water Well C-1, containing quite a high level of sodium, was not included in this transport modeling because of its location in the complex mixing zone of Frenchman Flat (Laczniak et al., 1996). In the absence of a measurement of the U concentration in Amargosa Tracer Well #2 during the same period, the simulated U concentration was compared with the measured range in wells (Koonce, 2004) in the Amargosa Desert region. The measured concentration

of U is still close to the simulated value, which has been exaggerated by the experimental conditions. These results indicate that leaching from the carbonate Karst system doesn't significantly account for U concentration in groundwater of Amargosa Tracer Well #2. They also show that U concentration is quite stable and that its variation likely resulted from changes in concentration in groundwater inflow.

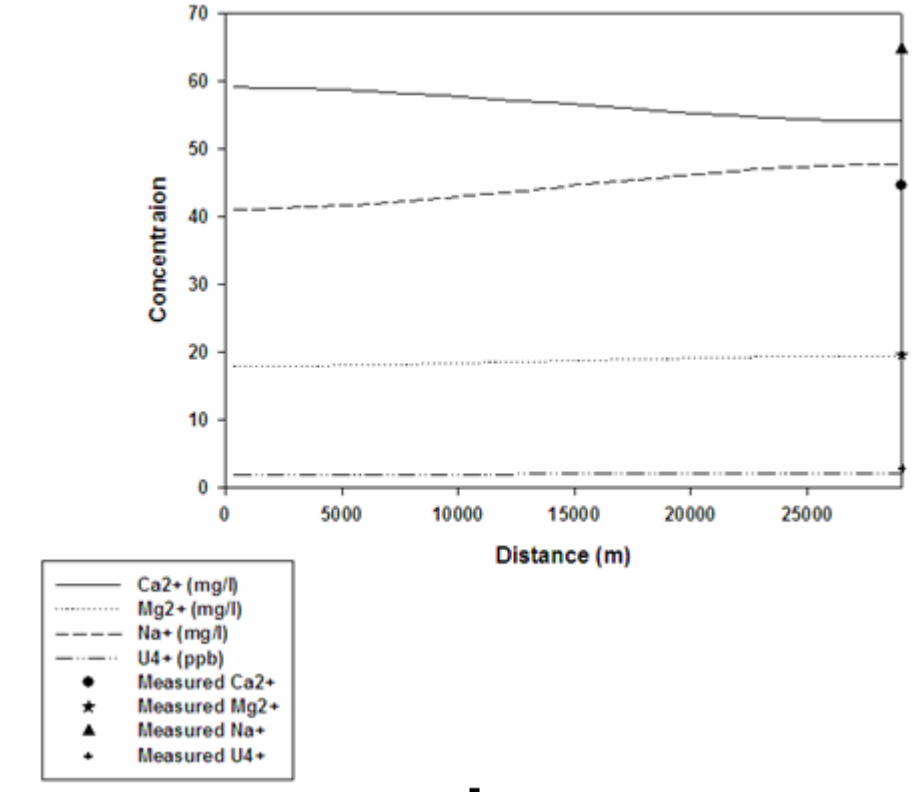

Figure 2.8 Simulated results of cation transport from the Spring Mountains to Amargosa Desert with comparison to the measured cation concentrations. Black solid line- simulated calcium concentration; black dot line- simulated magnesium concentration; black dashed line- simulated sodium concentration; black dot dashed line- simulated uranium concentration.

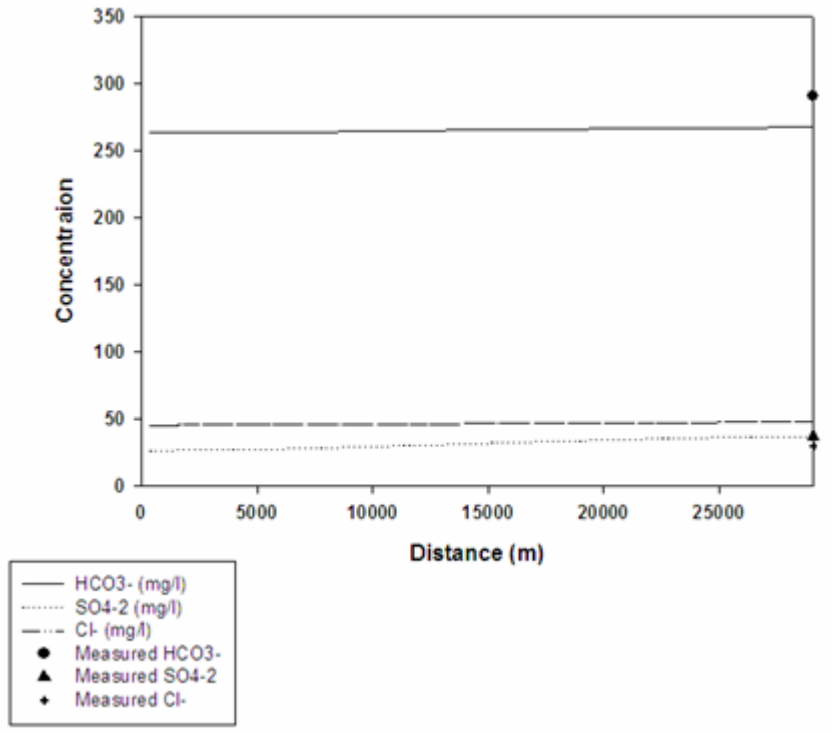

Figure 2.9 Simulated results of anion transport from the Spring Mountains to Amargosa Desert with comparison to the measured anion concentrations. Black solid line- simulated carbonate hydrate concentration; black dot line- simulated sulfate concentration; black dashed line- simulated chloride concentration.

Table 2.2 Measured and calculated concentrations of groundwater in Amargosa Tracer Well #2

	Major ion concentration (mg/L)						pH	Tracer element (ppb)
	Cl^-	$SO4^{2-}$	HCO_3^-	Ca^{2+}	Mg^{2+}	Na^+		U
Measured concentration	29.9	36.5	291	44.5	19.6	64.6	7.4	2.20-5.70[a]
Calculated concentration	46.2	36.7	271.7	54.1	19.5	47.8	7.5	2.34

Note: [a] measured values of the wells (Koonce, 2004) in the Amargosa Desert region.

2.5 Conclusions

The concentrations of trace elements in the leached solution are mainly controlled by geochemical and mineralogical factors. The abundance of trace elements in the bulk rock samples led directly to their elevated levels in the leaching solution. Comparison of the leaching results of the three formation rocks indicates that mineralogy also exerts significant influence on trace element leaching. The Bonanza King Formation showed less leachablility than rocks of the other two formations because of its dominant and secondary minerals. The reasons for this could be: (1) Bonanza King Formation has a long diagenetic history and stable minerals, so trace elements are not easily leached out of the rock; (2) different secondary minerals in fractures might cause decreased leachability of trace elements in Bonanza King Formation rocks; and (3) different pH values could affect the solubility of trace elements and saturation indices. Similarly, Zhou et al.'s (2006) research showed that the leaching solution from the Surprise Formation contained higher concentrations of rare earth elements (REEs) than that from the Bonanza King Formation. The host minerals' effect on the leaching of trace elements might be one of the reasons for this difference, e.g., the easily weathered and unstable glass or silicates (Piatak et al., 2004) contained in the Surprise Formation volcanic rocks (White et al., 1980). Geochemical simulation also calculated saturation indices of the Cambrian dolomite (Bonanza King Formation) that were consistently less than those of the Permian limestone (Toroweap Formation) and the Tertiary volcanic rock (Surprise

Formation). The lower saturation indices indicate that a lower amount of trace elements were leached from rocks in the Bonanza King Formation.

Leached trace elements showed a positive general trend with a longer duration of leaching, despite the existence of incongruent dissolution. The concentrations of the leached trace elements were obviously attenuated with increasing grain size, mainly because of the decreased particle interacting surface. However, it is difficult to rank the influences of grain size, leaching time, and pH value because these factors are measured with different and unconvertible units. Based on saturation calculation, it was shown that free ions Li^{+}, and its corresponding SO_4^{2-} complexes are the dominant species of this element. As for Mn^{2+}, free ions were the first dominant species, Mn^{2+} hydrolysis products were elevated, and Mn^{2+} and SO_4^{2-}complexes were attenuated with increasing pH. Saturation calculation showed that two kinds of mineral phases existed: a mineral phase with relatively constant solubility; and a mineral phase with variable solubility. The partial precipitation of mineral phases was mainly caused by the abundance of corresponding metals in bulk samples, while other geologically reasonable mineral phases were obviously under saturated.

Leaching experiments provided preliminary datasets for the conceptual model that quantified the fraction of trace elements released from the host rock, which is very useful to transport modeling. The derived leaching fractions were used in the fraction conceptual model to estimate the extra addition of U to groundwater due to rainfall infiltrating through aquifer rocks. The measured results matched well with the values

calculated by using the transport modeling of groundwater flow from Cold Creek Spring and Army #1 Water Well to Amargosa Tracer Well #2. The leaching fractions of U derived from leaching experiments were reasonable and were used as the preliminary datasets for the transport modeling. The results of the inverse and transport modeling also imply that rainfall on the Spring Mountains may recharge the groundwater system in Amargosa Desert or Ash Meadows, or both.

Further studies should be conducted to conceptualize models for quantifying the fractionation and redistribution of trace elements, with the inclusion of upscaling techniques, to delineate more complicated groundwater flow paths, and to investigate the important interaction between water and rock in Southern Nevada. These will be very beneficial to the transport modeling in the region.

2.6 References

Al-Masri, S.M., Amin, Y., Ibrahim, S., and Al-Bich, F., 2004. Distribution of some trace metals in Syrian phosphogypsum. Applied Geochemistry, 19, p. 747-753.

Berger, B.L., 1992. Lithologic properties of carbonate-rock aquifers at five test wells in the Coyote Spring Valley area, Southern Nevada, as determined from geophysical logs. U. S. Geological Survey, Water-Resources Investigations Report 91-4167, 27 pp.

CRTD, Center for Research and Technology Development (Publication), 2002. Strategy for remediation of groundwater contamination at the Nevada Test Site. American Society of Mechanical Engineers, 62, 207 pp.

D' Agnese, F., Turner, A.K., and Hill, M.C., 1997. Hydrogeologic evaluation and numerical simulation of the Death Valley regional ground-water flow system, Nevada and California. U. S. Geological Survey, Water-Resources Investigations Report 96-4300, p. 72-77.

Edet, E.A., Merkel, J.B., and Offiong, E.O., 2003. Trace element hydrochemical assessment of the Calabar Coastal Plain Aquifer, southeastern Nigeria using statistical methods. Environmental Geology, 44, p. 137-149.

Farnham, I.M., Johannesson, K.H., Singh, A.K., Hodge, V.F., and Stetzenbach, K.J., 2003. Factor analytical approaches for evaluating groundwater trace element chemistry data. Analytica Chimica Acta, 490, p. 123-138.

Flint, E.L., 1997. Characterization of hydrogeologic units using matrix properties, Yucca Mountain, Nevada. U. S. Geological Survey, Water-Resources Investigations Report 97-4243, 33 pp.

Gaskova, L.O., Bessonova, P.E., and Bortnikova, B.S., 2003. Leaching experiments on trace element release from the arsenic-bearing tailings of Khovu-Aksy (Tuva Republic, Russia). Applied Geochemistry, 18, p. 1361-1371.

Grasso, D.N., 1996. Hydrology of modern and late Holocene lakes, Death Valley, California. U.S. Geological Survey, Water-Resources Investigations Report 95-4237, 11-54 pp.

Gűler, C., and Thyne, D.G., 2004. Hydrologic and geologic factors controlling surface and groundwater chemistry in Indian Wells-Owens valley area, southeastern California, USA. Journal of Hydrology, 285, p.177-198.

Hershey, L.R., and Acheampong, Y.S., 1997. Estimation of groundwater velocities from Yucca Flat to the Amargosa Desert using geochemistry and environmental isotopes. Reno, Nevada, Water Resources Center, Desert Research Institute, p. 2-31.

Hodge, V., Johannesson, K.H., and Stetzenbach, K.J., 1996. Rhenium, molybdenum, and uranium in groundwater from the southern Great Basin,USA: Evidence for conservative behavior. Geochimica et Cosmochimica Acta, 60, p. 3197-3214.

Hughes, L.J., 1966. Some aspects of the hydrogeology of the Spring Mountainss and Pahrump Valley, Nevada, and environs, as determined by spring evaluation. Master's Thesis, University of Nevada, Reno, 116 pp.

Johannesson, K.H., and Zhou, X., 1999. Origin of middle rare earth element enrichments in acid waters of a Canadian High Arctic lake. Geochimica et Cosmochimica Acta, 63, p. 153-165.

Koonce, E.J., 2004. Geochemical interpretation on groundwater flow in the Southern Great Basin. Master of science thesis, University of Nevada, Las Vegas, 2-89 pp.

Koonce, E.J., Yu, Z., Farnham, I.M., and Stetzenbach, K.J., 2006. Geochemical interpretation of groundwater flow in the southern Great Basin. Geosphere, 2, p. 88-101.

Laczniak, R.J., Cole, J.C., Sawyer, D.A., and Trudeau, D.A., 1996. Summary of hydrogeologic controls on groundwater flow at the Nevada Test Site, Nye County, Nevada. U.S. Geological Survey, Water-Resources Investigations Report 96-4109, 30-59 pp.

Lee, K.P., Kang, J.M., Choi, H.S., and Touray, C.J., 2005. Sulfide oxidation and the neutral attenuation of arsenic and trace metals in the waste rocks of the abandoned Seobo tungsten mine, Korea. Applied Geochemistry, 20, p. 1687-1703.

Mariner, R.H., Presser, T.S., and Evans, W.C., 1983. Geochemistry of active geothermal systems in the northern Basin and Range Province. Geothermal Resources Council, Special Report, no.13, 95-119 pp.

Newsom, E.H., 1995, Composition of the Solar System, Planets, Meteorites, and Major Terrestrial Reservoirs. A Handbook of Physical Constants, the American Geophysical Union Reference Shelf 1, Copyright 1995 by the American Geophysical Union, 174. p. 159-188.

Parkhurst, D.L., 1995. User's guide to PHREEQC -- a computer program for speciation, reactionpath, advective-transport, and inverse geochemical calculations. U.S. Geological Survey, Water-Resources Investigations Report 95-4227, 20 pp.

Parsons, B.M., Bird, K.D., Einaudi, T.M., and Alpers, N.C., 2000. Geochemical and mineralogical controls on trace element release from the Penn Mine base-metal slag dump, California. Applied Geochemistry, 16, p. 1567-1593.

Piatak, M.N., Seal II, R.R., Hammarstrom, M.J., 2004. Mineralogical and geochemical controls on the release of trace elements from slag produced by base- and precious-metal smelting at abandoned mine sites. Applied Geochemistry, 19, p. 1039-1064.

Quejido, A.J., Perez Del Villar, L., Cozar, J.S., Fernandez-Diaz, M., Crespo, M.T., 2005. Distribution of trace elements in fracture fillings from the "Mina Fe" uranium deposit (Spain) by sequential leaching: Implications for the retention processes. Applied Geochemistry, 20, p. 487-506.

Scott, B.R., 1990. Structural geology of Yucca Mountain. Proceedings of the topical meeting on Nuclear waste isolation in the unsaturated zone, Focus '89. America Nuclear Society, La Grange Park, IL, United States .

Sohlenius, G.,O¨ born, I., 2004. Geochemistry and partitioning of trace metals in acid sulphate soils in Sweden and Finland before and after sulphide oxidation. Geoderma, 122, p. 167-175.

Wagner, J.N., and Hlatshwayo, B., 2005. The occurrence of potentially hazardous trace elements in five Highveld coals, South Africa. International Journal of Coal Geology, 63, p. 228-246.

White, A.F., Claassen, H.C., and Benson, L.V., 1980. The effect of dissolution of volcanic glass on the water chemistry in a tuffaceous aquifer, Ranier Mesa, Nevada. U.S. Geological Survey, Water Supply Paper, 1535-Q, 34 pp.

Winograd, I.J., and Thordarson, W., 1975, Hydrogeologic and hydrochemical framework, south-central Great Basin, Nevada-California, with special reference to the Nevada Test Site. U.S. Geological Survey, Professional Paper, 712-C.

Yu, Z., Hu, B., 2003. Studies on water movement and solute transport in arid regions. Journal of Hydrology. 275, p. 139-140.

Zhou, X., Stetzenbach, J.K., Yu, Z., Johennesson, H. K., 2006. Origin of rare earth elements signature in groundwaters of South Nevada, USA: implication from preliminary batch leach tests using aquifer rocks. In Johennesson, H. K., (Ed) Rare Earth Element in Groundwater Flow Systems, 2005 Springer Press, Netherlands, 141-160 pp.

Zhou, X., 2004. Trace Element Geochemistry of Groundwater Flow Systems in Southern Nevada and Eastern California. Ph.D. Dissertation, University of Nevada, Las Vegas, 116-120 pp.

CHAPTER 3

SORPTION AND SURFACE COMPLEXATION MODELING OF YTTERBIUM AND EUROPIUM ON VOLCANIC ROCKS AT THE NEVADA TEST SITE (NTS)

Batch adsorption experiments were conducted to investigate the adsorption behavior of rare earth elements (REEs) on the volcanic rocks at NTS. Observed adsorptions of ytterbium (Yb) and europium (Eu) were simulated respectively with two surface complexation models (SCM): the constant capacitance model (CCM) and triple-layer model (TLM) implemented in a geochemical model, HYDRAQL. Through comparison, TLM was selected as a preferred model being capable of yielding a better agreement with observed adsorption edges. Parameters of TLM were optimized including intrinsic acidity constants, surface binding constants and capacitance to reduce uncertainty of estimation. After parameter optimization and justification, the experimentally derived thermodynamic-based TLM was used to simulate adsorption isotherm and estimate distribution coefficients, K_d. In doing so, estimation error of K_d can be significantly reduced with TLM due to its advantage of wide application to ionic strength and pH. This research may suggest that the SCM can be coupled into transport models to describe adsorption reactions of REEs in the groundwater system of Nevada Test Site (NTS) and adjacent areas. This research is significant in studying adsorption reactions of REEs on the volcanic rocks and describing these reactions with thermodynamic SCM instead of empirically limited methods. This research may reduce prediction uncertainty of trivalent actinides transport by analogizing adsorption behaviors of REEs to those of trivalent

actinides (e.g., uranium, neptunium, plutonium), which can help us to better evaluate and operate the performance of Yucca Mountain repository.

3.1 Introduction

Sorption reactions have been studied extensively at the interface of water and individual minerals including quartz, hematite, goethite, kaolinite, biotite, magnetite, feldspar, and montmorillonite, among others (Chen et al., 2006; Peacock and Sherman, 2003; Harris, 2006; Takahashi et al., 2004). Many valuable studies have contributed to the understanding of sorption mechanisms and factors' impacts. Aamrani et al. (2001) investigated the sorption of uranium on olivine-rock under different pH, solid surface to volume ratio and uranium concentration. They found that the amount of carbonate complexation has a negative effect on the sorption of uranium. They also derived the stability constants of uranium species with a surface complexation model. Ikhsan et al. (2005) employed the surface complexation model and attenuated total reflectance-FTIR to study the sorption of multi-valence aminopyridine on montmorillonite. The research showed that different sorption behaviors of different aminopyridine complexation and calcium cation are more competitive than the potassium cation with aminopyridine for o-plane. However, as a fact, the absorbents in real environments are a mixture of amorpous/disordered phases and minerals. Based on the intensive sorption results of single mineral cases, how to come up with sorption behavior on mixed minerals is extremely worth studying. Pananelli et al. (2005) conducted a potentiometer titration and lead sorption on various minerals and their mixture. A unified model with a three peak

distribution function for proton affinity constants successfully simulated the lead sorption isotherms of individual and mixed minerals.

Based on studies (Choppin and Stout, 1989, Krauskopf, 1986, and Johannesson et al., 1993), it has been generally accepted that rare earth elements can be the chemical analogues of trivalent actinides due to their similar valences and group behaviors. Many studies about sorption behavior of REEs have been completed in the past decade (Dev et al., 1998; Gelis et al., 2003; and Zavarin et al., 2005). Many numerical models were proposed to simulate and reproduce experimental adsorption data. Surface complexation model (SCM) is one of these numerical models, which has superiority over the empirical techniques including distribution coefficient, Langmuir isotherm, and Freundlich isotherm. SCM has become a prevalent approach to analogize the interactions between water and solid surface based on thermodynamics. The derived intrinsic equilibrium constants from SCMs only are dependent on the identities of adsorbates and adsorbents, independent on the characterization of solutions such as pH, adsorbate load and solution composition (Koretsky, 2000). Microscopic and spectroscopic techniques (e.g., atomic force microscopy, X-ray absorption spectroscopy) are capable of characterizing mineral phases and geometric details of adsorbents. It is a current direction in adsorption studies to integrate microscopic and spectroscopic approaches for better investigating the water-solid interaction. Montavon et al. (2002) used a constant capacitance model (CCM) to simulate the sorption properties of europium (Eu) on mixed minerals under different metal ion concentration. Ternary surface sites were used in CCM in simulating Eu sorption in high

concentration solutions. The ternary sites were proved by the findings of a laser-induced fluorescence spectroscopy (LIFS). An extended X-ray absorption fine structure spectroscopy (EXAFS) was used by Schlegel et al. (2004) to study Eu retention by a calcium silicate hydrate. They found that Eu was sorbed or coprecipitated at Ca sites in a C-S-H-like environment. Quinn et al. (2006) used a surface complexation equation to calculate the competition and surface complexation of Yb and REEs onto amorphous ferric hydroxide. Equilibrium constants of Yb and REE surface species were estimated and compared with the previously published data. Chen et al., (2006) used macroscopic and spectroscopic techniques to study the metal sorption at the interface between water and oxides. Results of the two techniques showed strontium presented in outer-sphere complex, cobalt presented in solid phase, and lead presented in inner-sphere complex. In the solution of low ionic strengths, the prevalent adsorption mechanisms of cobalt and lead appeared different.

The risk of contamination of transuranic or actinide elements determines design and operation of nuclide waste repositories in the YM and NTS area. Sorption reactions have been regarded as one of most important processes for some radionuclide transport in this regional groundwater system (Ogard et al., 1984). The proposed waste repository of YM will be set in felsic volcanic rocks which are distributed widely in the NTS and YM area. The investigation of REEs adsorption on volcanic rocks can really help us understand the retention and predict the possible migration of transuranic radionuclides in this area. However, few studies about REEs sorption onto volcanic rocks have been published.

Furthermore, fewer studies of lanthanides were found than those of actinides, especially their sorption on natural rocks and the relevant modeling of surface complexation reactions. In order to enhance our understanding of adsorption, prediction of lanthanide transport and evaluation of potential contamination of radionuclides in the YM and NTS area, batch adsorption experiments and surface complexation modeling of Yb and Eu were conducted in this research.

In Katz and Hayes's study of surface complexation modeling (Katz and Hayes, 1994a), a self-consistent calibration approach was able to produce a unique set of surface ionization parameters through FITEQL optimization. Their research showed that the TLM can be used for the moderate sorption coverage even when the particle concentration changes by three orders of magnitude. The sorption and desorption of Yb(III) on hematite and alumina, respectively, were simulated with FITEQL based on experimental results (Marmier et al., 1996). There was a good agreement between measured and simulated sorption and desorption of Yb(III) with considering the hydroxylate surface complexation. Reversibility and irreversibility of sorption were fund respectively in the low and high surface loading solutions. Curtis et al. (2006) calculated the K_d of uranium by using a laboratory derived surface complexation model. Comparison of the laboratory derived K_d and in situ K_d indicated that SCM can be used to describe the sorption in the field. The surface complexation model has become the prevalent tool for simulating sorption reactions and providing crucial information for reactive pollutants transport. Obviously, the selection of key surface complexation reactions and calibration of reaction parameters are extremely

important. Katz and Hayes (1994 a, b) presented strategies to modeling the monomer complexation at moderate surface coverage and polymer complexation at moderate or high surface coverage. For the case of moderate surface coverage, different factors' effects on sorption results of various surface complexation models were analyzed. For the case of high surface coverage, three improved models were presented and exemplified to consider the co-precipitation in sorption process.

Based on the studies discussed above, the experimentally derived parameters of surface complexation reactions may be varied over several orders of magnitude under different conditions including ionic strength, pH and the ratio of surface area to particle concentration. In order to attenuate the impacts of factors and reduce the uncertainty of practical application, an optimization software, PEST-parameter estimation tool, was used to fit and optimize the derived parameters of Yb and Eu in this study. The detailed method of optimization was described by Katz and Hayes (1994a and 1994b). Here, the previous results of spectroscopic technique (Tertre et al., 2006; Piasecki and Sverjensky, 2008) were used to justify and interpret the observed adsorption phenomenon in this study as well.

According to batch reactor experiments, we derived the primary parameters of sorption and conceptualized SCM to simulate specific sorption processes of Yb and Eu, respectively. CCM and triple-layer model (TLM) embedded in HYDRAQL were used to simulate the sorption envelopes of Yb and Eu from six matrix/fracture sample sites in the YM and NTS area. By comparing simulated and experimental results, an appropriate SCM

was selected for optimization with PEST. Then the improved SCM can be incorporated into the flow and solute transport model with good transferability and reliability. This study has significance in studying the existence of the two lanthanides' adsorption behavior using batch reactor experiments and SCM. This study also can provide optimized thermodynamic parameters using PEST tool to obtain best fitted adsorption envelopes for the numerical modeling of the real water/rock interaction.

3.2 Materials and Methods

3.2.1 Materials

Rock samples were collected from five cores, respectively, from the Western Pahute Mesa (WPM) in the NTS site and around the YM region. These cores are UE18R2228, UE20C2908, UE20C2855, PM-14823 and PM-2-4177 shown in Figure 3.1 (Shundahai Network, 2007). In order to investigate the impact of the adsorbent surface's property on the adsorption behavior of solvents, the fracture and matrix samples were prepared. By cutting significant fracture surface from the core rocks, the two types of rock samples were obtained to tentatively evaluate the adsorption on oxidized surface and fresh surface respectively. The rock samples fall into the range from 44 μm to 149 μm after cutting, grinding, and sorting with different sieves.

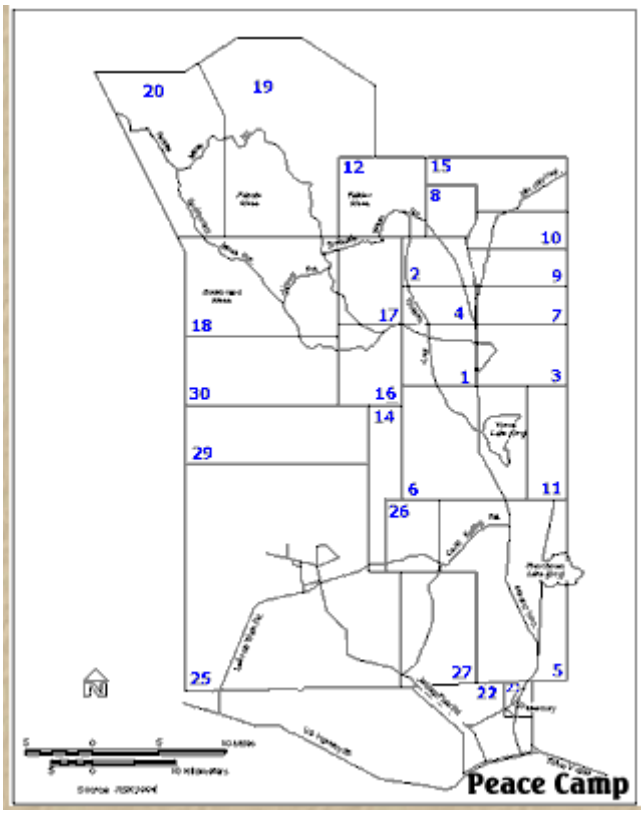

Figure 3.1 Rock sample site for batch reactor experiments- Pahute Mesa located in area 19 of Nevada Test Site
(from http://www.shundahai.org/area_19_nts.htm)

The mineralogy of the rock samples were analyzed by the Los Alamos National Laboratory (LANL) with X-ray diffraction (XRD). The XRD analysis showed that rock samples are mainly composed of quartz, feldspar and other minor amounts of smectite, hematite and mica, shown in Table 3.1 (Papelis and Um, 2002). The obvious dark coating of the fracture surfaces from three sample sites were identified as Mn and/or Fe oxides.

Table 3.1 Mineralogy composition of the rock samples from the sample sites in WPM

Sample site	Porosity (%)	Main minerals
UE18R2228 Fracture	3.65	Quartz (28%); Feldspar (66%)
UE18R2228 Matrix	2.0	Same as above
UE20C2908 Matrix	28.8	Quartz (37%); Feldspar (57%)
UE20C2855 Matrix	15.0	Quartz (34%); Feldspar (65%)
UE20C2855 Fracture	14.8	Same as above
PM-1-4823 Matrix	26.3	Quartz (39%); Feldspar (55%)
PM-1-4823 Fracture	28.0	Same as above
PM-2-4177 Matrix	13.0	Quartz (30%); Feldspar (50%)

3.2.2 Experiments

Yb and Eu adsorptions were studied through laboratory batch reactor experiments. Every 10 mL test tube was filled with WPM rock powders, synthetic groundwater of NTS and the metal ion of ytterbium and europium, respectively. Nitric acid and sodium hydroxide were used to obtain different desired pH values. The solid concentration was 3 g/L in the series of batch sorption experiments. The initial Yb concentration was 10^{-6} M made from a pure 99.999% ytterbium (III) chloride hexahydrate (Fisher Scientific); the initial Eu concentration was 10^{-7} M made from a pure 99.9% europium (III) nitrate hexahydrate (Fisher Scientific). In batch adsorption experiments, blank samples were prepared without rock adsorbents with pH ranging from about 3 to 9. The experimental

results showed that no larger than 3% of the relative change in concentrations were found. After 48 hours of end-over-end rotation, the equilibrium samples were centrifuged for 10 minutes at 7000 rpm to separate solid and solution. Then the supernatant solutions were diluted for the cation concentration analysis of interest with an atomic absorption spectroscopy (AA, PerkinElmer 4110ZL). All measurements of AA were made in duplicates for quality control and assurance. The pH of each remaining supernatant solution was measured with a pH meter and the temperature during the whole experiment process was controlled within 22±2 ^{o}C. Finally, the adsorption envelopes of Yb and Eu on the volcanic rocks from NTS were obtained by plotting uptake percentages vs. pHs.

In order to quantify sorption, SCMs were used to simulate the observed absorption edges of Yb and Eu, respectively. Specific surface areas of crushed rock samples, an important geochemical parameter in SCM, were measured by the static BET method and shown in Table 3.2 (Papelis and Um, 2002).

Table 3.2 Specific surface area of the rock samples from WPM

Sample site	Specific surface area (m^2/g)	Sample site	Specific surface area (m^2/g)
UE18R2228 Fracture	0.9996	UE20C2855 Fracture	3.259
UE18R2228 Matrix	1.147	PM-1-4823 Matrix	5.652
UE20C2908 Matrix	5.246	PM-1-4823 Fracture	4.987
UE20C2855 Matrix	3.759	PM-2-4177 Matrix	4.707

3.2.3 Surface Complexation Modeling

HYDRAQL 1.0 (Papelis et al., 1988) used in this study is a geochemical equilibrium model including four types of SCMs, which are constant capacitance model (CCM), electric double layer model (DLM), basic Stern model (BSM) and three layer model (TLM). Only CCM and TLM were selected to numerically model adsorption of Yb and Eu. In CCM, the potential of the electric double layer is constant and five parameters are needed including protonation, deprotonation, site density, specific surface area, and electric capacitance. TLM can be regarded as a transformed CCM by adding a middle layer to consider strong and weak binding forces. Surely, extra parameters are needed in TLM besides these five parameters mentioned above.

The acid-base surface reactions in CCM and TLM are expressed as follows:

$$XOH \Leftrightarrow XO^- + \mathrm{H}^+ \qquad K_{a1}^{\mathrm{int}} = \frac{[XO^-][H^+]}{[XOH]} \exp(-F\psi_0 / RT) \tag{3.1}$$

$$XOH + H^+ \Leftrightarrow XO\mathrm{H}_2^+ \qquad K_{a2}^{\mathrm{int}} = \frac{[XOH_2^+]}{[XOH][H^+]} \exp(F\psi_0 / RT) \tag{3.2}$$

where *XOH* is a reactive surface functional group, *XO* is a negative surface group caused by deprotonation of *XOH*, *F* is the Faraday constant, ψ_o is the potential at surface, *R* is the idea gas constant, *T* is the absolute temperature, and [] represent the activity.

3.2.3.1. Surface Complexation Reactions in CCM

The mineral acid-base properties of adsorbents were described with stability constants (stoichiometries) in CCM, while the interaction of electrolyte ions and variable ionic

strength were not taken into account. Only three parameters, including the specific surface area of the suspended solid, initial concentration of the suspended solid, and capacitance of the inner layer, are needed in surface modeling of CCM. Compared with TLM, CCM obviously has the merits of fewer parameters required and less interference of parameters due to the simpler mechanism.

For Yb adsorption, the two following surface complexation reactions were considered in CCM modeling:

$$XOH + Yb^{3+} - H^{+} \Leftrightarrow XOYb^{2+} \qquad \mathrm{K}_{\mathrm{Yb1}}^{\mathrm{int}} = \frac{[XOYb^{2+}][H^{+}]}{[XOH][Yb^{3+}]}\exp(2F\psi_0 / RT) \tag{3.3}$$

$$XOH + Yb^{3+} + 2H_2O \Leftrightarrow XOYb(OH)_2 + 3\mathrm{H}^{+} \qquad \mathrm{K}_{\mathrm{Yb2}}^{\mathrm{int}} = \frac{[XOYbOH^{+}][H^{+}]^3}{[XOH][Yb^{3+}]} \tag{3.4}$$

For Eu adsorption, the two surface complexation reactions similar to Yb adsorption were considered in CCM modeling:

$$XOH + Eu^{3+} - H^{+} \Leftrightarrow XOEu^{2+} \qquad \mathrm{K}_{\mathrm{Eu1}}^{\mathrm{int}} = \frac{[XOEu^{2+}][H^{+}]}{[XOH][Eu^{3+}]}\exp(2F\psi_0 / RT) \tag{3.5}$$

$$XOH + Eu^{3+} + 2H_2O \Leftrightarrow XOEu(OH)_2 + 3\mathrm{H}^{+} \qquad \mathrm{K}_{\mathrm{Eu2}}^{\mathrm{int}} = \frac{[XOEuOH^{+}][H^{+}]^3}{[XOH][Eu^{3+}]} \tag{3.6}$$

For a given adsorption system (sample site), the stability constants should be strictly determined by the adsorbent property, no matter what the medium composition is. Theoretically, the stability constants derived respectively from Yb and Eu adsorption experiments should be consistent for each sample spot.

3.2.3.2. Surface Complexation Reactions in TLM

In order to consider different binding strengths of adsorbents, an additional layer is added in TLM, resulting in an outer layer. Also the interaction of electrolyte ions and ionic strength are considered by two additional parameters describing concentrations and charges of electrolyte ions in the adsorption system. Thus, three more parameters including the capacitance of the outer layer, concentration of the symmetric electrolyte, and charge of the symmetric electrolyte, are needed in surface modeling of TLM. In this study, the Yb cation was placed in the o-plane; NO_3^- was placed in the β-plane. The reactions and stoichiometries for Yb in TLM are expressed as following:

$$XOH + Na^+ \Leftrightarrow XO - Na^+ + H^+ \qquad K_{cat}^{\text{int}} = \frac{[XO^- - Na^+][H^+]}{[XOH][Na^+]} \exp(F(\psi_\beta - \psi_0)/RT) \tag{3.7}$$

$$XOH + H^+ + NO_3^- \Leftrightarrow XOH_2^+ - NO_3^- \qquad K_{an}^{\text{int}} = \frac{[XOH_2^+ - NO_3^-]}{[XOH][H^+][NO_3^-]} \exp(F(\psi_0 - \psi_\beta)/RT) \tag{3.8}$$

$$XOH + Yb^{3+} \Leftrightarrow XOYb^{2+} + \mathrm{H}^+ \qquad \mathrm{K}_{\mathrm{Yb1}}^{\text{int}} = \frac{[XOYb^{2+}][H^+]}{[XOH][Yb^{3+}]} \exp(F\psi_0/RT) \tag{3.9}$$

$$XOH + Yb^{3+} + 2NO_3^- \Leftrightarrow XOYb(NO_3^-)_2 + \mathrm{H}^+ \quad \mathrm{K}_{\mathrm{Yb2}}^{\text{int}} = \frac{[XOYb(NO_3^-)_2][H^+]}{[XOH][Yb^{3+}][NO_3^-]^2} \exp(F(\psi_0 - \psi_\beta)/RT)$$

(3.10)

Similarly, the reactions and stoichiometries for Eu in the triple-layer model are expressed as following:

$$XOH + Na^+ \Leftrightarrow XO - Na^+ + H^+ \qquad K_{cat}^{\text{int}} = \frac{[XO^- - Na^+][H^+]}{[XOH][Na^+]} \exp(F(\psi_\beta - \psi_0)/RT) \tag{3.11}$$

$$XOH + H^+ + NO_3^- \Leftrightarrow XOH_2^+ - NO_3^- \qquad K_{an}^{\text{int}} = \frac{[XOH_2^+ - NO_3^-]}{[XOH][H^+][NO_3^-]} \exp(F(\psi_0 - \psi_\beta)/RT) \tag{3.12}$$

$$XOH + Eu^{3+} \Leftrightarrow XOEu^{2+} + \mathrm{H}^{+} \qquad \mathrm{K}_{\mathrm{Eu1}}^{\mathrm{int}} = \frac{[XOEu^{2+}][H^{+}]}{[XOH][Eu^{3+}]} \exp(F\psi_0 / RT) \tag{3.13}$$

$$XOH + Eu^{3+} + 2NO_3^{-} \Leftrightarrow XOEu(NO_3)_2 + \mathrm{H}^{+} \qquad \mathrm{K}_{\mathrm{Eu2}}^{\mathrm{int}} = \frac{[XOEu(NO_3^{-})_2][H^{+}]}{[XOH][Eu^{3+}][NO_3^{-}]^2} \exp(F(\psi_0 - \psi_\beta) / RT) \tag{3.14}$$

The stoichiometries, respectively, for adsorptions of Yb and Eu in each adsorption system (sample site) should be the same assuming that the experimentally derived parameters in TLM are self-consistent. The results will be discussed in detail and comparisons performed in the following section for different matrix and fracture surfaces of each sample site.

3.3 Results and Discussion

Both adsorptions of Yb and Eu showed pH-dependent behavior at the eight sample sites. From Figures 3.2 and 3.3, the adsorbed Yb was increased with increasing pH around pH of 3 from a small uptake for most of sample sets. When pH fell in the range from 5 to 6, adsorption attained a full saturation and continued to high pH values. Adsorption behavior of Yb^{3+} suggests that it is a moderately to weakly binding cation electrostatically attracted by the charged surface to form the outer-sphere complexation. Conclusively, the observed sorption of ytterbium at low pH was limited by ion exchange and sorption on the hydroxyl sites; while enhanced by the strong hydrolysis tendency at high pH. The reaction equations and simulation results of TLM can satisfactorily and qualitatively explain the competition among complexation of surface free hydroxyl groups and hydrolysis of Yb at different pHs.

The reversibility of Yb adsorption respectively on Hematite and Alumina may occur at low surface loading and no desorption of Yb at high surface loading (Marmier and Fromage, 1996). Coppin et al. (2002) used an isotopic exchange between clay and solution as an analogue of the microscopic reversibility of sorption of Sm and Yb on kaolinite and smectite. Their results showed that the sorption reversibility of Sm and Yb were not complete for both smectite and kaolinite. And lanthanides were easily to form as the outer-sphere complexes than atoms to be absorbed as inner-sphere complexes. There is a good agreement between the previous research and our simulation about Yb adsorption on volcanic rocks.

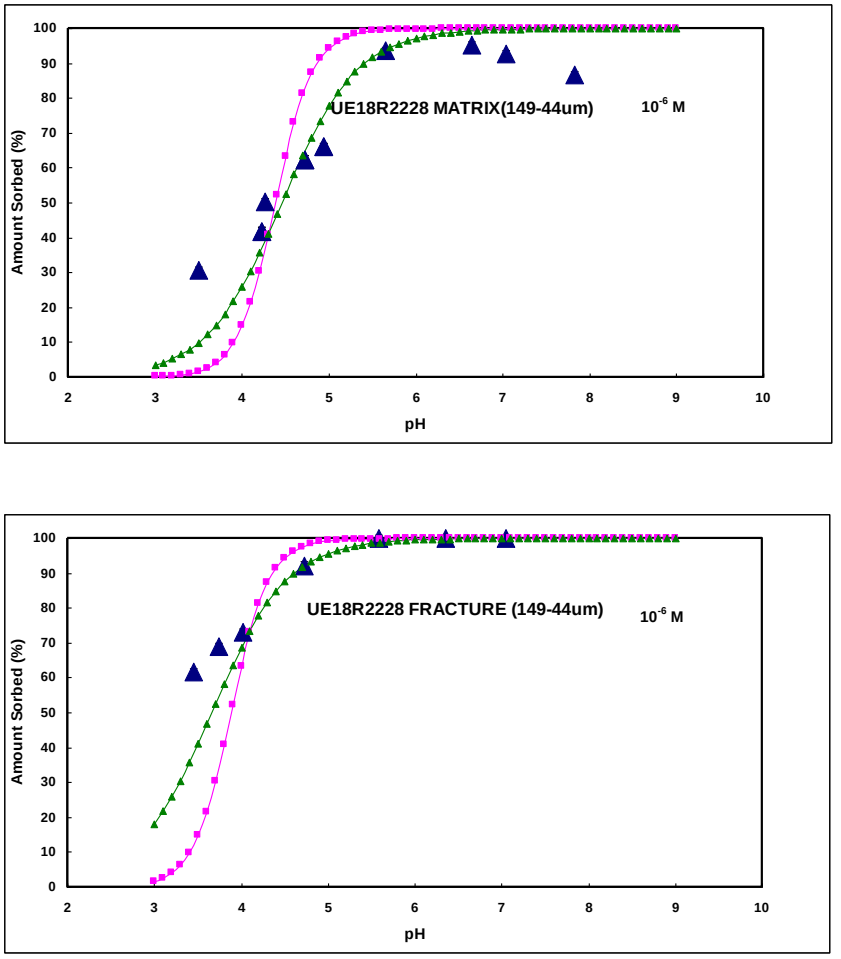

Figure 3.2 Adsorption envelope of Yb on the matrix and fracture surfaces of rock sample collected at UE18R-2228 site. The data show that adsorption of Yb was positively proportional to pH and became saturated around at pH 5-6.

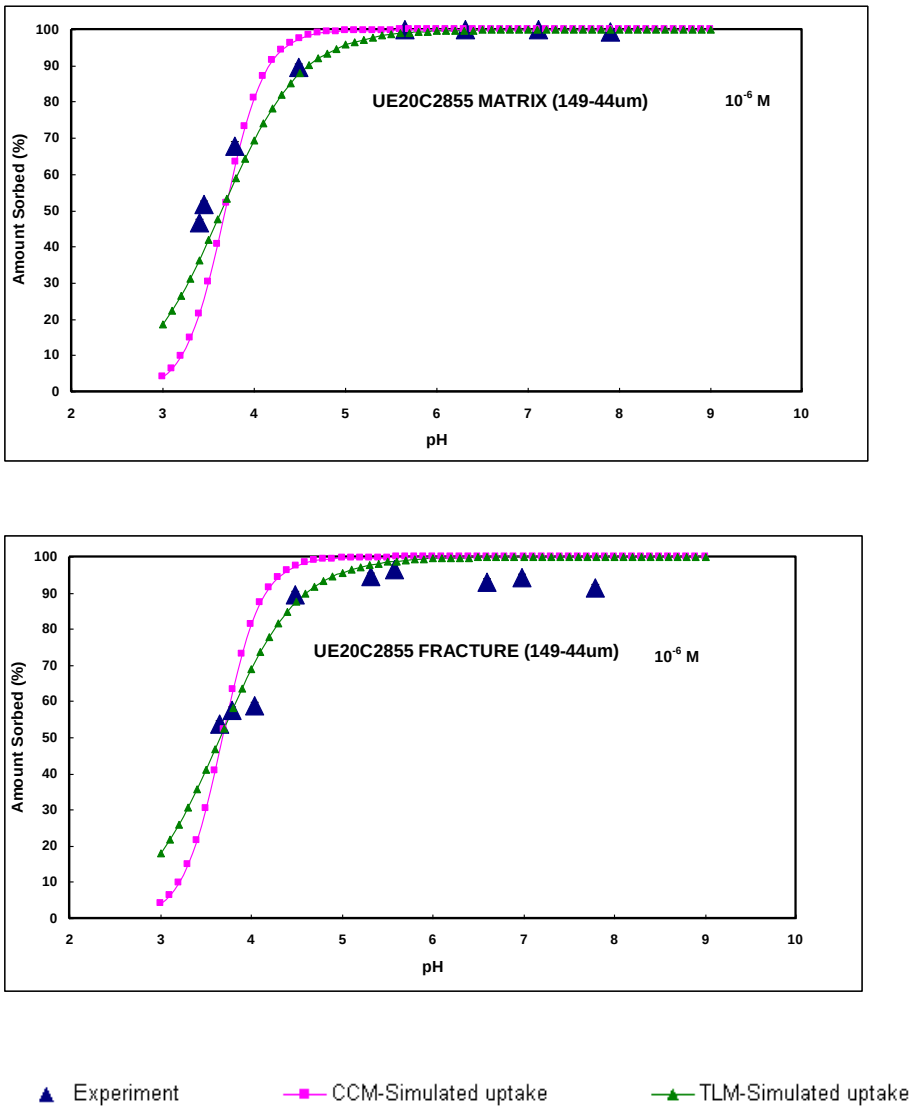

Figure 3.3 Adsorption envelope of Yb on the matrix and fracture surfaces of rock sample collected at UE20C-2855 site. The data show that adsorption of Yb was positively proportional to pH and became saturated around at pH 5-6.

Europium adsorption showed two different sorption mechanisms shown in Figures 3.4 and 3.5. With increasing pH, the adsorbed uptake of Eu was enhanced and obtained a peak at pH range from 6 to 7 and then decreased. So the mechanism of Eu adsorption seemed more complicated with two processes. The reaction equations and simulation

results of TLM can qualitatively demonstrate the ion exchange with hydrogen ions is dominant at low pH, whereas, the metal binding by specific sites might dominate at high pH. Based on the derived constants of the surface complexation reactions in TLM, the point of zero charges of the eight volcanic rock surfaces were the same at the pH of 5.3. The laboratory adsorption measurement agreed well with the calculated value. This value demonstrated that the volcanic rock surface is protonated when pH is lower than 5.3 and the adsorption is simple electrostatic interactions. When pH is higher than 5.3, the adsorption cannot be explained only as electrostatic ion exchange reactions. Some researchers also found the similar adsorption behavior of As (Decker et al., 2006). Clark et al. (1998) outlined that some factors of Eu adsorption in the sandy soils included pH, ionic strength, Eu concentration, competing cations and soil aging. Regarding the limitation of SCM on describing the real complicated geochemical situation, they suggested some factors which may help explain the measured Eu transport in the field.

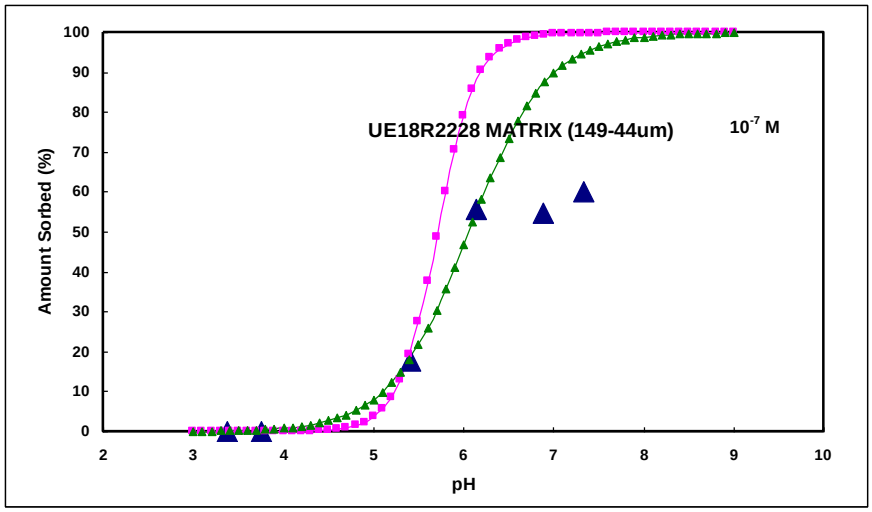

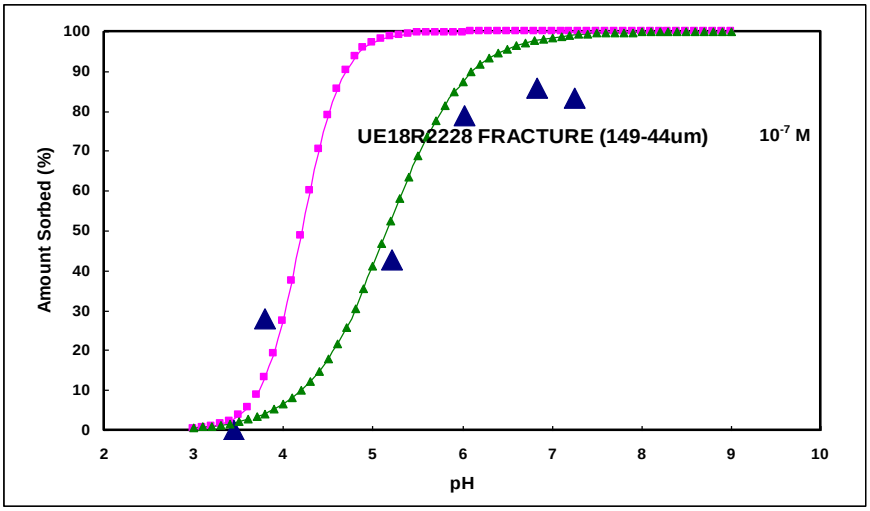

Experiment CCM-Simulated uptake TLM-Simulated uptake

Figure 3.4 Adsorption envelope of Eu on the matrix and fracture surfaces of rock sample collected at UE18R-2228 site. The data show that adsorption of Eu obtained a peak at pH 6-7.

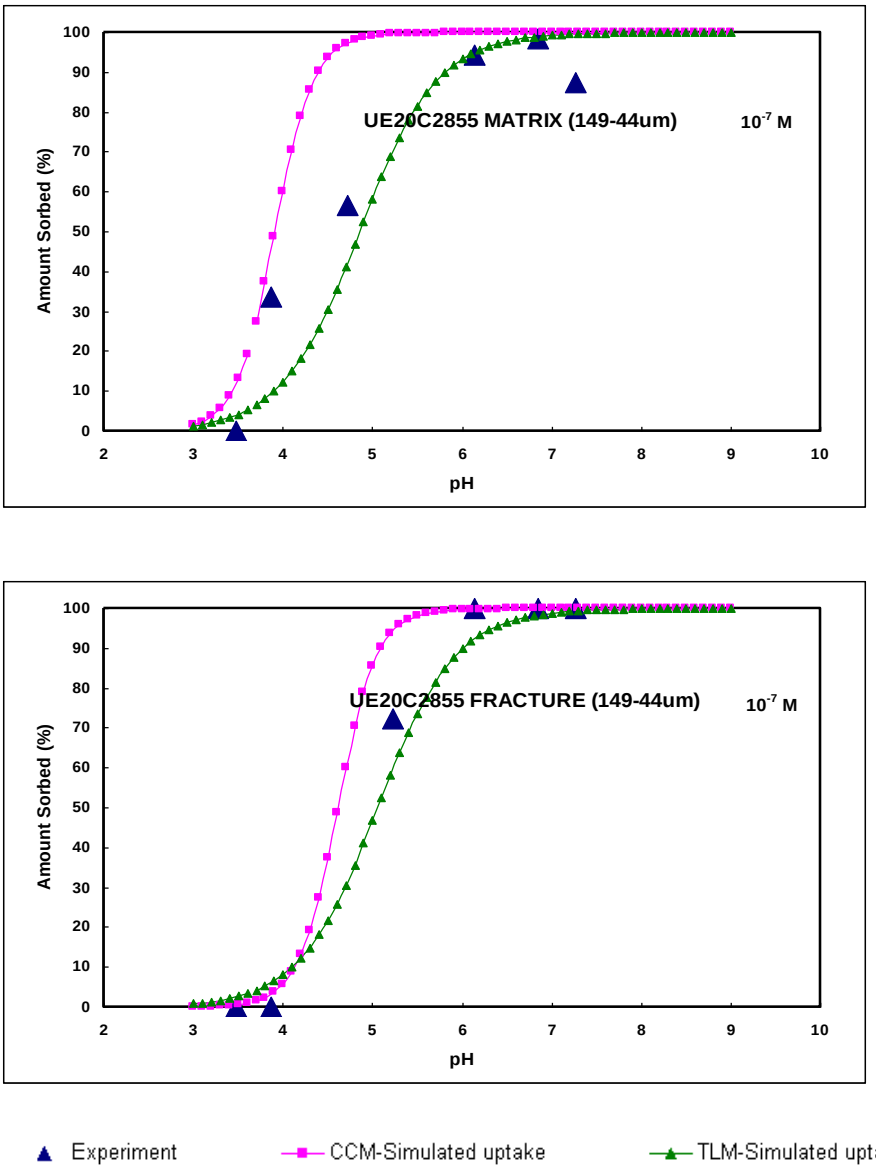

Figure 3.5 Adsorption envelope of Eu on the matrix and fracture surfaces of rock sample collected at UE20C-2855 site. The data show that adsorption of Eu obtained a peak at pH 6-7.

Apparently, there exist the buffering plateaus around the point of zero charges pH_{PZC} (or the pH of zero net protonization) for both adsorptions of ytterbium and europium.

3.3.1 Comparison between Sample Sites

It is obvious that the adsorption uptakes of Yb and Eu are both proportional to pH value. Higher pH value, the surface hydroxyl sorption sites are more negatively charged which leads to the higher adsorption of Yb and Eu. This may indicate that the retardations of Yb and Eu are unignorable in WPM aquifer and groundwater system. Additionally, the results showed that sorptions of Yb and Eu on matrix and fracture surfaces are not that different according to observed experiments and derived parameters of SCM for each same site. For the same rock sample, slight differences between adsorptions on matrix and fracture surfaces were also observed in the research of Papelis and Um (2003). The reason for limited impacts of adsorption surface is probably due to their similar mineralogy and close specific surface area.

3.3.2 Comparison between Surface Complexation Models

Generally, the model with complicated mechanism and parameters has more flexibility of correct simulation of surface complexation reactions. The parameters of CCM and TLM for different samples are listed in Tables 3.3 and 3.4 respectively. Compared with the TLM, the simulated sorption results of CCM are not as good as those of the TLM but with the advantage of less parameter estimation and less interference of parameters. In CCM, the competition of the sorbing ions cannot be accounted in this model even though they have different binding capacities. In TLM, the weakly binding ions can be considered into the sorption competition due to adding an extra plane-β plane.

The pHs of zero net surface charges, pH_{PZC}, of the eight solid surfaces are very close according to $\Delta(pK_{a1} - pK_{a1})$ of TLM.

Table 3.3 Parameters in the constant capacitance model (CCM) respectively for ytterbium and europium respectively

Ytterbium						
Sample sites	pK_{a1}	pK_{a2}	pK_{Yb1}	pK_{Yb2}	Capacitance (Fm^{-2})	Site density
UE18R2228 Fracture	10	8	-5	10.2	0.7	2
UE18R2228 Matrix	10	8	-5	9.2	0.7	2
UE20C2908 Matrix	10	8	-5	10.2	0.7	2
UE20C2855 Matrix	10	8	-4	10.6	0.7	2
UE20C2855 Fracture	10	8	-4	10.6	0.7	2
PM-14823 Matrix	10	8	-5	9.2	0.7	2
PM-1-4823 Fracture	10	8	-5	9.6	0.7	2
PM-2-4177 Matrix	10	8	-5	9.2	0.7	2
Europium						
Sample sites	pK_{a1}	pK_{a2}	pK_{Eu1}	pK_{Eu2}	Capacitance (Fm^{-2})	Site density
UE18R2228 Fracture	10	8	-4	10.2	0.7	2
UE18R2228 Matrix	10	8	-4	7.0	0.7	2
UE20C2908 Matrix	10	8	-4	12.0	0.7	2
UE20C2855 Matrix	10	8	-4	10.6	0.7	2
UE20C2855 Fracture	10	8	-4	9.2	0.7	2
PM-14823 Matrix	10	8	-4	8.7	0.7	2
PM-1-4823 Fracture	10	8	-4	6.2	0.7	2
PM-2-4177 Matrix	10	8	-4	7.0	0.7	2

Table 3.4 Parameters in the triple layer model (TLM) for ytterbium and europium respectively

Ytterbium								
Sample sites	pK_{a1}	pK_{a2}	pK_{cat}	pK_{an}	pK_{Yb1}	pK_{Yb2}	Capacitance (Fm^{-2})	Site density
UE18R2228 Fracture	-6.8	3.8	-8.5	8.5	10.1	4.7	0.7	2
UE18R2228 Matrix	-6.8	3.8	-8.5	8.5	9.3	4.7	0.7	2
UE20C2908 Matrix	-6.8	3.8	-8.5	8.5	9.7	4.7	0.7	2
UE20C2855 Matrix	-6.8	3.8	-8.5	8.5	10.3	4.7	0.7	2
UE20C2855 Fracture	-6.8	3.8	-8.5	8.5	10.1	4.7	0.7	2
PM-14823 Matrix	-6.8	3.8	-8.5	8.5	9.1	4.7	0.7	2
PM-1-4823 Fracture	-6.8	3.8	-8.5	8.5	9.1	4.7	0.7	2
PM-2-4177 Matrix	-6.8	3.8	-8.5	8.5	9.1	4.7	0.7	2
Europium								
Sample sites	pK_{a1}	pK_{a2}	pK_{cat}	pK_{an}	pK_{Eu1}	pK_{Eu2}	Capacitance (Fm^{-2})	Site density
UE18R2228 Fracture	-6.8	3.8	-8.5	8.5	9	4.7	0.7	2
UE18R2228 Matrix	-6.8	3.8	-8.5	8.5	8.1	4.7	0.7	2
UE20C2908 Matrix	-6.8	3.8	-8.5	8.5	11.2	4.7	0.7	2
UE20C2855 Matrix	-6.8	3.8	-8.5	8.5	9.3	4.7	0.7	2
UE20C2855 Fracture	-6.8	3.8	-8.5	8.5	9.1	4.7	0.7	2
PM-14823 Matrix	-6.8	3.8	-8.5	8.5	9.3	4.7	0.7	2
PM-1-4823 Fracture	-6.8	3.8	-8.5	8.5	8.5	4.7	0.7	2
PM-2-4177 Matrix	-6.8	3.8	-8.5	8.5	9.3	4.7	0.7	2

3.3.3 Parameter Optimization and Identification

Although surface complexation modeling has been intensively practiced in last three decades, there are many uncertainties in parameters estimation. The relevant investigation showed that a range of the intrinsic acidity constant and the background electorate surface complexation reaction constants can fit the experiment sorption results equally well. Unclear sorption mechanisms and amorphous parameter interferences impose uncertainty in numerical modeling. This situation makes optimization and justification of parameters quite necessary. According to the experimental protocols presented by Hayes et al. (1991), optimized parameters (the best fit) of TLM for Yb and Eu adsorptions on volcanic rocks were conducted as follows.

3.3.3.1 Optimization of TLM Parameters

Based on Hayes et al's sensitivity analysis (1991), a unique set of parameters for SCM can be obtained to match the observed adsorption behavior. In TLM, seven parameters can be optimized to match the measured adsorption edges, including two surface protolysis constant parameters (K_{a1} and K_{a2}), inner-layer capacitance (C_1), outer-layer capacitance (C_2), surface sites, and two electrolyte surface-binding constants (K_{an} and K_{Cat}). The site density can be derived from the measured values including surface area, site density and solids concentration. In this study, the site densities of different sample sites were not measured by using a standard tritium exchange measurement. Instead, a fixed site density of 2 sites nm^{-2} was used for each sample site because of its less influence (Hayes et al., 1991) and requirements of standardization of

surface complexation modeling (Davis and Kent, 1990). A usually selected value of outer capacitance, 0.2 F/m^2, was assigned to C_2 in TLM simulation. Hayes et al. (1991) found that the two optimized electrolyte binding constants are insensitive to change when ΔpK_a is equal to 4. There is no compelling way to directly measure integral capacitance (C_1), a suggested range from 0.6 F/m^2 to 1.2 F/m^2 was selected by referencing (Hayes et al., 1991).

The optimization was divided into two steps: (1) firstly, to perform the sensitivity analysis of C_1 by changing its value from 0.6 F/m^2 to 1.2 F/m^2 while keeping other parameters constant and to choose the suitable value of C_1 which should correspond with the minimum of calculated model fits; (2) secondly, to perform the sensitivity analysis of the two surface protolysis parameters by changing ΔpK_a from 0 to 8 while keeping the suitable C_1 and other parameters constant.

The adjustable parameters of TLM were optimized to obtain a unique best-fit by adopting a "standard" protocol for avoiding nonunique fits (Hayes et al., 1991). A nonlinear parameter estimation and optimization package, PEST - parameter estimation technique (Doherty, 2004), was linked with TLM to run together in the parameter optimization iteration. PEST is model-free meaning that this package is not limited by the existing models containing parameters to be estimated or optimized. PEST is able to be linked with a model, running to adjust the parameters until results of the existing model match well with measurements. The method of weighted least squares is applied in

PEST. Optimized parameters of TLM are listed in Table 3.5, which would be justified and compared with other relevant researches in the flowing section.

Table 3.5 Optimized intrinsic surface complexation constants of TLM

Yb					
Sample Site	pK_{a1}	pK_{a2}	pK_{cat}	pK_{an}	Capacitance (Fm^{-2})
UE18R2228 Fracture	-6.349	3.548	-8.500	1.000	1.200
UE18R2228 Matrix	-6.603	3.690	-8.500	1.000	1.200
UE20C2908 Matrix	-5.817	3.251	-8.500	9.541	1.200
UE20C2855 Matrix	-6.693	3.740	-8.500	12.00	0.657
UE20C2855 Fracture	-6.253	3.494	-8.500	8.500	0.651
PM-1-4823 Matrix	-6.611	3.694	-8.500	8.504	0.707
PM-1-4823 Fracture	-8.306	4.642	-8.500	1.000	1.200
PM-2-4177 Matrix	-6.800	3.800	-8.500	8.500	0.700
Eu					
Sample Site	pK_{a1}	pK_{a2}	pK_{cat}	pK_{an}	Capacitance (Fm^{-2})
UE18R2228 Fracture	-6.934	3.875	-8.500	12.000	0.700
UE18R2228 Matrix	-6.846	3.826	-8.500	11.648	0.600
UE20C2908 Matrix	-6.342	3.544	-8.500	8.500	0.600
UE20C2855 Matrix	-6.791	3.795	-8.500	9.206	1.200
UE20C2855 Fracture	-6.943	3.880	-8.500	8.500	1.200
PM-1-4823 Matrix	-6.162	3.443	-8.500	12.00	0.600
PM-1-4823 Fracture	-6.822	3.812	-8.500	1.00	0.600
PM-2-4177 Matrix	-4.058	2.267	-8.500	12.00	0.600

The "composite sensitivity" of each adjustable parameter expressed in Equation (3.19) were recorded and listed in Table 3.6 for the eight sample surfaces.

$$s_i = \frac{V_{ii}^{-1}}{m} \tag{3.19}$$

where, m is the number of laboratory observations; n is the number of adjustable parameters; $V_{ii} = (J^t Q J)_{ii}^{-1/2}$; J is the Jacobian matrix of a m×n matrix M, the function which maps n parameters into m observations; and Q is a m×m diagonal matrix composed of the square of the weight of each observation.

Parameters with larger sensitivities contribute more to parameter upgrade and optimization. The parameters with lowest sensitivities are likely to be temporarily held in the optimization iteration of PEST. This can explain that all pK_{cat} of eight sample surfaces do not change after the completion of optimization process due to its low sensitivity. It is important to mention that pK_{a1} and pK_{a2} were tied together in the optimization process. The parent parameter is pK_{a1} and pK_{a2} is the tried parameter. Sensitivity analysis showed that pK_{a1} always has the highest sensitivity among adjustable parameters of TLM.

Table 3.6 Sensitivity of adjustable parameters in TLM upon the completion of optimization process

Sensitivity for Yb				
Sample sites	pK_{a1}	pK_{cat}	pK_{an}	Inner Capacitance
UE18R2228 Fracture	8.002	0.000	5.199E-04	3.683E-03
UE18R2228 Matrix	8.507	0.000	6.368E-04	2.604E-03
UE20C2908 Matrix	4.702	0.000	3.880E-04	1.331E-02
UE20C2855 Matrix	8.271	0.000	1.500E-03	1.669E-02
UE20C2855 Fracture	4.290	0.000	8.403E-04	2.422E-17
PM-14823 Matrix	5.856	0.000	1.213E-03	1.443E-02
PM-1-4823 Fracture	4.850	0.000	4.419E-03	6.379E-03
PM-2-4177 Matrix	0.354	0.000	0.000	0.000
Sensitivity for Eu				
Sample sites	pK_{a1}	pK_{cat}	pK_{an}	Inner Capacitance
UE18R2228 Fracture	3.518	0.000	3.676E-04	0.000
UE18R2228 Matrix	7.680	0.000	5.155E-04	5.102E-03
UE20C2908 Matrix	5.878	0.000	0.000	2.976E-02
UE20C2855 Matrix	2.248	0.000	5.199E-04	4.464E-03
UE20C2855 Fracture	3.097	0.000	7.353E-04	2.305E-17
PM-14823 Matrix	1.951	0.000	2.604E-04	5.208E-03
PM-1-4823 Fracture	4.962	0.000	9.707E-04	1.378E-02
PM-2-4177 Matrix	1.746	0.000	0.000	7.366E-03

3.3.3.2 Justification of the Optimized Parameters

There might be nonunique fits to experimental adsorption data, and the parameter values of SCM are imperfectly known. Justification of parameters of TLM was conducted after optimization to further reduce the uncertainty of parameter estimation. As mentioned above, sample rocks are mainly composed of quartz and feldspar with a very close ratio of these two minerals. As we know, quartz and feldspar are the most common minerals on the earth's crust. Quartz is always composed of SiO_2 in spite of existing different varieties and structures. Feldspar is silicates of aluminum mainly including three types: Orthoclase ($KAlSi_3O_8$), Albite ($NaAlSi_3O_8$) and Anorthite ($CaAl_2Si_2O_8$).

Adsorptions on Quartz and Feldspar have been investigated in previous research, providing valuable information as reference. Discrepancy with the reported values in literature may provide clues to the reasonability of derived parameters to some extent. The smaller the discrepancy, the more acceptable are the parameters. Table 3.7 lists some surface complexation constants consistent to TLM adverting to wide ranges of ion strength for quartz and feldspar in literatures. The protonation constants and association constants of sample rocks are between those of quartz and silicate in Table 3.7. This can be explained by the mineralogy of sample rocks being mainly composed of quartz and feldspar.

Table 3.7 Literature values of TLM parameters in previous research

Solid	Electrolyte	pK_{a1}	pK_{a2}	pK_{cat}	pK_{an}	Inner Capacitance (Fm^{-2})
Magnetite (Fe_3O_4 : 96%; SiO_2: 2.4%)[a]				-6.43 $XOHEu^{3+}$	14.87 $XOEu(OH)^2$	
Synthetic Hematite (Fe_2O_3: 99%)[b]		-9.81	6.38	-5.6 $XOHYb^{3+}$		
Quartz (SiO_2: 99.9%)[c]			5.62			
Natural sediment (Si: 29.53%)[d]						1.6
Quartz[e]	NaCl	-4.83	1.64			0.97
Quartz[f]	NaCl					1.00
Quartz[f]	$CaCl_2$	-6.2	2.2	-	0.2	0.81
Quartz[g]	KNO_3	-6.2	2.2	0.2	2.0	1.05
SiO_2[h]	NaCl	-7.2	2.0	-	6.7	1.40

Note: % is mass percentage; [a] is from Catalette et al., (1998); [b] from Marmier et al., (1997); [c]from Arnold et al., (1999); [d] from Wen et al., (1998); [e] from Criscenti and (1999); [f] from Riese (1982); and [g]from Huang (1996).

Research of Tertre et al. (2005) showed that Eu adsorbed onto kaolinite and montmorillonite in the form of inner and outer sphere complexes investigated by using time resolved laser fluorescence spectroscopy (TRLFS). Ytterbium is adsorbed on rutile in the form of tetranuclear species and possibly two to four coexisting cations hydrolysis states according to X-ray results of Piasecki and Sverjensky's research (2008). These spectroscopic results are consistent with Yb and Eu complexes and the stoichiometry of reactions constrained in Equations (3.1)-(3.18).

3.3.4 Calculation of Distribution Coefficients with the Laboratory-derived Surface Complexation Model

The research of Sauve et al., (2000) showed that most of the variability in the distribution coefficient, K_d, up to several orders of magnitude, are attributed to pH. A dramatic change in distribution coefficient of Yb was observed around at pH 9.0 in Wang et al.'s experiments (2000). Estimation of K_d with SCM, can constrain the estimation error to dramatically lower level than direct estimation. Having a wide application range of ionic strength, the laboratory-derived TLM with the optimized parameters was used to simulate adsorption isotherms of Yb and Eu, respectively. Then, an important parameter of transport modeling, K_d, was calculated according to simulated adsorption isotherms.

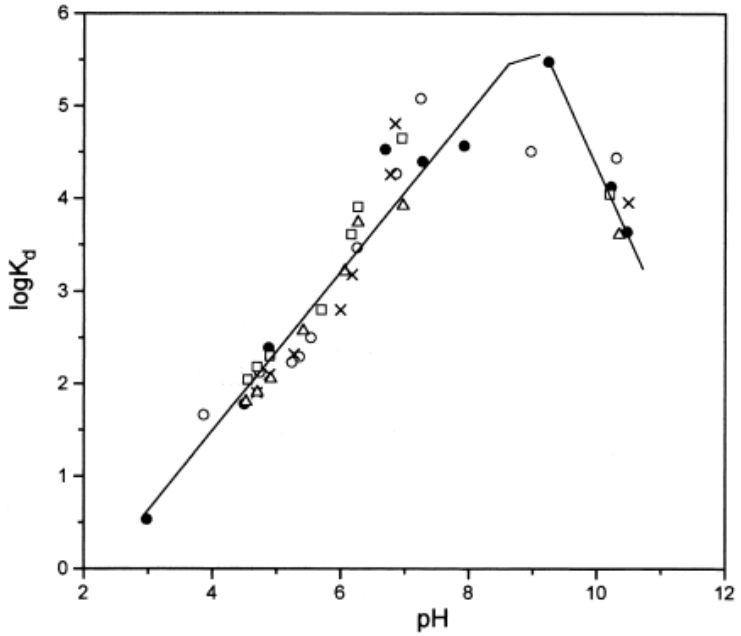

Figure 3.6 Variation of the logarithm of distribution coefficient of Yb with pH: (•) 0.01 mol/l $NaNO_3$; (o) 0.1 mol/l $NaNO_3$; (×) 0.5 mol/l $NaNO_3$; (Δ) 1.0 mol/l $NaNO_3$; (□) 2.0 mol/l $NaNO_3$ (from Wang et al., 2000)

Adsorption isotherms were simulated at pH 8.5, 0.1 M of ionic strength, and 25 ºC. The reason for selecting the above pH value is that the groundwater typically varies around 8 to 9 in the study area. A Langmuir isotherm expressed in Equation (3.20) was used for comparison and fitting of distribution coefficients.

$$C = \frac{C_{\max} \cdot K_d \cdot C_{aqu}}{1 + K_d \cdot C_{aqu}} \tag{3.20}$$

where, C is the adsorbed concentration of the adsorbate; and C_{max} is the maximum adsorption capacity of the adsorbate; K_d is the distribution coefficient; and C_{aqu} is the aqueous concentration of adsorbate at equilibrium.

For the eight rock surfaces, calculated adsorption isotherms of Yb and Eu were compared and shown in Figures 3.7 and 3.8, respectively. The solid lines with various markers represent the TLM fit with optimized intrinsic constants. The dash line with circle markers stands for Langmuir fit for the averaged adsorption isotherm of all eight rock surfaces.

The fitted averaged distribution coefficient and averaged maximum adsorption capacity of Yb are 0.0499 (L/meq) and 32.47 (g Yb^{3+}/ g adsorbent); those of Eu are 0.0525 (L/meq) and 29.91 (g Yb^{3+}/ g adsorbent) under the above geochemical condition. Calculation results show that Yb is bound to be adsorbed on the volcanic rock surfaces equally to Eu under same condition. This is expected because of their very close atom mass numbers. The calculated K_d by Langmuir fitting are listed in Table 3.8 for each sample rock surface.

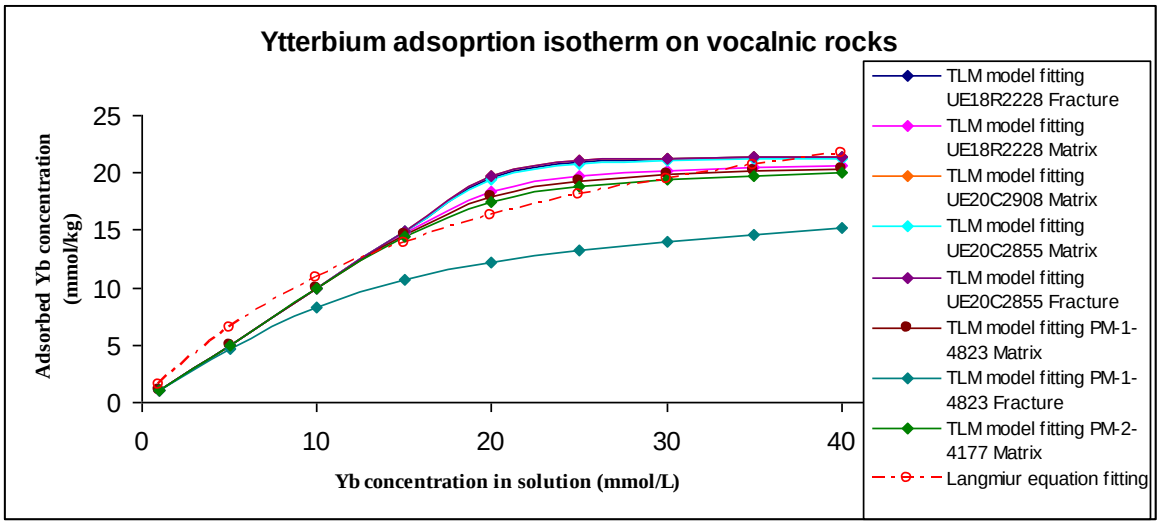

Figure 3.7 Ytterbium adsorption isotherms on the volcanic rocks at pH=8.5, I=0.1M, and T=25ºC. The plot shows a Langmuir adsorption isotherm can averagely fit the adsorption of Yb on volcanic rocks.

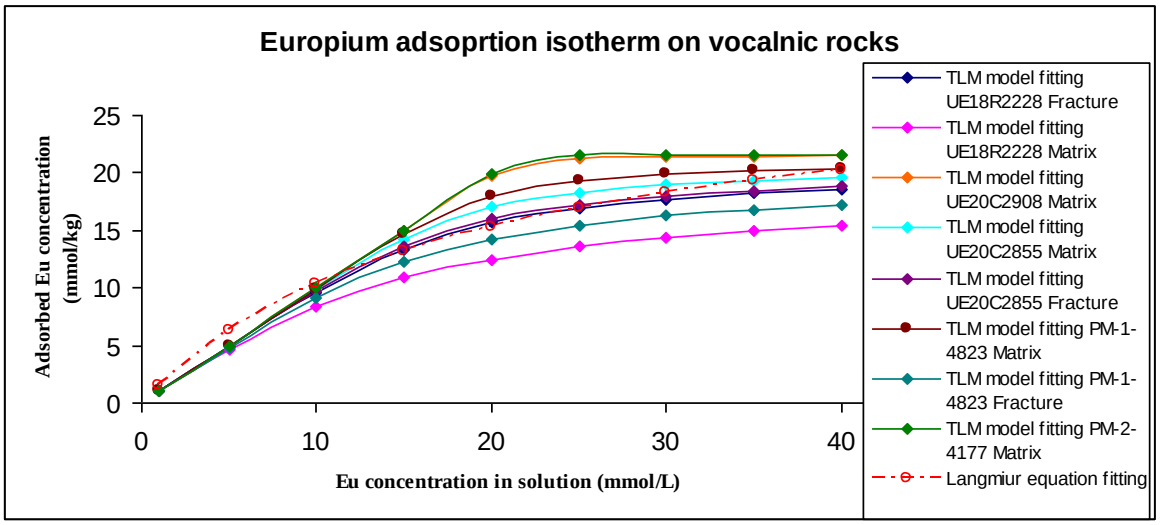

Figure 3.8 Europium adsorption isotherms on the volcanic rocks at pH=8.5, I=0.1M, and T=25ºC. The plot shows a Langmuir adsorption isotherm can averagely fit the adsorption of Eu on volcanic rocks.

Table 3.8 Calculated distribution coefficients of Yb and Eu for each sample rock surface

Distribution coefficient of Yb		
Sample sites	C_{max}	K_d g adsorbate/ g adsorbent
UE18R2228 Fracture	35.3600	0.0476
UE18R2228 Matrix	33.0910	0.0500
UE20C2908 Matrix	35.4071	0.0476
UE20C2855 Matrix	35.0797	0.0480
UE20C2855 Fracture	35.4206	0.0476
PM-14823 Matrix	32.2483	0.0511
PM-1-4823 Fracture	21.6461	0.0616
PM-2-4177 Matrix	31.4876	0.0519
Distribution coefficient of Eu		
Sample sites	C_{max}	K_d g adsorbate/ g adsorbent
UE18R2228 Fracture	28.1453	0.0554
UE18R2228 Matrix	22.1932	0.0608
UE20C2908 Matrix	35.6947	0.0473
UE20C2855 Matrix	30.5781	0.0528
UE20C2855 Fracture	28.6578	0.0549
PM-14823 Matrix	32.4592	0.0508
PM-1-4823 Fracture	25.4889	0.0580
PM-2-4177 Matrix	36.1139	0.0468

3.4 Conclusions

The batch reactor experiments were conducted to investigate the adsorption behavior of Yb and Eu on volcanic rocks in the YM and NTS area. A synthetic typical groundwater of the study area was used in experiments to reflect the real groundwater environment. Experimental results show that both adsorptions of Yb and Eu are pH dependent and moderately to weakly binding. With increasing pH, the adsorbed uptakes of Yb attain a peak plateau around pH of 5 to 6, indicating hydrolysis adsorption mechanism at high pH conditions. However, after reaching an adsorption peak, uptakes of Eu behaved differently without remaining but reducing. This cannot be explained only by hydrolysis adsorption mechanism.

On the basis of observed adsorption edges of Yb and Eu, two kinds of SCM including CCM and TLM were applied to describe the specific adsorption reactions for the eight rock surfaces. Through comparison of simulation with CCM, TLM is a more desired model to simulate adsorptions of Yb and Eu on volcanic rocks of concern. The reason is that TLM is more feasible and capable of counting for weakly binding and ion competition than CCM. Simulated adsorption edges with TLM match better with observed ones than those of CCM for both of Yb and Eu.

To reduce uncertainty of estimated parameters in TLM, parameter optimization was preformed for protolysis constants, capacitance constant, and surface binding constants by linking PEST. Through iteration, the five parameters of TLM were optimized and relevant sensitivity analysis was conducted as well. Goodness-of-fit and sensitivity

analysis showed that pK_1 has the highest sensitivity and pK_{cat} has the lowest sensitivity among adjustable parameters of TLM. This provides some insightful information for parameter justification of TLM, indicating protonation and association constants may be the most concern because of their relatively significant impacts in model fitting.

Parameter justification was performed by comparing with relevant microscopic and spectroscopic researches about quartz and feldspar, main compositions of sample rocks. It can be found that the derived surface reaction constants have acceptable differences from reported parameter values in literature. Furthermore, spectroscopic results showed that Yb and Eu have inner and outer spheres of adsorption mechanism. This is in agreement with the adopted surface complexation reactions and simulation results in this study.

The TLM with optimized parameters was used to simulate the adsorption isotherm under typical geochemical condition of groundwater in the study area. Consequently, distribution coefficients of Yb and Eu were estimated, respectively, by using Langmuir isotherm fitting. It can be found that Yb is equally apt to be adsorbed on volcanic rocks with respect to Eu because of their similar weight of cations.

3.5 References

Aamrani, Z.F., Duro, L., Pabloa, J., and Brunoc, J., 2001. Experimental study and modeling of the sorption of uranium (VI) onto olivine-rock. Applied Geochemistry, 17, p. 399-408.

Arnold, T., Zorn, T., Bernhard, G., Nitsche, H., 1999. Applying the DDLM to model the

sorption of uranium onto quartz and muscovite. Report FZR-272, Forschungszentrum Rossendorf e.V., Institute of Radiochemistry, Annual Report, 25 pp.

Charles, F.B,. and Mesmer, R.E., 1986. Hydrolysis of Cations, Krieger publishing company, Malabar, FL, 489 pp.

Chia, C.C., Coleman, M., and Katz, E.L., 2006. Bridging the Gap between Macroscopic and Spectroscopic Studies of Metal Ion Sorption at the Oxide/Water Interface: Sr(II), Co(II), and Pb(II) Sorption to Quartz. Environmental Science & Technology, 40, p. 142-148.

Choppin, R.G., and Stout, E.B., 1989. Actinide behavior in natural waters. Science of the Total Environment, 83, p. 203-216.

Clark, B.S., Bryce, L.A., Lueking, D.A., Gariboldi, J., and Serkiz, M.S., 1998. Factors affecting trivalent f-element adsorption to an acidic sandy soil. In: E.A. Jenne (Editor), Adsorption of metals by geomedia. Academic Press, San Diego, pp. 149-162.

Coppin, F., Castet, S., Berger, G., and Loubet, M., 2003. Microscopic reversibility of Sm and Yb sorption onto smectite and kaolinite: Experimental evidence. Geochimica et Cosmochimica Acta, 67, p. 2515–2527.

Criscenti, J.L., and Sverjensky, A.D., 1999. The role of electrolyte anions (ClO_4^-, NO_3^-, and Cl^-) in divalent metal (M^{2+}) adsorption on oxide and hydroxide surfaces in salt solutions. American Journal of Science, 299, p. 828-899.

Curtis, P.G., Davis, A.J., and Naftz, L.D., 2006. Simulation of reactive transport of uranium(VI) in groundwater with variable chemical conditions. Water Resources Research, 42, WR4044, p. 1-15.

Davis, J.A., and Kent, D.B., 1990. Surface complexation modeling in aqueous geochemistry. Rev. Mineral, 23, p. 177–260.

Decker, D., and Papelis, C., 2003. Evaluation of Surface complexation models for radionuclides transport at Nevada Test Site: data availability and parameter evaluation. U.S. Department of Energy Report, Nevada Operations Office U.S. Department of Energy, Las Vegas, Nevada. Publication No. 45185. 67 pp.

Decker, D.L., Papelis, C., Tyler, S.W., Logsdon, M.J., and Simunek, J., 2006. Arsenate and arsenite sorption on carbonate hosted precious metals ore. Vadose Zone Journal. 5, p. 419-429.

Dev, K., Pathak, R., and Rao, N.G., 1998. Sorption behaviour of lanthanum(III), neodymium(III), terbium(III), thorium(IV) and uranium(VI) on Amberlite XAD-4 resin functionalized with bicine ligands. Talanta, 48, p. 579-584.

Doherty, J., 2004. PEST model-independent parameter estimation user manual, 5th Edition. Watermark Numerical Computing, 336 pp.

Farquhar, M.L., Vaughab, C.R., Hughes, J.M., Charnock, J.M., and England, K.E.R., 1997. Experimental studies of the interaction of aqueous metal cations with substrates: Lead, cadmium and copper with perthitic feldspar, muscovite and biotite. Geochimica et Cosmochimica Acta, 61, p. 3051-3064

Gelis, M.V., Chuveleva, A.E., Firsova, A.L., and Bashlykova, B.I., 2003. Sorption of REEs and TPEs on sorbents containing ferrocyanide and ferricyanide ions. Radiochemistry, 45, p. 373-376.

Goldberg, S., Criscenti, J.L., Turner, R.D., Davis, A.J., and Cantrell, J.K., 2007. Adsorption-desorption processes in subsurface reactive transport modeling. Vadose Zone Journal, 6, p. 407-435.

Harris, R.G., Wells, D.J., Angove, J.M., Johnson, B.B., 2006. Modeling the adsorption of organic dye molecules to kaolinite. Clays and Clay Minerals, 54, p. 456-465.

Hayes, F.K., Redden, G., Ela, W., and Leckie, O.J., 1991. Surface complexation models: An evaluation of model parameter estimation using FITEQL and oxide mineral titration data. Journal of Colloid and Interface Science, 142, p. 448-469.

Huang, P., 1996. The effects of the adsorption of metal ions and surfactant behavior on the interfacial behavior of silicate minerals. Ph.D. thesis, University of California, Berkeley, 174 pp.

Ikhsan, J., Wells, D.J., Johnson, B.B., and Angove, J.M., 2005. Surface complexation modeling of the sorption of Zn(II) by Montmorillonite. Colloids and Surfaces A: Physicochemical and Engineering Aspects, 252, p. 33–41.

Johannesson, H.K., Lyons, B.W., Fee, H.J., Gaudette, E.H., and McArthur, M.J., 1993. Geochemical processes affecting the acidic groundwaters of Lake Gilmore, Yilgarn Block, Western Australia: a preliminary study using neodymium, samarium, and dysprosium. Journal of Hydrology, 154, p. 217-289.

Johannesson, H.K., and Stetzenbach, K.J., 1995. Speciation of the rare earth element neodymium in groundwaters of the Nevada Test Site and Yucca Mountain and implications for actinide solubility. Applied Geochemistry, 10, p. 565-572.

Johannesson, H.K., Stetzenbach, K.J., Hodge, V.F., Kreamer, D.K., and Zhou, X., 1997. Delieaton of groundwater flow systems in the southern Great Basin using aqueous rare earth element distribution. Ground Water, 35, p. 807-819.

Katz, E.L., and Hayes, F.K., 1994a. Surface complexation modeling I. Strategy for modeling monomer complex formation at moderate surface coverage. Journal of Colloid and Interface Science, 170, p. 477-490.

Katz, E.L., and Hayes, F.K., 1994b. Surafce complexation modeling II. Strategy for modeling polymer and precipitation reactions at high surface coverage. Journal of Colloid and Interface Science, 170, p. 491-501.

Koretsky, C., 2000. The significance of surface complexation reactions in hydrologic systems: a geochemist's perspective. Journal of Hydrology, 230, p. 127-171.

Krauskopf, K.B., 1986. Thorium and rare-earth metals as analogues for actinide elements. Chem. Geol., 55, p. 323–335.

Marmier, N., Dumonceau, J., and Fromage, F., 1996. Surface complexation modeling of Yb(III) sorption and desorption on hematite and alumina. Journal of Contaminant Hydrology, 26, p. 159-167.

Montavon, G., Markai, S., Andres,Y., and Grambow, B., 2002. Complexation studies of Eu(III) with alumina-bound polymaleic acid: effect of organic polymer loading

and metal ion concentration. Environmental Science & Technology, 36, p. 3303-3309.

Ogard, E. A., Wolfsberg, K., Daniels, W.R., Kerrisk, J., Rundberg, R.S., and Thomas, K.W., 1984. Retardation of radionuclides by rock units along the path to the accessible environment. Materials Research Society Symposia Proceedings, 26, p. 329-336.

Pagnanelli, F., Bornoroni, L., Moscardini, E., and Toro, L., 2005. Non-electrostatic surface complexation models for protons and lead (II) sorption onto single minerals and their mixture. Chemosphere, 63, p. 1063-1073.

Papelis, C., Hayes, F.K., and Leckie, O.J., 1988. HYDRAQL: A Program for the Computation of Chemical Equilibrium Composition of Aqueous Batch Systems Including Surface-Complexation Modeling of Ion Adsorption at the Oxide/Solution Interface, 1.0 version. Department of Civil Engineering, Stanford University, San Francisco, CA. 89 pp.

Papelis, C., and Um, W., 2002. Evaluation of cesium, strontium, and lead sorption, desorption, and diffusion in cores from Western Pahute Mesa, Nevada Test Site, Based on Macroscopic and Spectroscopic Investigations. Publication No. 45187, U.S. Department of Energy Report, Nevada Operations Office U.S. Department of Energy, Las Vegas, NV. 62 pp.

Peacock, C.L., and Sherman, D.M., 2003. Copper (II) sorption onto goethite, hematite and lepidocrocite: A surface complexation model based on an initio molecular

geometries and EXAFS spectroscopy. Geochimica et Cosmochimica Acta, 68, p. 2623-2637.

Piasecki, W., and Sverjensky, A.D., 2008. Speciation of adsorbed yttrium and rare earth elements on oxide surfaces. Geochimica et Cosmochimica Acta, 72, p. 3964-3979.

Quinn, A.K., Byrne, H.R., and Schijf, J., 2006. Sorption of yttrium and rare earth elements by amorphous ferric hydroxide: Influence of solution complexation with carbonate. Geochimica et Cosmochimica Acta, 70, p. 4151-4165.

Riese, A.C., 1982. Adsorption of radium and thorium onto quartz and kaolinite: A comparison of solution/surface equilibrium models. Ph.D. thesis. Colorado School of Mines.

Ruzic, I., 1996. Trace metal complexation at heterogeneous binding sites in aquatic systems. Marine Chemistry, 53, p. 1-15.

Sauve, S., Hendershot, W., and Allen, E.H., 2000. Solid–solution partitioning of metals in contaminated soils: Dependence on pH, total metal burden, and organic matter. Environmental Science & Technology, 34, p. 1125–1131.

Schlegel, L.M., Pointeau, I., Coreau, N., and Reliller, P., 2004. Mechanism of europium retention by calcium silicate hydrates: An EXAFS study. Environmental Science & Technology, 38, p. 4423-4431.

Shundahai Network. Nov 12th 2007. website of Shundahai network, http://www.shundahai.org/area_19_nts.htm.

Takahashi, Y., Tada, A., and Shimizu, H., 2004. Distribution pattern of rare earth Ions between water and montmorillonite and its relation to the sorbed speicies of the ions. Analytical Sciences, l20, p. 1301-1306.

Tertre, E., Berger, G., Simoni, E., Castet, S., Giffaut, E., Loubet, M., and Catalette, H., 2006. Europium retention onto clay minerals from 25 to 150 degrees C; experimental measurements, spectroscopic features and sorption modeling. Geochimica et Cosmochimica Acta, 70, p. 4563-4578.

Wang, X., Dong, W., Dai X., Wang, A., Du, J., and Tao, Z., 2000. Sorption and desorption of Eu and Yb on alumina: mechanisms and effect of fulvic acid. Applied Radiation and Isotopes, 52, p. 165-173.

Wen, X.H., Qin, D., and Tang, H.X., 1998. Surface complexation model for the heavy metal adsorption on natural sediment. Environmental Science & Technology, 32, p. 870-875.

Zavarin, M., Roberts, S.K., Hakem, N., Sawvel, A.M., and Kersting, A.B., 2005. Eu(III), Sm(III), Np(V), Pu(V), and Pu(IV) sorption to calcite. Radiochimica Acta, 93, p. 93-102.

CHAPTER 4

TRANSPORT MODELING OF RARE EARTH ELEMENTS (REES) IN THE YUCCA MOUNTAIN (YM) AREA

One of important processes for radionuclides in the saturated zone is the sorption onto matrix surfaces in the YM area. However, the sorption reaction is simply accounted for by a constant, distribution coefficient, or other empirical adsorption isotherms in most practices. In this study, a thermodynamic surface complexation model was coupled with a groundwater transport model to simulate adsorption reactions. By doing so, the adsorption (retardation) effects on radionuclide transport can be simulated as close as possible to real environments. As analogues of trivalent actinides, two rare earth elements (REEs), ytterbium (Yb) and europium (Eu) were simulated with a PHAST3D model of the site-scale saturated zone of YM, incorporated with a surface complexation model. PHAST3D is a versatile three-dimensional multi-component geochemical transport simulator, consisted of flow model HST3D and geochemical simulator PHREEQC. The experimentally derived surface complexation reaction equations derived from our previous research were included in the geochemical input file of PHREEQC. The hydrogeology model frame was constructed on different rock types and confining layers. The simulated concentration contours showed that adsorption reactions may impede radionuclide transport significantly. Additional characteristic information and observations, such as tracer testing, borehole log, are needed for model calibration and verification in the future.

4.1 Introduction

Previous studies show that processes important to radionuclide transport in the saturated zone are advection, dispersion, diffusion, and sorption and colloid-facilitated transport (SNL, 2007). Presently the groundwater model has been a prevalent tool capable of simulating complex underground environments. The two kinds of models are different in the purposes of study and usages in practice. Usually, the regional model is used to evaluate the global response to groundwater withdrawal, estimate the travel time of solute transport, and provide boundaries for local groundwater models. The local model is used to study a specific area and detailed information of interest. In southern Nevada, most of the local models are related to radionuclide transport under YM and NTS.

Finite element heat and mass transfer code (FEHM) and transport of unsaturated groundwater and heat version 2 (TOUGH2) are widely used for performing evaluations of YM repository in the past two decades (Arnold et al., 2003; Eddebbarh et al., 2003; Robinson et al., 2003; Zyvoloski et al., 2003; Wu et al., 2004; Pan et al., 2004; Liu et al., 2003; Vrugt et al., 2008; Zhang et a., 2003). Both of them have been modified and improved by incorporating into more field measurements and updated hydrogeologic characteristics. Although both of them have capability of transport simulation of unsaturated and saturated zones, FEHM is more apt to be used for saturated zone and TOUGH2 for unsaturated zone. With the enhanced hydrogeologic understanding and in-situ experiments of YM groundwater system, FEHM and TOUGH2 have been increasingly improved through the calibration and validation. However, the prediction

uncertainty of models is still our main concern because of model-based assumptions and simplifications. It is well accepted that adsorption is one of important processes of radionuclide transport in the YM groundwater. There is no module of surface complexation model (SCM) in the existing FEHM and TOUGH2 for describing thermodynamic adsorption reactions. A constant, K_d, is used in TOUGH2 to count for the adsorbed solutes on the interface between groundwater and solids (Pruess, 1991). Some empirical adsorption isotherms are applied in FEHM to reflect adsorption behavior of reactants along the groundwater flow path (Birdsell et al., 1995; Zyvoloski et al., 1997; Zyvoloski et al., 1999). Actually, adsorption reactions are complicated in the natural environment as they are, highly dependent on the chemistry of the solution and solid rock surfaces. The K_ds and simple isotherms are empirical and sensitive with limitations in applications. It is an enigma how much adsorption reactions impacts radionuclide transport in the YM groundwater system.

A thermodynamically related SCM is needed to decipher the retardation of adsorption reactions on radionuclide transport in the YM groundwater system. Process-based SCM is superior over K_d and empirical adsorption isotherms by closely describing the adsorption behaviors of radionuclides in natural circumstances. In previous researches, different experiments and numerical modeling were proposed in various application cases or practical environments according to specific purposes. Incorporating of a surface complexation model into transport model has been investigated and implemented to

simulate the realistic configurations of geological media (Goldberg et al., 2008; Montarnal et al., 2007; Jacques et al., 2008; Zachara et al., 2007; Graf and Therrien, 2007). Goldberg et al. (2008) used a constant capacitance model (CCM) to simulate adsorption of arsenic (As) and selenium (Se) on soils around ash disposal. In addition, the anion surface complexation constant was optimized and coupled into transport model to predict the attenuation of As and Se in various geochemical conditions. Montarnal et al. (2007) incorporated various chemical codes into flow codes in order to assess validation of numerical tools in prediction of radionuclide transport. Chemical models used in this research are PHREEQC and CHESS, while flow models combined are CAST3M, MT3D and TRACES. Different combinations of chemical and flow modules were applied to simulate uranium transport and clay-cement interactions, respectively. Surface complexation reaction was included to describe the realistic circumstances. Jacques et al. (2008) applied the HP1 multi-component reactive model to simulate the migration of Ca, P and U in a field soil. In this case study, surface complexation reactions and cation exchange were considered in the interactions between water and solid. The variances of distribution coefficients were found more than three orders of magnitude due to change in pH values in solution.

4.2 Evaluation of PHAST3D

Solute transport will be simulated by combining surface complexation modeling with a mountain-scale transport model of YM in this study. The mountain-scale transport model is conceptualized on the basis of PHAST3D, a 3-D reactive multi-component geochemical

model as well for the simulation of groundwater flow, heat and multi-components reactive solute transport (Parkhurst et al., 2004). This model consists of a groundwater flow model, HST3D, and a geochemical model, PHREEQC (Parkhurst and Appelo, 2004). The HST3D is a program for heat- and solute-transport simulation in a 3-D saturated groundwater system with variable density and viscosity (Kipp, 1997). Many geochemical equilibrium and kinetic reactions can be simulated with PHREEQC involving aqueous, mineral, gas, solid-solution, surface-complexation, and ion-exchange reactions (Parkhurst and Appelo, 1999). In each time step, the transport of multiple components is firstly solved by using HST3D with a finite difference method and reactions in each computational cell is solved by using PHREEQC. The transport and reactions are repeated in each transient stress period until the simulation is completed (Parkhurst et al., 2004).

PHAST3D has versatile capabilities of applications providing convenient options for boundary conditions and friendly input/output interface. The evaluation of PHAST3D has been conducted with some typical benchmark problems prior to practical applications to rare earth element transport in the YM area in this study. Three diverse well-documented literature benchmarks were selected in this paper and the simulated results were compared with the analytic solutions and/or results of other similar models. For comparison, simulation results of some bench marks with PHAST3D were against with those with PHT3D, a reactive multicomponent transport model for saturated porous media (Prommer, 1999). PHT3D is incorporated in the transport model MT3DMS (Zheng and Wang, 1998)

and geochemical model, PHREEQC-2 (Parkhurst and Appelo, 1999). PHT3D is able to simulate various equilibrium reactions (speciation, cation exchange, dissolution and precipitation) and kinetic reactions (biodegrading, dissolution and precipitation) (Prommer, 1999).

4.2.1 One-Dimensional Transport Controlled By Kinetic Reactions

Firstly, the problem of one-dimensional transport controlled by kinetic biodegradation was used as one of benchmarks (Parlange et al., 1984; Essaid and Bekins 1997):

$$x = \frac{v}{v_{\max}}[K \ln(\frac{C}{C_0}) + C_0 - C] \tag{4.1}$$

with $$\frac{\partial C}{\partial x} = 0 \quad at \quad x = L \tag{4.2}$$

where x is the axis of distance, L is the maximum distance between at the inflow and outflow boundaries, v is effective velocity, v_{max} is maximum effective velocity, C is solute concentration, C_0 is initial concentration at the inflow boundary, and K is half saturation concentration.

The simulated results with PHAST3D and PHT3D were compared with Essaid and Bekins's analytic solution (1997) shown in Figure 4.1. The hydrogeologic and geochemical parameters used in this benchmark simulation with PHT3D and PHAST3D are listed respectively in Table 4.1.

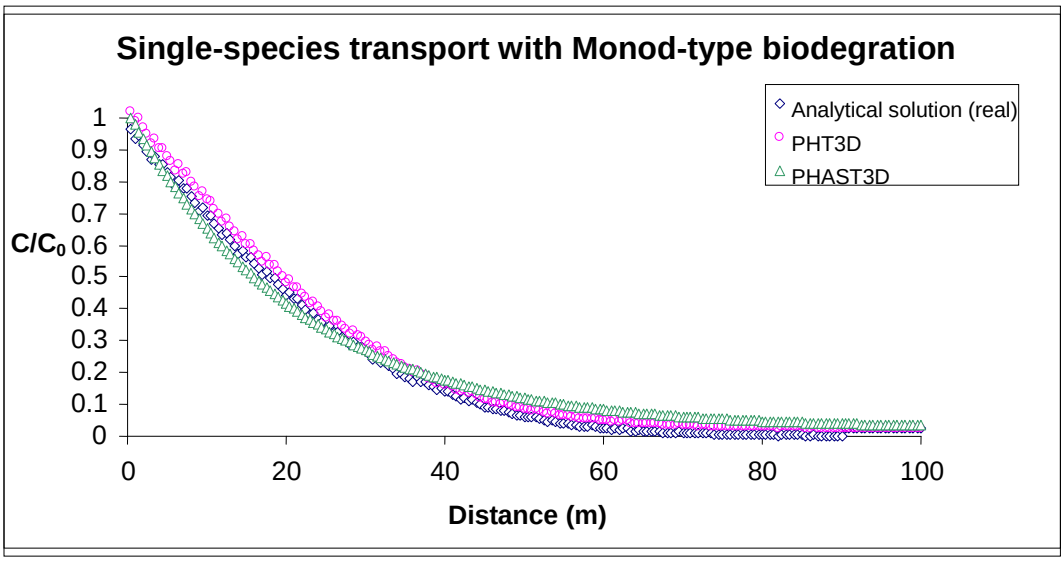

Figure 4.1 Comparison among simulated results of PHT3D (pink circle), simulated results of PHAST3D (green triangle) and analytical solutions (blue diamond). This plot shows that the simulated results of PHT3D and PHAST3D both match with the analytical solutions.

Table 4.1 The parameters used for Parlange et al (1984) and Essaid and Bekins (1997) benchmarks

Parameter	Value
Flow simulation	Steady state
Simulation time	1826days
Time step	0.25 days
Model length	150 m
Grid spacing	1 m
Effective velocity	0.1 m/day
Dispersive	0 m
Inflow concentration	1.0 mmol/l
Half saturation concentration	0.5 mmol/l
Maximum effective velocity	4.77×10^{-3}/day
Porosity	0.25

Note: the simulated results of PHAST3D are lower than those of PHT3D in close area of inflow.

4.2.2 Multiple Species Transport with Kinetic, Sequential/Parallel Degradation

This benchmark (problem with known analytical solutions) is conducted with one dimensional transport, associated with physical reactions and chemical reactions presented by Sun et al. (1999) with the analytical solution. Physical reactions include advection and dispersion, and chemical reactions refer to a series of one-order kinetic, sequential degradations of 5 species described as following:

$$\frac{\partial C_A}{\partial t} - D\frac{\partial C_A^2}{\partial x^2} + v\frac{\partial C_A}{\partial x} = k_A C_A \tag{4.3}$$

$$\frac{\partial C_B}{\partial t} - D\frac{\partial C_B^2}{\partial x^2} + v\frac{\partial C_B}{\partial x} = y_B k_B C_A - k_B C_B \tag{4.4}$$

$$\frac{\partial C_{C1}}{\partial t} - D\frac{\partial C_{C1}^2}{\partial x^2} + v\frac{\partial C_{C1}}{\partial x} = y_{C1} k_B C_B - k_{C1} C_{C1} \tag{4.5}$$

$$\frac{\partial C_{C2}}{\partial t} - D\frac{\partial C_{C2}^2}{\partial x^2} + v\frac{\partial C_{C2}}{\partial x} = y_{C2} k_B C_B - k_{C2} C_{C2} \tag{4.6}$$

$$\frac{\partial C_{C3}}{\partial t} - D\frac{\partial C_{C3}^2}{\partial x^2} + v\frac{\partial C_{C3}}{\partial x} = y_{C3} k_B C_B - k_{C3} C_{C3} \tag{4.7}$$

where, C_A, C_B, C_{C1}, C_{C2}, and C_{C3} are the concentrations of species A, B, C1, C2 and C3 respectively; y_A, y_B, y_{C1}, y_{C2}, and y_{C3} are the stoichiometric coefficients; and k_A, k_B, k_{C1}, k_{C2}, and k_{C3} are first-order reaction rate constants.

Also the simulated results with PHT3D and PHAST3D were compared with the analytical solutions presented by Sun et al. (1999). The parameters used in the modeling are listed in Table 4.2 and the comparison of simulated and analytical results are shown in Figure 4.2.

Table 4.2 Hydrogeological and geochemical parameters used in Sun et al (1999) benchmark

Parameter	Value
Flow simulation	Steady state
Simulation time	40 days
Time step	Days
Model length	40 m
Grid spacing	1 m
Effective velocity	0.4 m/day
Dispersive	10 m
Inflow concentration	1.0 mol/l
Porosity	1.0
First order rate constants k_A, k_B, k_C, k_{C2}, k_{C3}	0.2/day, 0.1/day, 0.02/day, 0.02/day, 0.02/day
Stoichiometric yield y_A, y_B, y_{C1}, y_{C2}, y_{C3}	0.5, 0.3, 0.2, 0.1, 0.0
Initial concentration of all species	0.0
Boundary inflow concentration for species A, B, C1, C2, C3	1.0, 0.0, 0.0, 0.0, 0.0

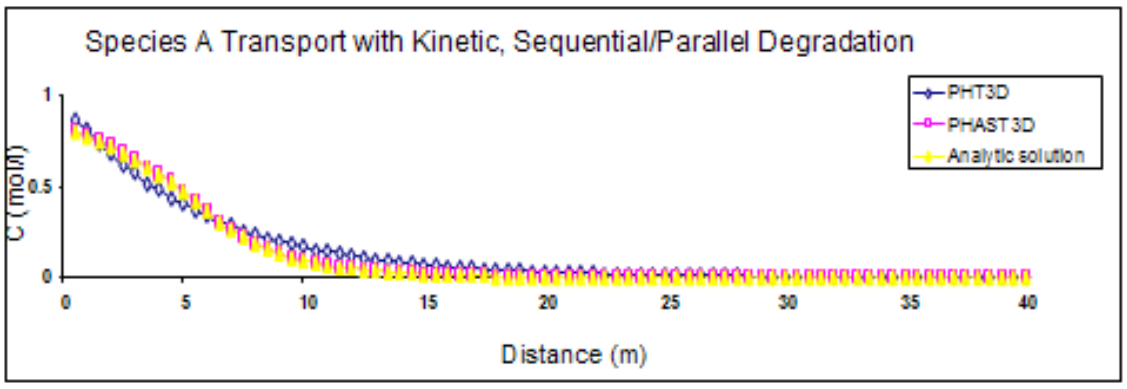

Figure 4.2 Concentration variations of species A with distances based on simulated results of PHT3D (blue diamond), simulated results of PHAST3D (pink square) and analytical solutions (yellow solid diamond), respectively. This plot shows that the simulated results of PHT3D and PHAST3D both match with the analytical solutions.

4.2.3 Biodegradation

In the real environment, the growth and decay of bacteria are involved in different kinetic reactions of solutes. Clement (1997) presented benchmarks about complex pH dependent bacteria with kinetic reactions. The first order degradation of PCE and Monod-type degradation of BTEX under certain conditions of electron-acceptors were included in this benchmark. The reaction rate of BTEX-type hydrocarbons are the synthetic contributions of the degradations of O_2, Fe^{2+}, NO^{3-}, and CH_4. The respective degradation rates of the four species are expressed as follows:

$$r_{NO_3^-} = -k_{NO_3^-} C_{hc} \frac{K_{inh,O_2}}{K_{inh,O_2} + C_{O_2}} \frac{C_{NO3^-}}{K_{NO_3^-} + C_{NO_3^-}} \tag{4.8}$$

$$r_{Fe^{2+}} = -k_{Fe^{2+}} C_{hc} \frac{K_{inh,O_2}}{K_{inh,O_2} + C_{O_2}} \frac{K_{inh,NO_3^-}}{K_{inh,NO_3^-} + C_{NO_3^-}} \frac{C_{Fe^{3+}}}{K_{Fe^{3+}} + C_{Fe^{3+}}} \tag{4.9}$$

$$r_{SO_4^{2-}} = -k_{SO_4^{2-}} C_{hc} \frac{K_{inh,O_2}}{K_{inh,O_2} + C_{O_2}} \frac{K_{inh,NO_3^-}}{K_{inh,NO_3^-} + C_{NO_3^-}} \frac{K_{inh,Fe^{3+}}}{K_{inh,Fe^{3+}} + C_{Fe^{3+}}} \frac{C_{SO_4^{2-}}}{K_{SO_4^{2-}} + C_{SO_4^{2-}}} \tag{4.10}$$

$$r_{CH_4} = -k_{CH_4} C_{hc} \frac{K_{inh,O_2}}{K_{inh,O_2} + C_{O_2}} \frac{K_{inh,NO_3^-}}{K_{inh,NO_3^-} + C_{NO_3^-}} \frac{K_{inh,Fe^{3+}}}{K_{inh,Fe^{3+}} + C_{Fe^{3+}}} \frac{K_{inh,SO_4^{2-}}}{K_{inh,SO_4^{2-}} + C_{SO_4^{2-}}} \frac{C_{CO_2}}{K_{CH_4} + C_{CO_2}} \tag{4.11}$$

where, C_{O2}, C_{Fe2+}, C_{NO3-}, and C_{CH4} are the concentrations of oxygen, iron, nitrate and methane respectively; K_{O2}, K_{Fe2+}, K_{NO3}, and K_{CH4} are the half saturation constants for oxygen, iron, nitrate and methane respectively; and $K_{inh,O2}$, $K_{inh,Fe2+}$, and $K_{inh,NO3}$ are the inhibition constants for oxygen, iron, and sulfate respectively. It must be mentioned that the injection well is located at 155×155 m in the simulation domain.

The comparison was done with the modeling results with PHT3D and PHAST3D and results for both of the models matched well with analytic solutions.

Table 4.3 Hydrogeological and geochemical parameters used in Clement's (1997) benchmark

Parameter	Value	
Simulation time	1100 days	
Time step	55	
Model extension	510×310 m	
Grid spacing	10×10 m	
Porosity	0.30	
Hydraulic conductivity	50 m/d	
Aquifer thickness	10 m	
Head difference between inflow/outflow boundary	1 m	
Dispersivity	10 m	
Well injection rate at contamination source	2 m^3/d	
PCE source concentration (mol/L)	6.031×10^{-3}	
First order rate constants $k_{PCE->TCE}$, $k_{TCE->DCE}$, $k_{DCE->VC}$, $k_{VC->ETH}$	5.787×10^{-8}/d, 3.472×10^{-8}/d 2.314×10^{-8}/d, 1.157×10^{-8}/d	
PH	Initial 7.0	Inflow N/A
Pe	Initial 14.0	Inflow N/A
Hy_carb (mol/L)	Initial 0.0	Inflow 1.09×10^{-2}
O(0) (mol/L)	Initial 2.5×10^{-4}	Inflow 0.0
N(5) (mol/L)	Initial 3.23×10^{-4}	Inflow 0.0
Fe(2) (mol/L)	Initial 0.0	Inflow 0.0
S(6) (mol/L)	Initial 1.04×10^{-4}	Inflow 0.0
Meth (mol/L)	Initial 0.0	Inflow 0.0
Na (mol/L)	Initial 1.0×10^{-3}	Inflow 1.0×10^{-3}
Cl (mol/L)	Initial 1.0×10^{-3}	Inflow 1.0×10^{-3}

The comparison between the calculated results of PHT3D and PHAST3D, and the observed data are shown in Figure 4.3. It is obvious that the two models agree well with each other and both of them have the function of modeling the compound biodegradation. The dependence of the compound biodegradation on the chemical environment including the electrical acceptor and donators can be considered in the simulation.

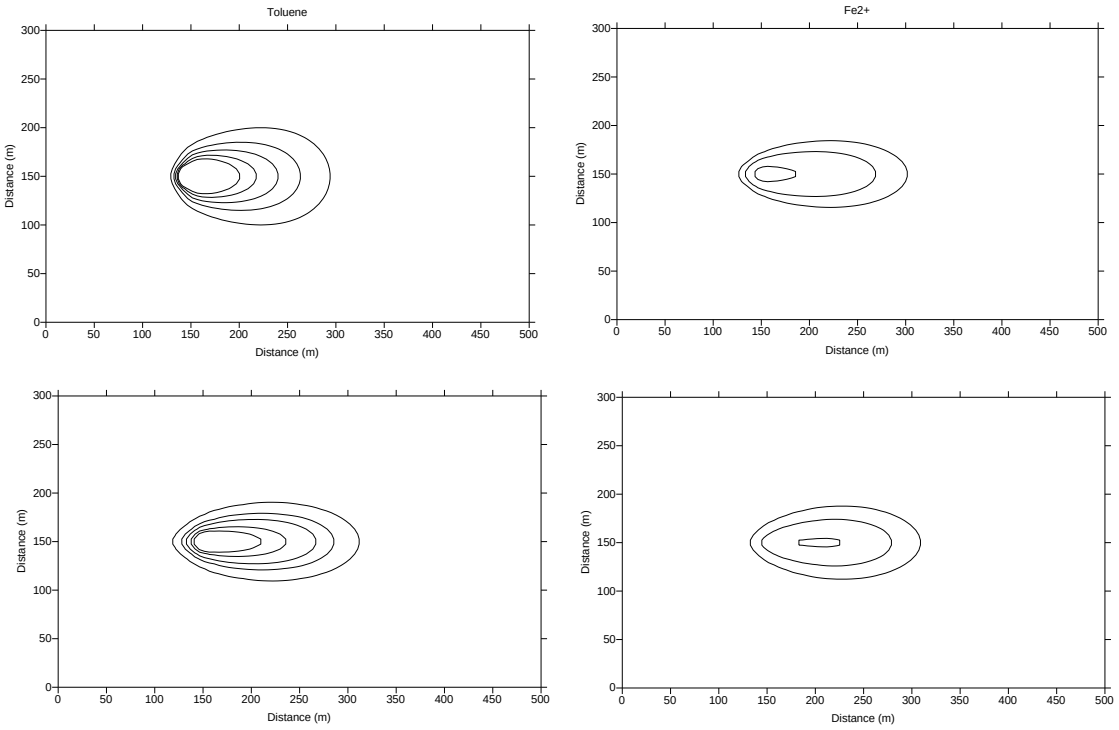

Figure 4.3 Comparison of concentration contours between PHAST3D (upper) and PHT3D (lower) simulations for hydrocarbon HCO^{-}_{3} (1, 5, 10, 20, and 30 mg/l), and dissolved iron Fe^{2+} (2, 8, and 24 mg/l). This plot shows that the simulated results of PHT3D and PHAST3D are comparable.

As presented above, simulation results of PHAST3D match well with those of PHT3D. In the first two cases, simulation results of these two models are in agreement with the analytic solutions. This shows that PHAST3D can be used for simulating solute transport

associated with different geochemical reactions. As for the execution efficiency, PHT3D and PHAST3D models are on the same level. One limitation of PHT3D is that it is unsupportive to surface complexation model (SCM) with respect to PHAST3D. In this study, the surface complexation reaction is one of essential processes for REEs migration (analogues of trivalent actinides) in the YM groundwater system. Thus, PHAST3D is employed to construct the site-scale model for simulating the REEs transport in the YM area.

Obviously, the reliability of simulated results is highly dependent on the hydrogeological and geochemical knowledge. The simplification and description of practical cases must be carefully evaluated; otherwise the simulated results may not be representative.

4.3 Methods and Materials

The evaluation of PHAST3D model demonstrates that this model is reliable in the transport simulation by comparing results with analytic solutions and/or results of PHT3D. The reliability of simulated results of PHAST3D model could be verified further by comparing with the field-measured data if they are available. In this study, the transport simulation of REEs was carried out using the PHAST3D to investigate REE transport behavior in the YM groundwater system.

4.3.1 Governing Equations

PHAST3D can be used in a variety of scales from laboratory experiments, to local and regional field scales according to the purpose of research. The governing equations include

flow, transport, and geochemical equations, which are solved by operator splitting in a sequential way (Parkhurst et al., 2004).

4.3.1.1 Groundwater Flow Equation

$$S_s \frac{\partial(h)}{\partial t} = \nabla \bullet k \nabla h + q \tag{4.12}$$

where, S_s is the storage coefficient (m^{-1}); h is the potential head (m), $h = \frac{p}{\rho g} + z$; t is the time (s); ∇ is the gradient operator for scalar and divergence operator for vectors; k is the hydraulic conductivity (m/s); q is the fluid-source flow rate intensity (m^3/m^3-s); p is the pressure (Pa); ρ is the water density (kg/m^3); g is the gravitational acceleration (m/s^2); and, z is the elevation coordinate (m); and v is the pore velocity, $v = -\frac{k}{\varepsilon}(\nabla h)$.

4.3.1.2 Solute Transport Equation

$$\frac{\partial(\varepsilon \rho c_j)}{\partial t} = \nabla \bullet \varepsilon D \nabla \rho c_j - \nabla \bullet \varepsilon v \rho c_j - \sum_{e=1}^{N_E} \nu_{j,e}^{E} \frac{\partial}{\partial t}(\varepsilon \rho \overline{c_e}) + \sum_{k=1}^{N_K} \nu_{j,k}^{K} \varepsilon \rho R_k + q \varepsilon \rho \hat{c}_j; \quad j = 1,...N_c \tag{4.13}$$

where, c_j is the total aqueous concentration of components j (mol/L); D dispersion-coefficient tensor (m^2/s); N_E is the number of heterogeneous equilibrium reactions; $\nu_{j,e}^{E}$ is the stoichiometric coefficient of component j in heterogeneous equilibrium reaction e; $\overline{c_e}$ is the concentration of solid reactant e (mol/L); N_K is the number of kinetic reactions; $\nu_{j,k}^{K}$ is the stoichiometric coefficient of component j in kinetic reaction k; R_k is the rate of kinetic reaction k (mol $L^{-1}s^{-1}$); $\hat{c}_j$ is the total aqueous concentration of component j in the source water (mol/L); and Nc is the number of chemical components in the system.

The finite difference method is used to discretize the partial-differential equations and boundary conditions. The equations are solved numerically sequentially from the groundwater flow equation to solute transport equations for each component. A set of nonlinear algebraic chemical-reaction equations are incorporated into solving solute transport equations, which count for changes in component concentrations that result from equilibrium and kinetic reactions. The surface complexation reactions are coupled into the equilibrium reactions of Equation (4.13) and the derived surface complexation coefficients are substituted by $v_{j,e}^{E}$ to simulate the adsorption behavior of solutes.

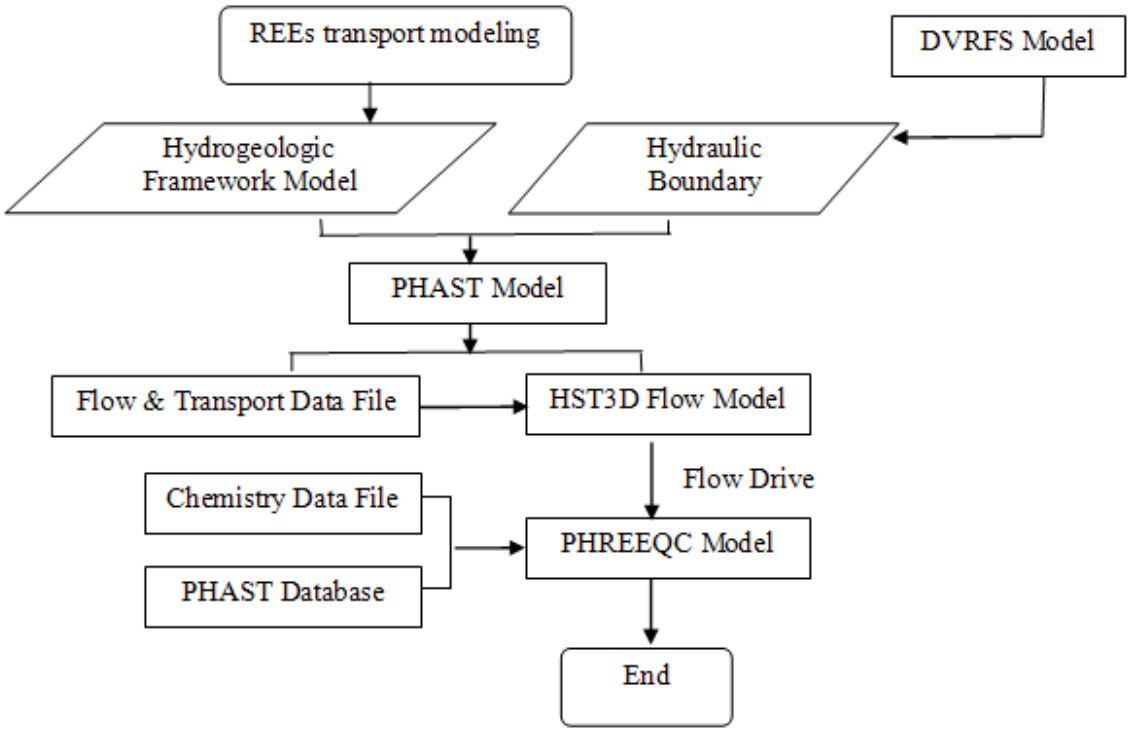

Figure 4.4 Flowchart of REEs transport modeling driven by the HST3D flow model and PHREEQC reaction model

4.3.2 Experimentally Derived Surface Complexation Reactions of REEs

In PHAST3D, the embedded surface complexation model is the constant capacity model (CCM) instead of the three-layer model (TLM). Based on our previous adsorption study of ytterbium (Yb) and europium (Eu), the experimentally derived surface complexation reactions are presented in Equations (3.1)-(3.6). The curve-fitted parameters of the surface complexation reactions in CCM are listed in Table 3.3.

4.4 Numerical Modeling

4.4.1 Model Description

A site-scale YM model was conceptualized by extracting model domain and hydrogeologic property from the regional DVRFS model (shown in Figure 4.5). The simulated hydraulic head, flux of DVRFS model were used for defining the initial and boundary conditions for the site-scale model.

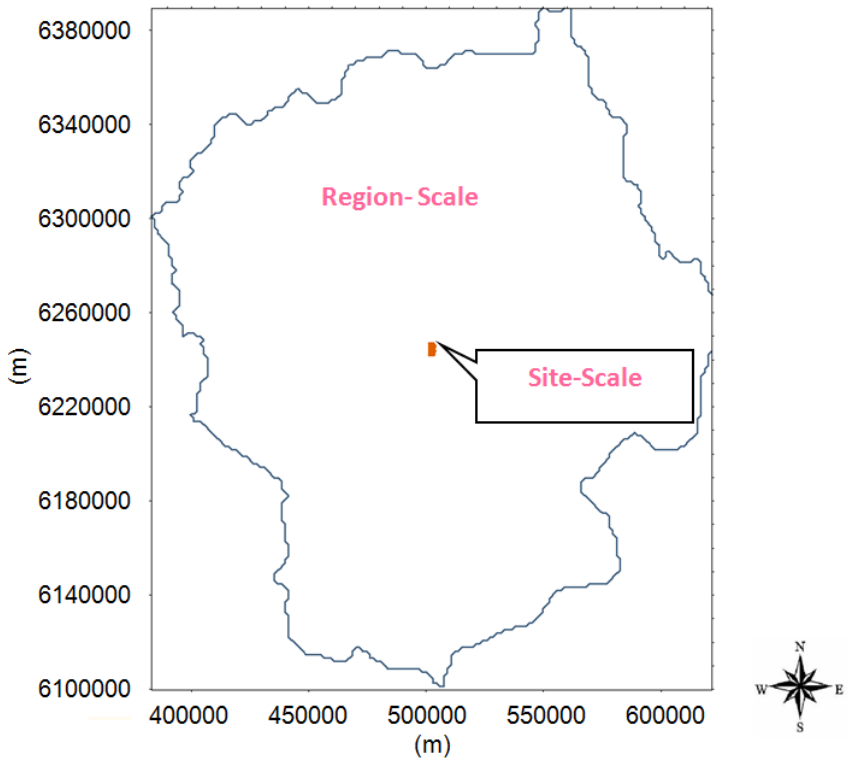

Figure 4.5 Study areas of region-scale and site-scale model. The blue solid line represents the boundary of region-scale model; the small orange solid polygon represents the computational domain of site-scale model

There are twenty five hydrostratigraphic units in four main rock types including confining units, basin-fill units (green color), volcanic-rock units (orange and red color), and carbonate-rock aquifer (blue and dark color) in the DVRFS model shown in Figure 4.6. The vertical exaggeration is approximately 4:1 (Belcher, editor, 2004).

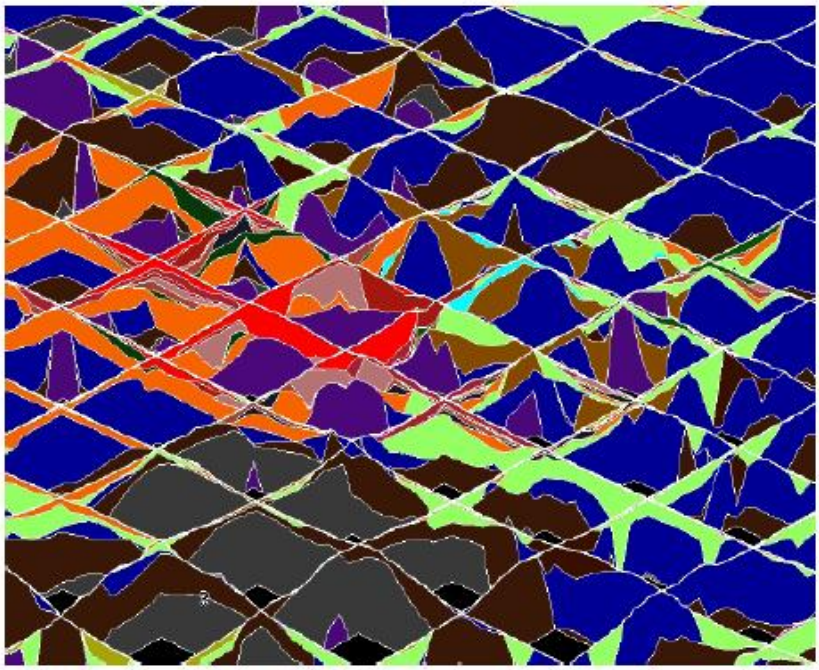

Figure 4.6 Vertical north-south and east-west slices in well-calibrated HFM of DVRFS. The slice horizontal spacing is 15 km and vertical extension is down to 4km below sea level. Volcanic rock is in red or orange color; Tertiary sedimentary rocks in green color; Paleozoic carbonate rock in blue color; Paleozoic and older siliciclastic and metamorphic rock in dark color (from Belcher, 2004).

As shown in Figure 4.7, barrier functions of large faults distributed in YM were considered in the conceptualization of the mountain-scale model, including Solitario Canyon Fault and Ghost Dance Fault. Also, the contaminant source, the burial site for high-level nuclear waste was included as a linkage boundary in the model conceptualization. Borehole tests show that the repository crosses through several faults, which may provide geological barriers or paths for the nuclide migration (Eckhardt, 2000). The hydrostratigraphic units are anisotropic by assigning a default ratio of horizontal and vertical hydraulic conductivity as 10 given unavailability of field measurements.

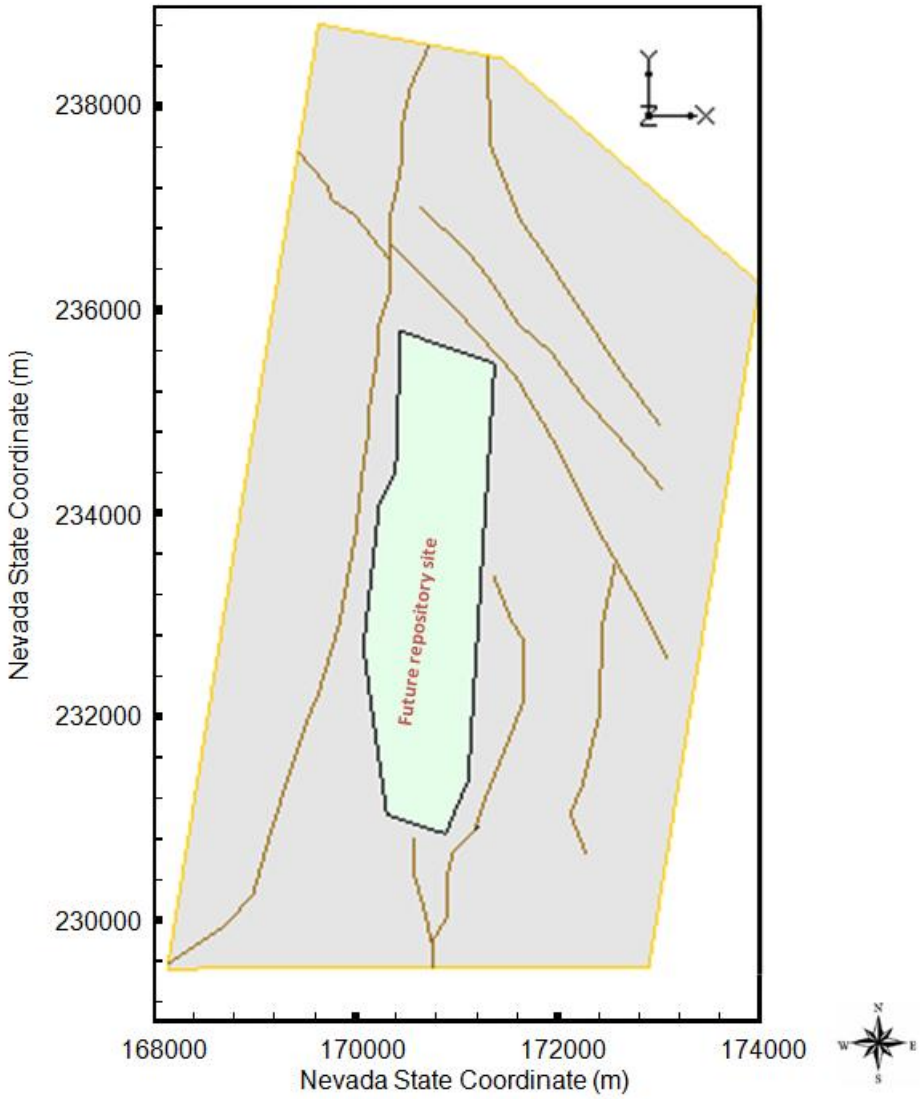

Figure 4.7 Conceptualization of the site-scale model of YM (including the proposed future nuclear waste repository and faults).

In this study, the discretization of the model was set at a lateral spacing interval of 100 m and vertical varied spacing interval of 10 m, referenced to Zyvoloski et al.'s (2003) study. The top elevation of layer 1 (water table) was extracted from the bottom elevation of the lowest layer in the TOUGH2 unsaturated model (Wu et al., 2006).

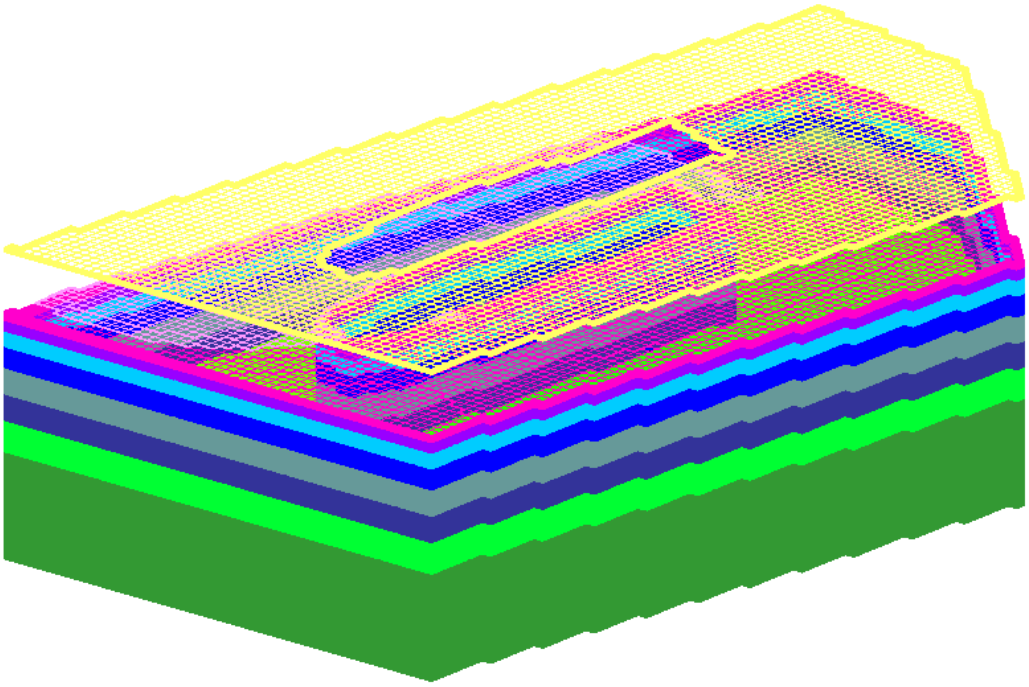

Figure 4.8 Oblique view of the conceptual site-scale model consisted of 15 layers extracted from DVRFS. Layers 2 to 7 were shown as transparent gap between the yellow layer (upper) and the pink layer (lower) in order to show the grids in the two layers.

4.4.2 Modeling Approach

In this study, a base model was used to investigate two scenarios with and without surface complexation modeling of REEs adsorption. By comparing the migration of REEs under the two scenarios, the impacts of adsorption were quantified by contamination plume. The surface complexation was simulated with the CCM embedded in PHREEQC using the experimentally derived surface complexation reactions and optimized reaction constants.

The mountain-scale base model was not calibrated after setting up in this study for few reasons. Firstly, the regional-scale model-DVRFS has been keeping calibrated and updated since 1997. Secondly, this research was focused on the impact of adsorption other than characterizing the appropriate geological and hydrologic property. Thirdly, we do not have the access to the extensive field measurements in YM, which require some specific requirements.

4.4.3 Initial and Boundary Conditions

For the site-scale saturated model, the water table is taken as the top model boundary, which is treated as Dirichlet-type condition with spatially specified head water (shown in Figure 4.9). The bottom model boundary was set as no flux boundary at 4000 m below sea level. All lateral boundaries were treated as flux boundary, whose values were derived from simulation results of DVRFS (Claudia et al., 2004). The extracted flow fluxes for four lateral boundaries are listed in Table 4.4.

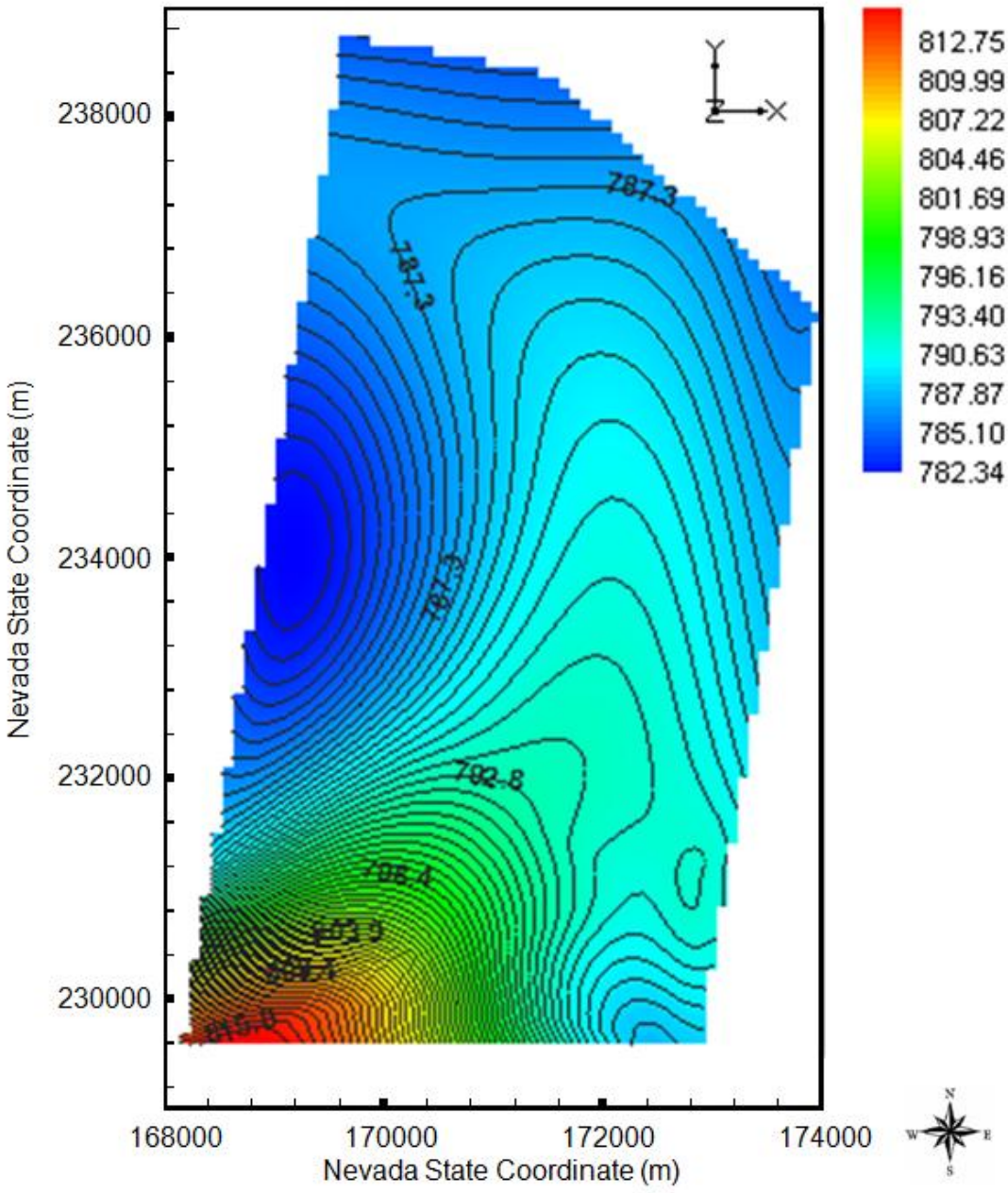

Figure 4.9 Initial hydraulic head (m) distribution at the top model layer. This plot shows the initial hydraulic gradient of water table is relatively high at the southwestern corner of the computational domain.

Table 4.4 Flow flux from the regional model for boundaries (negative flux indicating outflow, and positive flux indicating inflow)

Layer No.	Flow Flux along West Boundary (m3/day)	Flow Flux along East Boundary (m3/day)	Flow Flux along North Boundary (m3/day)	Flow Flux along South Boundary (m3/day)
1	862.4073	788.15	1323.11	-1148.99
2	709.3697	716.7	1400.13	-1148.87
3	517.9393	656.91	1356.77	-1175.15
4	1053.555	1203.86	2869.62	-2486.62
5	290.7644	1057.78	2924.23	-2635.09
6	-45.8554	1176.68	2926.04	-2642.84
7	-46.601	1102.65	2869.65	-2463.49
8	-222.438	1165.09	1955.32	-2131.55
9	-389.051	1202.45	1712.3	-1799.37
10	-670.784	1159.95	1729.24	-1954.97
11	-1055.9	1530.64	2202.42	-2056.64
12	-1588.66	1727.95	149.53	-3527.18
13	-1980.73	1397.15	1.85	-3639.85
14	-2350.96	1456.68	1.63	-2554.99
15	-1181.9	1736.04	2.00	-4038.08

The future repository site was treated as a leakage boundary (source/sink terms). The water table might be recharged by infiltration or leakage from the unsaturated zone where the burial site is located. The infiltration rate was assigned as 1.25 mm/year according to Wu et al's research (2006).

4.4.4 Model Parameters

Input parameters including hydraulic conductivity, storage, and porosity are extracted from those of the YM area in the DVRFS model. The extracted parameter values for 22 zones (including horizontal-flow barriers) are listed in Table 4.5.

Table 4.5 Hydraulic property parameters of model sub-zones

Zone No.	Hydraulic conductivity (m/d)	Anisotropy Factor	Storage	Porosity
1	1.5	5000	1.0×10^{-5}	0.25
2	3	5000	5.0×10^{-5}	0.25
3	0.1	1	0	0.20
4	0.06	5000	0	0.15
5	0.01	1	0	0.15
6	0.02	1	0	0.15
7	0.2	3	0	0.20
8	0.3	3	0	0.20
9	0.05	1	0	0.15
10	0.4	3	0	0.20
11	0.3	3	0	0.20
12	0.004	1	0	0.15
13	0.01	1.26	7.0×10^{-8}	0.15
14	0.002	1.267	0	0.15
15	0.1	5000	7.0×10^{-8}	0.20
16	0.00002	1.26	7.0×10^{-8}	0.15
17	4.45×10^{-5}	1	0	0.30
18	4.45×10^{-5}	1	0	0.30
19	4.45×10^{-5}	1	0	0.30
20	4.45×10^{-5}	1	0	0.30
21	4.45×10^{-5}	1	0	0.30
22	4.45×10^{-5}	1	0	0.30

According to the estimation of Claudia et al. (2004), a longitudinal dispersivity of 10 m and a horizontal dispersivity of 3 m were applied to entire simulation domain, which may be improved once reliable measured values become available. The model calibration was not conducted because: 1) all the model parameters were extracted from

well-calibrated DVRFS model or site-scale TOUGH2 model; 2) the main research objective was to investigate the impacts of adsorption reactions on the solute transport instead of characterizing fluid flow in YM area; 3) model calibration needs extensive field measurements in YM.

4.5 Flow Pattern and Analyses

Groundwater flow and solute transport are simulated with the PHAST3D model to study the adsorption behavior of REEs in the YM area. Specifically, the transport simulation was conducted to investigate the differences between concentration contours of REEs under two conditions with and without surface complexation modeling (SCM). In this study, the studied REES were ytterbium (Yb) and europium (Eu) previously examined with batch reactor experiments and SCM.

4.5.1 Groundwater Flow Simulation

In this study, the flow simulation was conducted at steady state based on the extracted boundary and initial conditions from regional DVRFS and mountain-scale TOUGH2. But the transport simulation was conducted at a transient state using some stress periods to predict the designed safe storage period for nuclear wastes.

After the steady-state simulation, the hydraulic heads were obtained (shown in Figure 4.10). Relatively high hydraulic heads were found at the area close to the west and north boundaries (in red color contour). The flow direction of groundwater is mainly from the northwestern to southeastern in the study area accompanying with some local complex flows.

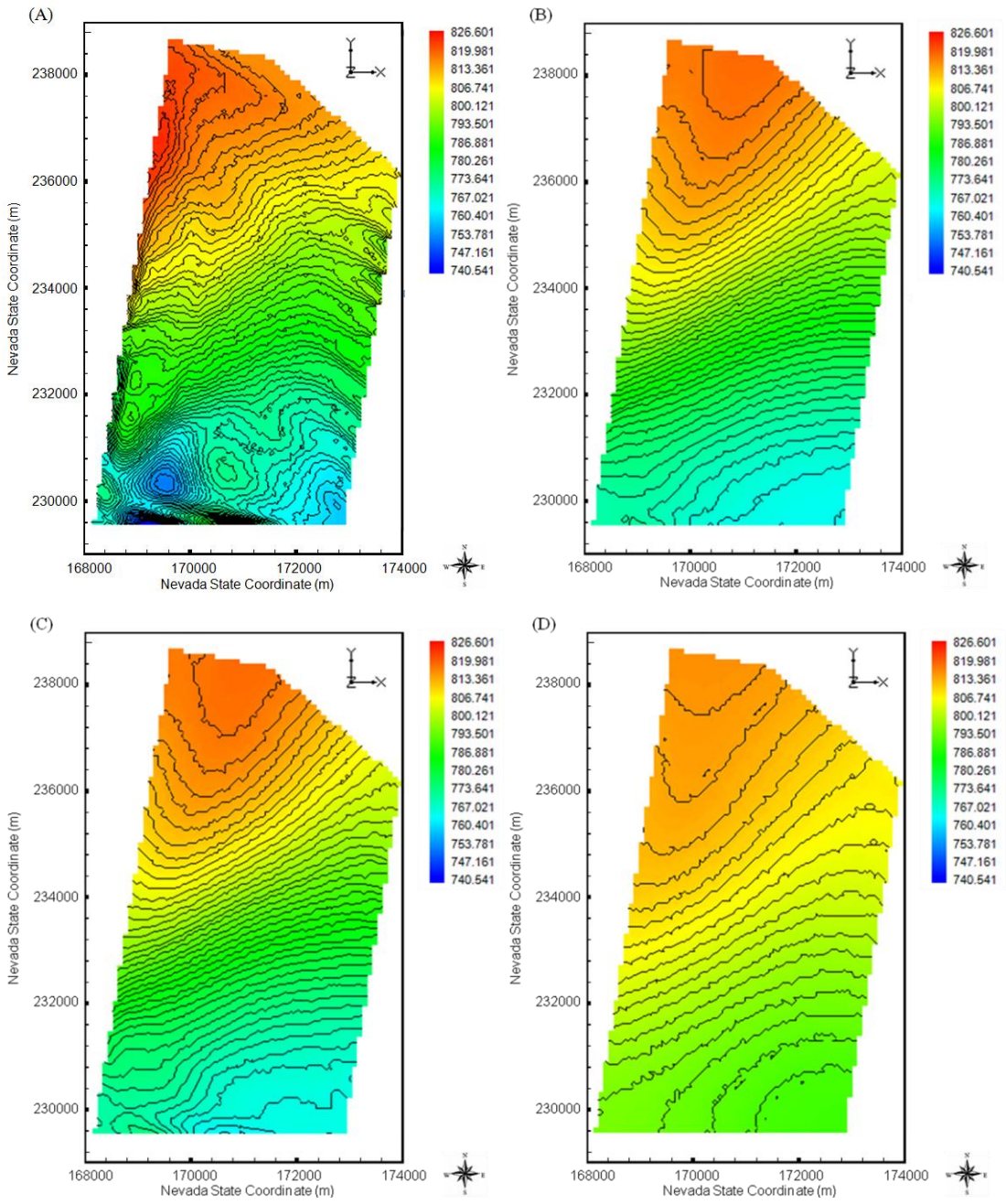

Figure 4.10 Simulated hydraulic heads (m) of the top four layers in steady state: (A) the first layer; (B) the second layer; (C) the third layer; (D) the fourth layer. This plot shows that water mostly moves faster at upper layers than at lower layers.

Under the same color scale and linear interval (Figure 4.10), the hydraulic head gradient became flatter with the increasing depth from the top ground.

In Figure 4.11, the length of the arrow is proportional to the magnitude of the velocity vector. The normalized fluxes rates ranged from 0.0 m/day to 0.044 m/day (mean value 0.0008 m/day, median value 0.00011 m/day) in the simulation at steady state. Mostly, the maximum flux usually occurred around the east boundary, and the second maximum flux occurred around the west boundary of the study area.

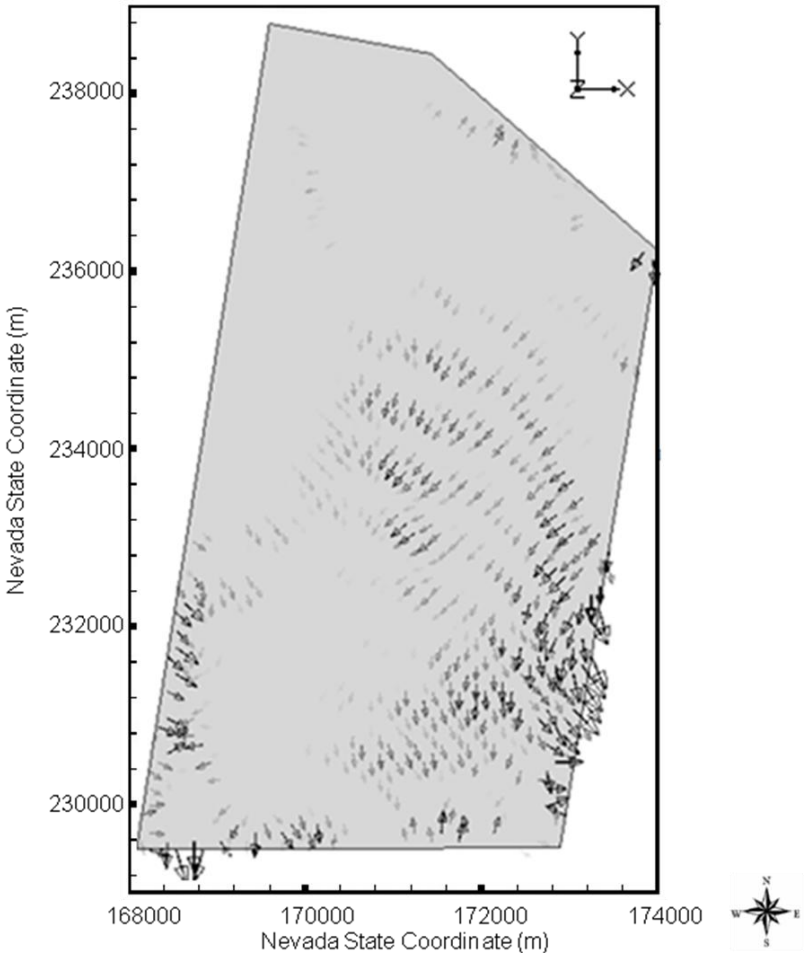

Figure 4.11 Simulated flux rates in the steady state. This plot shows that the high flux occurred around the east and the west boundary of the study area.

Sensitivity analysis can help us evaluate how much the prediction uncertainty could have resulted from the variation of the model parameters. By linking PEST with the mountain-scale model, a preliminary sensitivity analysis was conducted. The simulated flow field didn't significantly change if the field measured hydraulic conductivities were quite few. So a comprehensive sensitivity analysis requires abundant good-quality field observations to investigate the model's response to changes in parameters. In this study, sensitivity analysis was ignored by assuming that the extracted mountain-scale model can properly characterize the hydrogeology of the YM area. If not, the results of modeling will be impaired and unreliable because of large uncertainties.

4.5.2 Transport Modeling

Transport simulations with SCM and without sorption were conducted for ytterbium and europium, respectively. Comparison between simulation results of the two scenarios can provide insight on retardation effects of the studied groundwater system.

4.5.2.1 Transport modeling with SCM

In order to reduce the uncertainty of prediction, the curve-fitted parameters of the surface complexation reactions (listed in Table 3.3) in CCM were optimized using PEST. The optimized reactions parameters are listed in Table 4.6 as follows:

Table 4.6 Optimized intrinsic surface complexation constants of CCM

Yb					
Sample Site	pK_{a1}	pK_{a2}	pK_{cat}	pK_{an}	*Capacitance* (Fm^{-2})
UE18R2228 Fracture	-6.800	3.800	-8.500	8.500	0.700
UE18R2228 Matrix	-6.621	3.700	-8.500	8.500	0.700
UE20C2908 Matrix	-6.800	3.800	-8.500	8.500	0.700
UE20C2855 Matrix	-6.575	3.675	-8.500	8.510	0.700
UE20C2855 Fracture	-6.580	3.677	-8.500	8.500	0.700
PM-1-4823 Matrix	-6.592	3.684	-8.500	8.500	0.700
PM-1-4823 Fracture	-6.655	3.719	-8.500	8.500	0.700
PM-2-4177 Matrix	-6.582	3.678	-8.500	8.500	0.700
Eu					
Sample Site	pK_{a1}	pK_{a2}	pK_{cat}	pK_{an}	*Capacitance* (Fm^{-2})
UE18R2228 Fracture	-6.800	3.800	-8.500	8.500	0.700
UE18R2228 Matrix	-6.800	3.800	-8.500	8.500	0.700
UE20C2908 Matrix	-6.342	3.544	-8.500	8.500	0.700
UE20C2855 Matrix	-6.800	3.800	-8.500	8.500	0.700
UE20C2855 Fracture	-6.661	3.722	-8.500	8.592	0.700
PM-1-4823 Matrix	-6.615	3.367	-8.500	8.500	0.700
PM-1-4823 Fracture	-6.627	3.703	-8.500	8.500	0.700
PM-2-4177 Matrix	-6.538	3.654	-8.500	8.500	0.700

The parameters of adsorption reactions were quite close among the eight volcanic rock samples because of their similar mineralogy and surface area. Averaged values of the eight samples were used for the type of volcanic rocks in the mountain-scale model.

There were no experimentally derived adsorption reactions for the basin-fill alluvium and carbonate rocks. The averaged reaction parameters of volcanic rocks were applied to the other two rock types by adding them in the thermodynamic database file. There are two main reasons for doing so: 1) the chemical reactions defined in the thermodynamic database and chemical input file are universally applicable to all the computational grids; and 2) volcanic rocks play a very important role in the nuclide transport in the YM area.

In the chemical input file, the composition of the groundwater solution was defined in Table 4.7:

Table 4.7 Concentrations of groundwater used in transport simulation (Hershey and Acheampong, 1997)

	Major ion concentration (mg/L)						
Species	Cl^-	SO_4^{2-}	HCO_3^-	Ca^{2+}	Mg^{2+}	Na^+	pH
Concentration	29.9	36.5	291	44.5	19.6	64.6	7.4

Transport simulations were run to some certain time in the future under the groundwater steady flow condition. It was assumed that contaminant sources of Yb and Eu were located inside the leaky boundary (underneath the future repository site) on the first top lay of the mountain-scale model. The contaminant source has a constant concentration of Yb at 10^{-3} mmol/L and Eu at 10^{-4} mmol/L at the beginning of the simulation, respectively. The initial concentrations of Yb and Eu were same with those of previous batch reactor experiments conducted for deriving key adsorption reactions and related parameters.

Longer predicting into future, more extensive computer power is needed such as parallel computing. Given the unavailability of computer cluster, total simulation duration of 100 years was selected in transport simulation of Yb and Eu. The simulated horizontal and vertical concentration contours of Yb were shown in Figures 4.12- 4.13.

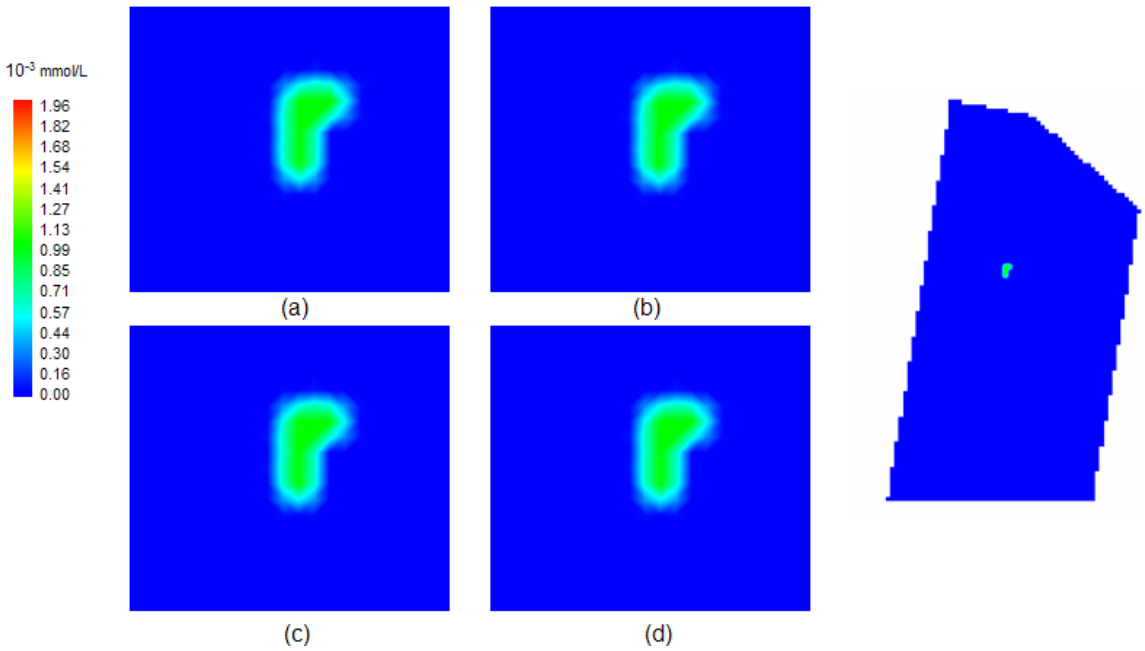

Figure 4.12 Concentration contour of Yb at (a) 25 years; (b) 50 years; (c) 75 years; and (d) 100 years

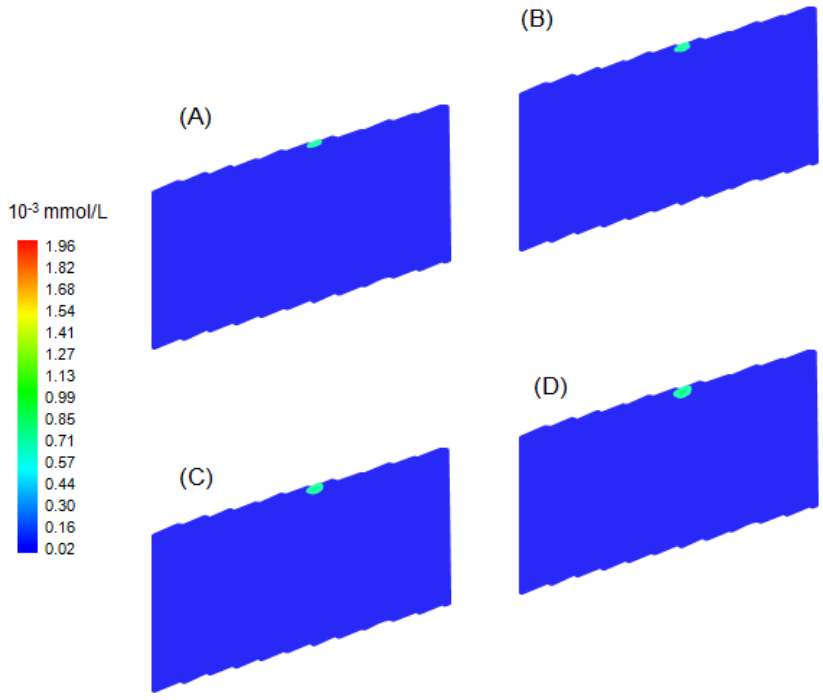

Figure 4. 13 Concentration profile of Yb in N-S vertical cross section at (A) 25 years; (B) 50 years; (C) 75 years; and (D) 100 years

The simulated horizontal concentration contours of Eu were shown in Figure 4.14. As expected, the behaviors of Yb and Eu were pretty similar in groundwater except one magnitude of concentration difference caused by one magnitude of difference in initial concentrations of the two REEs (Yb at 10^{-3} mmol/L and Eu at 10^{-4} mmol/L). There are three reasons for that: (1) same hydrologic and chemical conditions were used in the transport simulation; (2) the surface complexation reactions were similar in CCM; and (3) parameters in CCM were quite similar after optimization.

Calculated concentrations of Yb and Eu with SCM at 100 m and 500 m downstream of the contaminant source (Southeastern) are listed in Table 4.8.

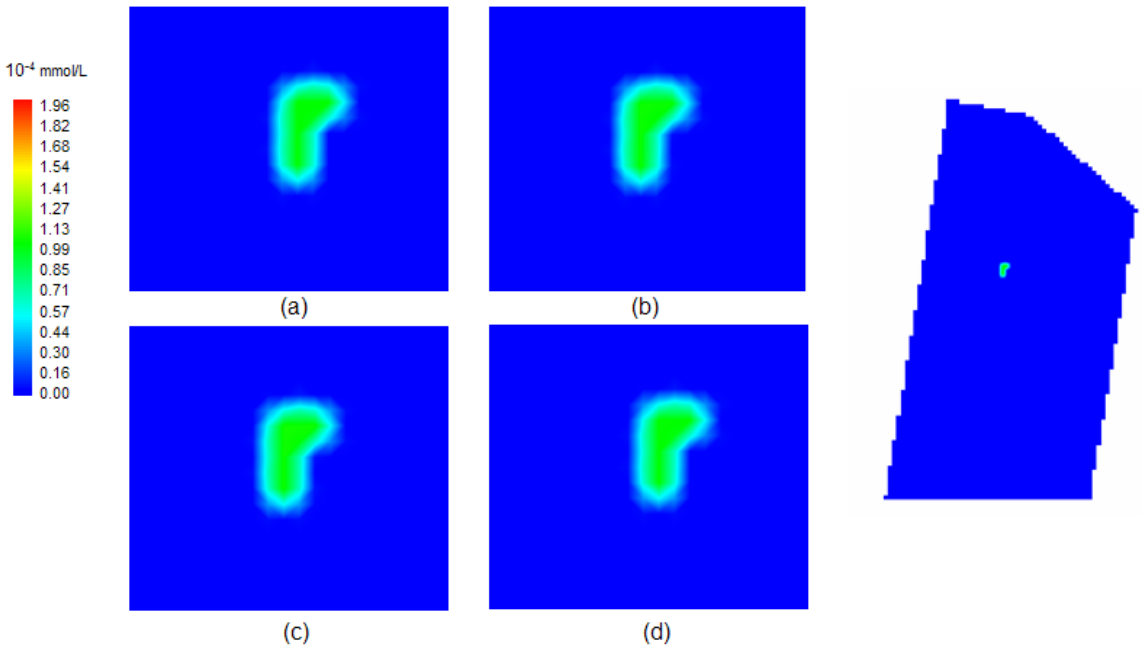

Figure 4.14 Concentration contour of Eu at (a) 25 years; (b) 50 years; (c) 75 years; and (d) 100 years

Table 4.8 Concentrations of calculated Yb and Eu with SCM at 100 m and 500 m downstream of the contaminant source (Southeastern)

Time Interval / **Location**	**Yb Concentration (10^{-3} mmol/L)**			
	25 years	50 years	75 years	100 years
100 m downstream	1.010	1.020	1.030	1.039
500 m downstream	0.0008	0.0023	0.0029	0.0038
	Eu Concentration (10^{-4} mmol/L)			
100 m downstream	1.016	1.032	1.049	1.047
500 m downstream	0.0007	0.0022	0.0026	0.0036

The simulation results showed that the transport of Yb and Eu were highly similar because of pretty close chemical characteristics, derived adsorption reactions and

intrinsic surface complexation constants. Minor differences between these two REEs has been largely dampened by the slow and steady groundwater flow. This might suggest that REEs fractionation and migrates in similar way along groundwater flow paths.

4.5.2.1 Transport modeling without SCM

For the case without SCM, Yb was simulated as a reactive tracer without adsorption in transport. Transport of Eu was not conducted without SCM because of the similarity between Yb and Eu. The SURFACE_SPECIES and SURFACE data blocks were removed from the chemical input file of PHAST3D in order to discount surface complexation reactions.

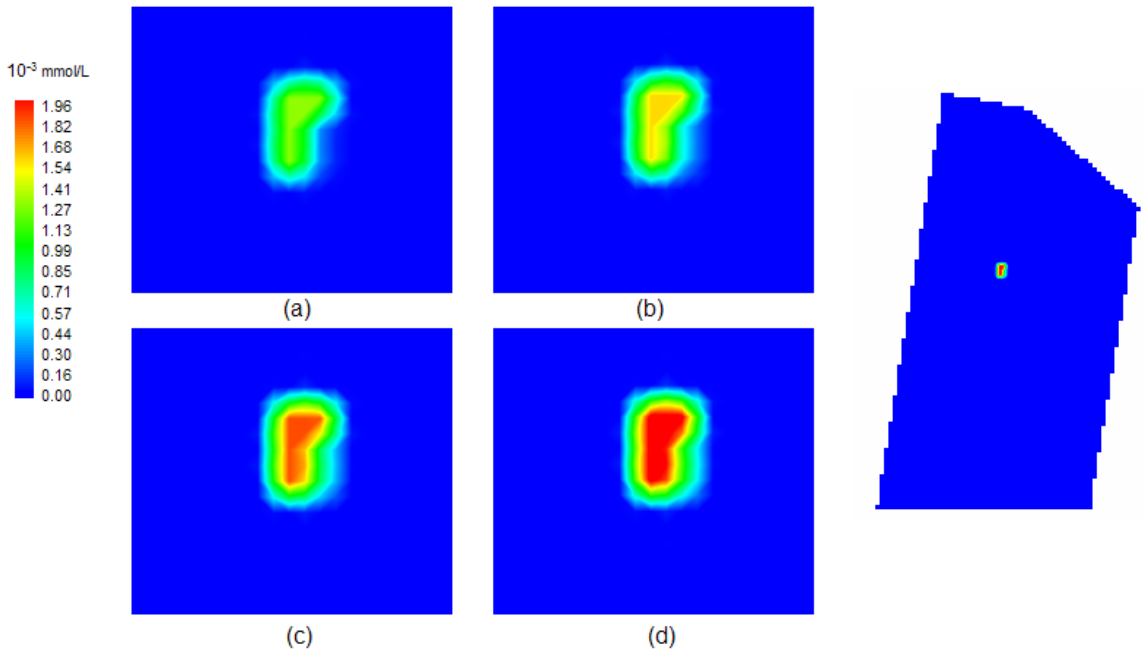

Figure 4.15 Simulated concentration contour of Yb without SCM at (a) 25 years; (b) 50 years; (c) 75 years; and (d) 100 years

The simulated Yb concentrations contours are shown in Figure 4.15 for 25 eyars, 50 years, 75 years and 100 years, respectively. Also the simulated Yb concentrations in different time intervals were listed in Table 4.9 for two imaginary observation cross sections. As we know, the laboratory batch reactor experiment largely accelerates the reaction rate with respect to the actual environments. There is no well-developed method to convert experimental results to field conditions. The retardation of solute transport was certainly overestimated by using the experimentally derived intrinsic surface complexation constants. These laboratory-derived adsorption constants might be adjusted by comparing with the field-measured K_d. However, many unverified assumptions have to be made for the adjustment.

Through curve fitting laboratory adsorption envelopes with the Langmuir isotherm, the derived K_ds are about several hundred times of field-measured ones. Here is a method proposed to convert experimentally derived adsorption results to field environments by making certain assumption. For example, we assumed that the experimentally fitted *Kd* was overestimated by 100 times leading to a reasonable field K_d of Yb is 0.0005068. So the K_d was transformed to equilibrium constants for surface species in such a way that linear sorption is simulated accurately:

$$XO^- + Yb^{3+} \Leftrightarrow XO - Yb^{2+} \tag{4.20}$$

$$Log(K_{cat}^{\text{int}}) = Log(XO - Yb^{2+}) - Log(Yb^{3+}) - Log(XO^-) \tag{4.21}$$

If K_d is 0.0005068, and the number of surface sites is 10^{10} moles, the equilibrium constant can be obtained by substituting Equation (4.20):

$$Log(K_d) = Log(K_{cat}^{\text{int}}) + 10 \Rightarrow K_{cat}^{\text{int}} = 10^{-13.295} \quad (4.22)$$

Then the equilibrium constant was implemented in the chemical data file to simulate the adsorption reactions equivalent to the linear adsorption effect of a K_d=0.0005068.

Table 4.9 Concentrations of calculated Yb without SCM and with an equivalent SCM at imaginary observation cross sections

Time Interval / **Location**	**Without SCM (sorption)** **Yb Concentration (10^{-3} mmol/L)**			
	25 years	50 years	75 years	100 years
100 m downstream	1.283	1.555	1.827	2.088
500 m downstream	0.218	0.621	0.774	1.024
	An equivalent SCM (K_d=5.068×10^{-4}, conversion from lab to field) Yb Concentration (10^{-3} mmol/L)			
100 m downstream	1.091	1.162	1.233	1.421
500 m downstream	0.072	0.212	0.307	0.337

As demonstrated above, the surface complexation modeling is important in the solute transport in the YM area. How to describe and simulate the retardation needs more effort and further study.

4.6 Summary and Conclusions

This study was conducted to simulate REEs transport using a 3-D mountain-scale saturated flow model, developed for investigating the retardation effects of surface complexation reactions. Simulation results showed that the adsorption behaviors of Yb and Eu are quite similar in having close equilibrium constants in SCM and similar simulated contaminant plumes (contours). The REEs transport could be considerably retarded due to adsorption using surface complexation modeling. So far, only CCM and diffusion-layer model (DLM) have been embedded in some groundwater flow models. Efforts of TLM embeding are an absolute necessity to describe ion competition and weak binding in a variety of solutions. However, how to convert obtained results from laboratory scale to field scale is still not well resolved because of the complexity of nature and imperfect knowledge. Additionally, the fact that not only a single set of stoichiometric coefficients yield best fit experimental adsorption results may cause a non-negligible uncertainty.

In summary, this study showed a significant impact of adsorption reactions on REEs transport in the groundwater system in the YM area. The mountain-scale model needs to be calibrated and verified once extensive field measurements are available in order to generate more realistic and reasonable simulations.

4.7 References

Arnold, B.A., Kuzio, S.P., and Robinson, B.A., 2003. Radionuclide Transport Simulation and Uncertainty Analyses with the Saturated-Zone Site-Scale Model at Yucca

Mountain, Nevada. Journal of Contaminant Hydrology, 62-63, p. 401-419.

Belcher, W.R., (editor) 2004. Death Valley regional ground-water flow system, Nevada and California -- hydrogeologic framework and transient ground-water flow model, WRI 2004-5205. U. S. Geological Survey, Denver, Colorado, 408 pp.

Birdsell, K., Soil, W., Rosenberg, N., and Robinson, B., 1995. Numerical modeling of unsaturated groundwater flow and radionuclide transport at MDAG. LA-UR-95-2735, Los Alamos National Laboratory, NM

Clement, T.P., 1997. A modular computer code for simulating reactive multispecies transport in 3-dimensional groundwater aquifers. Technical report, Pacific Northwest National Laboratory, Richland. 59 pp.

Eckhardt, R.C., 2000. Yucca Mountain Looking ten thousand years into the future. Los Alamos Science Number 26 LA-UR-00-4100, p. 464-489.

Eddebbarh, A.A., Zyvoloski, G.A., Robinson, B.A., Kwicklis, E.M., Reimus, P.W., Arnold, B. A., Corbet, W.T., Kuzio, S.P., and Faunt, C., 2003. The Saturated Zone at Yucca Mountain: An Overview of the Characterization and Assessment of the Saturated Zone as a Barrier to Potential Radionuclide Migration. Journal of Contaminant Hydrology, 62-63, p. 477-493.

Essaid, H.I., and Bekins, B.A., 1997. BIOMOC, A multispecies transport model with biodegradation. Technical report, U.S. Geological Survey techniques of Water-Resources Investigations Report 97-4022, 77 pp.

Graf, T., and Therrien, R., 2007. Coupled thermohaline groundwater flow and single-species reactive solute transport in fractured porous media. Advances in Water Resources, 30, p. 742-771.

Goldberg, S., Hyun, S., and Lee, S.L., 2008. Chemical modeling of arsenic(III, V) and selenium(IV, VI) adsorption by soils surrounding ash disposal facilities. Vadose Zone Journal, 7, p.1231-1238.

Hershey, L.R., and Acheampong, Y.S., 1997. Estimation of groundwater velocities from Yucca Flat to the Amargosa Desert using geochemistry and environmental isotopes. Reno, Nevada, Water Resources Center, Desert Research Institute, 2-31 pp.

Jacques, D., Simunek, J., Mallants, D., van Genuchten., and Martinus T., 2008. Modeling coupled hydrologic and chemical processes; long-term uranium transport following phosphorus fertilization. Vadose Zone Journal, 7, p. 698-711.

Kipp, L.K., 1997. Guide to the Revised Heat and Solute Transport Simulator: HST3D -- Version 2. Water-Resources Investigations Report 97-4157, U.S. Geological Survey, Denver, Colorado, 149 pp.

Liu, H.H., Haukwa, C.B., Ahlers, C.F., Bodvarsson, G.S., Flint, A.L., and Guertal, W.B., 2003. Modeling flow and transport in unsaturated fractured rock; an evaluation of the continuum approach. Journal of Contaminant Hydrology, 62-63, p.173-188.

Montarnal, P., Muegler, C., Colin, J., Descostes, M., Dimier, A., and Jacquot, E, 2007. Presentation and use of a reactive transport code in porous media. Physics and Chemistry of the Earth, 32, p. 507-517.

Pan, L., Wu, Y.S., and Zhang, K.N., 2004. A modeling study of flow diversion and focusing in unsaturated fractured rocks. Vadose Zone Journal, 3, p. 233-246.

Parkhurst, D.L. and Appelo, C.A.J., 1999. User's guide to PHREEQC (Version2)—A computer program for speciation, batch-reaction, one-dimensional transport, and inverse geochemical calculations: U.S. Geological Survey Water-Resources Investigations Report 99-4259, U.S. Geological Survey, Denver, Colorado, 310 pp.

Parkhurst, D.L., Kipp, L.K., Engesgaard, Peter, and Charlton, S.R., 2004. PHAST--A program for simulating ground-water flow, solute transport, and multicomponent geochemical reactions. U.S. Geological Survey Techniques and Methods 6-A8, U.S. Geological Survey, Denver, Colorado, 154 pp.

Parlange, J.Y., Starr, J.L., Barry, D.A., and Braddock, R.D., 1984. Some approximate solutions of the transport equation with irreversible reactions. Soil Science Society of America Journal, 137, p. 434-442.

Pawloski, G.A., Tompson, A.F.B., Carle, S.F., Bourcier, W.L., Bruton, C.J., Daniels, J.I., Maxwell, R.M., Shumaker, D.E., Smith, D.K., and Zavarin, M., 2001. Evaluation of the hydrologic source term from underground nuclear tests on Pahute Mesa at the Nevada Test Site: the CHESHIRE Test. W-7405-ENG-48, US Department of Energy.

Prommer, H., Davis, G.B., and Barry, D. A. 1999. PHT3D - A three dimensional biogeochemical transport model for modeling natural and enhanced remediation. In Johnston, C.D., editor, Proceedings of the 1999 Contaminated site re-mediation: Challenges posed by urban and industrial contaminants, Fremantle, Western Australia, p. 351-358.

Pruess, K., 1991. TOUGH2: A general numerical simulator for multiphase fluid and heat flow. LBL-29400, Lawrence Berkeley Laboratory, Berkeley, California, 210 pp.

Robinson, B.A., Li, C., and Ho, C.K., 2003. Performance Assessment Model Development and Analysis of Radionuclide Transport in the Unsaturated Zone, Yucca Mountain, Nevada. Journal of Contaminant Hydrology, 62-63, p. 249-268.

SNL (Sandia National Laboratories), 2007. Site-Scale Saturated Zone Transport. MDL-NBS-HS-000010 REV 03, ACC: DOC.20070822.0003, Sandia National Laboratories, Las Vegas, Nevada, 422 pp.

Sun, Y., Petersen, J.N., Clement, T.P., and Skeen, R.S., 1999. Development of analytical solutions for multispecies transport with serial and parallel reactions. Water Resources Research, 35, p. 185-190.

Vrugt, J.A., Stauffer, P.H., Woehling, T., Robinson, B.A., and Vesselinov, V.V., 2008. Inverse modeling of subsurface flow and transport properties; a review with new developments. Vadose Zone Journal, 7, p.843-864.

Wu, Y.S., Liu, H., and Bodvarsson, G.S., 2004. A triple-continuum approach for modeling flow and transport processes in fractured rock. Journal of Contaminant Hydrology, 73, p.145-179.

Wu, Y.S., Mukhopadhyay, S., Zhang, K. and Bodvarsson, G.S. 2006. A mountain-scale thermal-hydrologic model for simulating fluid flow and heat transfer in unsaturated fractured rock. Journal of Contaminant Hydrology, 86, p. 128-159.

Wolfsberg, A., Glascoe, L., Lu, G., Olson, A., Lichtner, P., McGraw, M., Cherry, T., and Roemer, G., 2002. Tybo / Benham: Model analysis of groundwater flow and radionuclide migration from underground nuclear tests in southwestern Pahute Mesa, Nevada. LA-13977, Los Alamos National Laboratory, NM, 490 pp.

Zachara, John M; Serne, Jeff; Freshley, Mark; Mann, Frederick M; Anderson, Frank; Wood, Marcus I; Jones, Tom; Myers, Dave, 2007. Geochemical processes controlling migration of tank wastes in Hanford's vadoze zone. Vadose Zone Journal, 6, p. 985-1003.

Zhang, K.N., Wu, Y.S., Bodvarsson, G.S., 2003. Parallel computing simulation of fluid flow in the unsaturated zone of Yucca Mountain, Nevada. Journal of Contaminant Hydrology, 62-63, p. 381-399.

Zheng, C., and Wang, P.P., 1998. MT3DMS, A Modular Three-dimensional Transport Model. Technical report, US Army Corps of Engineers, Waterways Experiment Station, Vicksburg, Miss.

Zyvoloski, A.G., Robinson, A.B., Dash, V.Z., and Trease, L.L., 1997. User's Manual for the FEHM Application-A Finite-Element Heat- and Mass-Transfer Code. OSTI ID 14902, Los Alamos National Laboratory, Los Alamos, NM, 155 pp.

Zyvoloski, A.G., Robinson, A.B., Dash, V.Z., and Trease, L.L., 1999. Models and methods summary for the FEHM application. SC-194, Los Alamos National Laboratory, Los Alamos, NM, 74 pp.

Zyvoloski, A.G., Kwicklis, E., Eddebbarh, A.A., Arnold, B.A., Faunt, C., and Robinson. B.A., 2003. The Site-Scale Saturated Zone Flow Model for Yucca Mountain: Calibration of Different Conceptual Models and Their Impact on Flow Paths. Journal of Contaminant Hydrology, 62-63, p. 731-750.

CHAPTER 5

CONCLUSIONS

This dissertation mainly focuses on the flow and solute transport in the YM and NTS area in the Southern Nevada. Three studies were presented which include leaching of trace elements (including some of REEs), adsorption behavior and simulation of Yb and Eu, and numerical simulation of REEs transport in the YM groundwater system.

The first study (Chapter 2) addressed the impacts of geochemical and mineralogical factors on the leaching of trace elements in the study area. Four studied factors are host rock, pH values, grain size, and leaching duration. Based on the experiment analysis, it was found that the concentrations of trace elements in the leached solution are directly proportional to the abundance of trace elements in the bulk rock samples. The Bonanza King Formation showed less leachablility than the Toroweap Formation and Surprise Formation. With respect to the other formations, the Bonanza King Formation has a long diagenetic history, contains some stable minerals and some secondary minerals in fractures which may cause decreased leachability of trace elements. Different ranges of pH could affect the solubility of trace elements and saturation indices. Previous research showed that the leaching solution from the Surprise Formation contained higher concentrations of REEs than that from the Bonanza King Formation. Geochemical calculation also showed that leachates from the Bonanza King Formation had lower saturation indices. However, leached trace elements showed a positive general trend with a longer duration of leaching, despite the existence of incongruent dissolution. The concentrations of the leached trace

elements were obviously attenuated with increasing grain size. The influences of grain size, leaching time, and pH value were difficult to compare because these factors are measured with different and unconvertible units. Leaching experiments provided preliminary datasets for the conceptual model that quantified the fraction of trace elements released from the host rock, which is very useful for tracing sources. Based on some assumptions, the derived leaching fractions were used in the fraction conceptual model to estimate the extra addition of U to groundwater due to rainfall infiltrating through aquifer rocks.

The second study (Chapter 3) addresses the adsorption of REEs onto the volcanic rocks using an integrated method of experiment and numerical modeling. Based on the results of batch reactor experiments, CCM and TLM were deployed to describe the adsorption reactions and estimate the associated reaction constants. The ybtterbium and europium showed pH dependent adsorption behaviors and moderately to weakly binding. Through comparison, TLM provided a better fit with experiments than CCM at expense of more model parameters. TLM is capable of counting for weakly binding and ion competition as CCM is not. Protolysis constants, capacitance constant, and surface binding constants were optimized by using the PEST. The sensitivity analysis showed that pK_1 has the highest sensitivity and pK_{cat} has the lowest sensitivity among adjustable parameters of TLM. Thus, the estimation of protonation and association constants needs to be carefully examined when using TLM. The derived K_ds of Yb and Eu through Langmuir isotherm fitting were quite close. The adsorption of Yb and Eu may be

amplified by hundreds times as compared to these under a laboratory condition.

The third study (Chapter 4) focused on the implementation of a local-scale 3D model to investigate the retardation of REEs in the YM groundwater system. The PHAST3D was selected in this study because of its embedded SCM. The local-scale model was extracted mainly from a well-calibrated regional-scale model, DVRFS. Two scenarios were simulated for Yb and Eu: one is reactive solute transport with SCM; and another is reactive solute transport without SCM. The comparison between simulated concentrations at observation points showed that adsorption reaction considerably attenuate the simulated concentrations of REEs. Based on certain assumptions, the experimentally derived equilibrium constants were transformed to these for a field condition. The simulated concentrations of REEs were still significantly less than those without adsorption reactions. The study showed the important role of adsorption in the REEs transport in the YM area.

Some additional recommendations are included here for future studies:

a. The adsorption behaviors of Yb and Eu needs more and further investigation, especially on the determination, optimization, and justification of reaction parameters;
b. REEs could be considerably retarded due to adsorption, which could be better simulated using the surface complexation model to consider associated thermodynamic geochemical reactions instead of a simple lumped distribution

coefficient. However, the conversion from laboratory scale to field scale is still not a well-resolved problem;

c. Not a single set of stoichiometric coefficients can fit laboratory adsorption results. How to estimate the uncertainty of stoichiometric coefficients in SCM in curve fitting adsorption envelope or isotherm is still a crucial issue;

d. The mountain-scale model needs to be calibrated and verified using extensive field measurements before being applied to produce more realistic and reasonable simulations.

VITA

Graduate College
University of Nevada, Las Vegas

Liqiong Zhang

Degrees:
Bachelor of Engineering, Hydrology and Water Resources, 1994
Science & Technology University of Chengdu, China

Master of Science, Hydrology and Water Resources Management, 2000
Hohai University, China

Special Honors and Awards:

- UNLV-DRI hydrology/hydrogeology research fellowship, 2003-2006
- Research Grant of Graduate & Professional Student Association (GPSA) of UNLV, 2005
- Graduate Research Grant of Geological Society of America (GSA), 2004

Publications:

- **Zhang, L.,** Yu, Z., Zhou, X., Papelis, C., and Stetzenbach, K., 2009. Leaching characterization and transport modeling of trace metals from different rocks in Southern Nevada Region. J. of Contaminant Hydrology (in review).
- **Zhang, L.,** Zhao, D., and Shen, H. W., 2006. An integrated approach for simulating and predicting the scour around abutments. International Journal of Sediment Research, Vol. 21, No. 3, p. 238-247

Dissertation Title: Study of Rare Earth Element Transport in the Yucca Mountain Region

Dissertation Examination Committee:
Chair, Dr. Zhongbo Yu, Ph. D.
Co-Chair, Dr. Lambis Papelis, Ph. D.
Committee Member, Dr. Wanda Taylor, Ph. D.
Committee Member, Dr. Matthew Lachniet, Ph.D.
Graduate Faculty Representative, Dr. Zhonghai Ding, Ph. D.